Scientific Research and Essays

Volume 10 Number 6 30 March 2015
ISSN 1992-2248

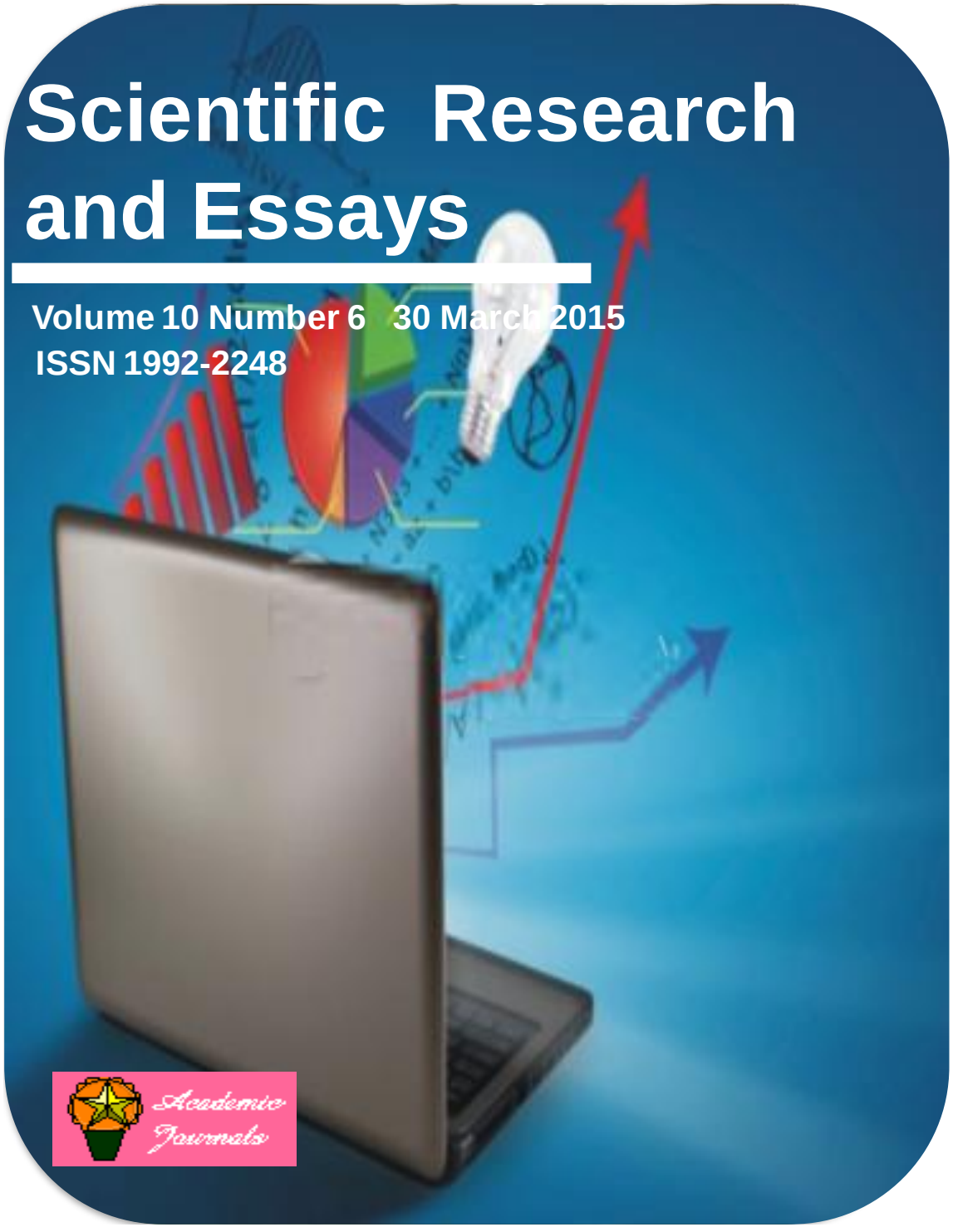

Academic Journals

ABOUT SRE

The **Scientific Research and Essays (SRE)** is published twice monthly (one volume per year) by Academic Journals.

Scientific Research and Essays (SRE) is an open access journal with the objective of publishing quality research articles in science, medicine, agriculture and engineering such as Nanotechnology, Climate Change and Global Warming, Air Pollution Management and Electronics etc. All papers published by SRE are blind peer reviewed.

SubmissionofManuscript

Submit manuscripts as email attachment to the Editorial Office at sre@academicjournals.org. A manuscript number will be mailed to the corresponding author shortly after submission.

The Scientific Research and Essays will only accept manuscripts submitted as e-mail attachments.

Please read the **Instructions for Authors** before submitting your manuscript. The manuscript files should be given the last name of the first author.

Editors

EditorialBoard

Fees and Charges: Authors are required to pay a $550 handling fee. Publication of an article in the Scientific Research and Essays is not contingent upon the author's ability to pay the charges. Neither is acceptance to pay the handling fee a guarantee that the paper will be accepted for publication. Authors may still request (in advance) that the editorial office waive some of the handling fee under special circumstances.

ScientificResearchandEssays

Table of Contents: Volume 10 Number 5 15 March, 2015

ARTICLES

Research Articles

academicJournals

Vol. 10(6), pp. 210-217, 30 March, 2015
DOI: 10.5897/SRE2015.6151
Article Number:CB06B6451817
ISSN 1992-2248

http://www.academicjournals.org/SRE

Scientific Research and Essays

Full Length Research Paper

Evaluation of pavement noise emission model: A case study in Tehran

Ali Mansour Khaki[1]*, Amir Esmael Forouhid[2] and Hootan Chegini[3]

[1]Civil Department, School of Civil Engineering, Iran University of Science and Technology, Narmak, Tehran, Iran.
[2]Road and Transportation Engineering, School of Civil Engineering, Iran University of Science and Technology, Narmak, Tehran, Iran.
[3]Transportation Engineering, Azad University of Tehran-South Unit, Tehran, Iran.

Received 1 January, 2015; Accepted 20 March, 2015

Noise pollution and its influence on environment and life quality of human beings may be considered as a hot topic in scientific research. Since there are no sufficient studies on noise pollution in Tehran, this study was carried out to determine noise levels of pavement in Tehran City. SMM1 (The first standard of noise measurement method) model is one of the most common models used in calculating noise emission in Tehran City. Because factors which this model uses are close to Tehran traffic situation, in this study, SMM1 noise emission model has been modified by including pavement statement factor. In other words, the pavement age will affect noise emission in environment. Thus, a case-study is chosen and its pavement statement factor is added to SMM1 noise emission model. Equivalent noise level changes in different distances with sound noise. This effect is calculated and indicated in this paper. Another factor that could affect the sound level is traffic volume, which is also shown in this paper. In this study, it is concluded that when asphalt pavement is fresh and new, equivalent noise level is 2 (dB) less than when the pavement becomes old due to congestion of pavement and its decreasing void. The results showed that pavement noise should be mentioned among the major environmental problems, and studies aim at preventing it should have great priority.

Key words: Noise, traffic, pavement, pollution.

INTRODUCTION

Sound is a physical phenomenon that is caused by air pressure waves, which emanate from a vibrating source, and alerts the hearing sense of human beings. While sound is an energy type that emits waves, noise is simply an unwanted sound. The magnitude of the highway traffic noise is analyzed in this study. Discrete sources of noise from industrial units like factories, construction, aircrafts or vehicles in a flowing traffic, turn into a linear source, the most stable of all known random noise sources in the city (Turgut and Zübeyde, 2012). Like other engineering problems, there are two major ways of analyzing the problem of noise emissions in residential areas. One way is by using sound level meters (SLMs) in the study area by which the level of the generated sound in the area is

*Corresponding author. E-mail: amiresmaelf@yahoo.com

directly measured and the necessary considerations will be thought. Using SLMs is a very precise technique for studying sound level in the area. On the other hand, sound measuring in each certain area would take a considerable time and be costly (Golmohammadi et al., 2007). This is because the level of noise emitted by vehicles in streets varies depending on traffic condition and such parameters should be considered in measurements. Noise pollution is recognized as a major problem for the quality of life in urban areas all over the world ((ElifEbru and Emin, 2011; Olayinka, 2012). Because of the increase in the number of cars and industrialization, noise pollution has also increased. Noise in cities, especially along main arteries, has reached up disturbing levels. Residences far from noise sources and near silent secondary roads are currently very popular. People prefer to live in places far from noisy urban areas (Serkan et al., 2009).

Another way used to measure noise pollution in a certain area is employing noise pollution model, which indeed is a mathematical technique. Mostly traffic-based parameters, which are very diverse, are used as the model's inputs. There are many factors that may affect sound emission in the space; hence, numerous models have been developed in this area so far. Some of these models are described in this reference (Garg and Maji, 2014). Most of them are physical factors which cover sound properties. Measuring and examining such parameters is very difficult and complicated. However, other parameters including traffic-related ones such as velocity of vehicles and traffic flow are measured very easily (Ranjbar et al., 2012).

First attempts of making a traffic noise prediction can be collocated into 1950/1960 decades; they mainly evaluate the percentile L_{50}, defined as the sound level exceeded by the signal in 50% of the measurement period. These models refer principally to a fluid continuous flux, considering a common constant velocity with no distinction between vehicle typologies. One of the first models, developed in 1952, is the one reported in Handbook of Acoustic Noise Control (Johnson and Saunders, 1968). This model states that the 50 percentile of traffic noise for speed of 35-45 mph (about 55-75 Km/h) and distances greater than 20 feet (about 6 m) are given by:

$$L_{50} = 68 + 8.5Log(Q) - 20Log(d) \quad (dBA) \qquad (1)$$

Where Q is traffic volume in vehicles per hour and d is the distance from observation point to center of the traffic lane, in feet; no specification is included about vehicles and types of roads.

The CoRTN procedure (Calculation of Road Traffic Noise) was developed by the Transport and Road Research Laboratory and Department of Transport of the United Kingdom in 1975 and was modified in 1988 (Department of Transport, 2008). It estimates the basic noise level L_{10} both at 1h and 18 h reference time. This level is obtained at a reference distance of 10 m from the nearest carriage way edge of the highway. The parameters involved in this model are: traffic flow and composition, mean speed, gradientof the road and type of road surface. The basic hypotheses of the model are a moderate wind velocity and a dried road surface. Operatively, the basic hourly noise level is predicted at a distance of 10 m from the nearest carriage way, according to the following equation:

$$L_{10}(1h) = 42.2 + 10Log(q) \quad (dBA) \qquad (2)$$

and the basic noise level in terms of total 18-hour flow is:

$$L_{10}(18h) = 29.1 + 10Log(q) \quad (dBA) \qquad (3)$$

Where q and Q are the hourly traffic flow (vehicles/hour) and 18 h flow (vehicles/hour), respectively. Here it is assumed that the basic velocity is v = 75 km/h; the percentage of heavy vehicles is P = 0 and road's gradient is G = 0%. It is also assumed that the source line is 3.5 m from the edge of the road for carriage ways separated by less than 5.0 m.

Tire/pavement interaction is not the only source of traffic noise, but it is the dominant component for passenger cars traveling at highway speeds (McNerney et al., 2000). Reducing traffic noise at the source by placing a noise reducing pavement surface is becoming an attractive option for many highway agencies. A noise reducing surface is defined as "a road surface which, when interacting with a rolling tire, influences vehicle noise by causing at least 3 dB (A) lower vehicle noise than what is obtained on conventional and most common road surfaces" (Sandberg and Ejsmont, 2002). Literature shows that open graded asphalt mixes in Europe can reduce traffic noise (Sandberg, 2005; Colwill et al., 1993; Camomilla et al., 1990).

Tire/pavement noise is evidently affected by the characteristics of the tires and the pavement. Only the latter factor is addressed in this paper. The physical properties of the materials that constitute the upper structural layer of the pavement play a major role in the generation of noise. Pavement mixes with higher air void contents porosity are known to reduce noise levels. There are two noise reduction mechanisms for open graded (porous) surfaces: noise absorption and noise propagation. The presence of air voids in the surface layer helps dissipate trapped air in the tire's tread grooves. This results in reduced air pumping, and therefore decreased noise emissions (Nelson, 1994). Porosity also gives the pavement acoustical absorption properties where sound waves are dissipated into heat within the voids of the surface layer (Sandberg and Ejsmont, 2002). This study tried to analyze a traffic model developed in Germany. The effect of asphalt life span on noise emission through asphalt was considered as the

pavement correction factor. Its proper adaptability with the studied area, which is a street in Tehran City, is why this model and its correction factor are used.

A mathematical model was used to design noise emissions level around the studied traffic axis. This model is useful for measuring level of equivalent noise or environmental noise pollution level through road traffic standards and various types of vehicles that cross the mentioned axis. For this model, various parameters were studied and applied which will be pointed out as follows. First of all, there is need to show you the general equation of equivalent noise level (Ranjbar, 2012):

$$L_{eq} = E + C_{opt} + C_{ref} - D_{afs} - D_{lucht} - D_{bodem} - D_{meteo} - D_{barrier} \quad (4)$$

In this equation, the sole unknown factor, which is important for this study, is equivalent sound level in decibel, which is represented by symbol L_{eq}. Other parameters defined in other sides of the equation are the ones that can be measured regarding the traffic factors. All parameters of the equations are summarized in Table 1. For road surface, Table 3, which concerns the pavement characteristic and as a factor used in the SMM1 model, was used. For the other factors in the model, the parameter that is described in Table 2 was used. As the table indicates, there is a main parameter, represented by symbol E, for measuring noise level. Other parameters are applied to reform this parameter. In the equation E, there are three noise related parameters for different sorts of vehicles including light, medium and heavy. The equation designed for these three parameters is (Ranjbar et al., 2012):

$$E_{lv} = 69.4 + 27.6\log\left(\frac{V_{lv}}{V0}\right) + 10\log\left(\frac{Q_{lv}}{V_{lv}}\right) + C_{wegdek,lv} \quad (5)$$

$$E_{mv} = 73.2 + 19.0\log\left(\frac{V_{mv}}{V0}\right) + 10\log\left(\frac{Q_{mv}}{V_{mv}}\right) + C_{wegdek,mv} \quad (6)$$

$$E_{hv} = 76.0 + 17.9\log\left(\frac{V_{hv}}{V0}\right) + 10\log\left(\frac{Q_{hv}}{V_{hv}}\right) + C_{wegdek,hv} \quad (7)$$

Where, l_v, m_v and h_v indexes are used for light, medium and heavy vehicles, respectively. V represents velocity, while Q is used to represent traffic flow in a certain time period. E is the equivalent noise level for each class of vehicle.

At the end of these equations, there is a factor which is the noise correction regarding the type of pavement. For the standard model, the factor has been defined separately for each class of pavements. However, what is complicated is the pavement lifespan, which can be an effective factor in pavement porosity and hence the sound emission level through pavement (Hampshire, 2009). In this study, we tried to achieve a certain level of correction through analyzing the pavement lifespan effect in noise emission using as a case study one of Tehran City streets. It helps the designed model to function more precisely.

METHODOLOGY

As already mentioned, this study focuses on the noise on pavements with a model that has a parameter that is related to asphalt pavements on highways. When possible, noise emission from light and heavy vehicles is analyzed separately. The areas for pavement and noise investigation are shown in Figures 1 and 2. Azadegan Expressway has been aligned from Northwest to Southeast of Tehran City. The expressway reaches Tehran-Karaj Freeway from Northwest and ends at Afsariyeh (Basij-e Mostaza'fin) three-way from Southeast. After crossing Tehran-Karaj Freeway, Azadegan Expressway in its path towards southeast meets the following highways: ShahidLashgari Expressway, Fat'h Highway, Tehran-Saveh Freeway, Ayatollah Saeedi Highway (Saveh Road), Khalije Fars Freeway (Tehran-Qom) at Jahad Square, Behesht-e Zahra Highway, ShahidRajaie Highway, Dowlatabad Highway (under construction) and Afsariyeh Three-way (Basij-e Mostazafin). Thus, the freeway is connected to Shahr-e Rey via ShahidRajaie Highway. Azadegan Freeway is located in North to South Zone and is stretched from Northwest to Southeast of Tehran. According to the traffic terminology, it is a super highway which is among the entrance and exit ways of Tehran. Azadegan Expressway is connected to Shahre-Rey through Shahid Rajaie Highway in order to generate a somehow fundamental way for passengers who intend to leave Tehran. Its traffic load is very heavy in vacations and weekends (Wikipedia, 2014).

This study aims at analyzing the effect of road pavement on how noise pollution is emitted. Reduction of empty space in pavement due to compression over time is the main reason why sound emissions patterns are changed after pavement installation (Department of Transportation and Road of Tehran, 2007). When there is wider empty space in the asphalt, the noise generated from tire rolling over the road pavement as well as that generated by the car's engine, which reaches the pavement surface, is trapped in the pavement's empty space, leading to a considerable loss of its energy. Now, if the empty space within the road pavement becomes smaller due to heavy car traffics and more compressed pavement, the sound wave will be further echoed and emitted around after colliding with the pavement surface. Accordingly, scientists started to fabricate a type of pavement with more porosity that can keep higher levels of sound. As a result, they have to invent porous asphalt, which indeed is very useful and practical in residential regions (Jalilzadeh et al., 2004).

Therefore, it can be concluded that both time and more durable pavements can affect the noise emissions level in the peripheral environment. The German standard sound emission model, that is, SMM1 will be analyzed in this study and pavement lifespan effect coefficient on the model will be considered in its coefficients based on the surveys made in the studied area. The interchange between Sattari Street and Azadegan Expressway in Tehran City was chosen as our study area. As mentioned before, this area was chosen because of applying new pavement for repairing a part of the street during this study. Therefore, comparing simultaneously the noise emission level in the repaired and unrepaired areas is very easy. As a result, the effect of new asphalt on sound emission can be studied (Figures 1 and 2).

RESULTS

The computational algorithm sample of the model is described in Table 2. For the case study area, all the parameters are explained, and for pavement age, Table 3 and the technical data in Figure 3 are used. The

Table 1. Definition of equivalent noise level equation parameters.

Parameter	Equation	Definition
E	$E = 10.\log(10^{\frac{E_{lv}}{10}} + 10^{\frac{E_{mv}}{10}} + 10^{\frac{E_{hv}}{10}})$	Noise Level
C_{opt}	0	Sound of vehicle break
C_{ref}	$C_{ref} = 1.5 \times f_{obj}$	Noise reflection by walls
D_{afs}	$D_{afs} = 10\log(r)$	Distance effect
D_{lucht}	$D_{lucht} = 0.01 \times r^{0.9}$	Air absorption effect
D_{bodem}	$D_{bodem} = B[2 + 4(1 - e^{-0.04\,r}).\left(e^{-0.65\,hw} + e^{-0.65\,(hweg-0.75)}\right)]$	Earth absorption effect
D_{meteo}	$D_{meteo} = 3.5 - 3.5\,e^{\frac{-0.04\,r}{(hweg+hw+0.75)}}$	Weather effect
$D_{barrier}$	-	Barriers and structures effect

Table 2. Computational algorithm model used in the case study.

Equation				
$L_{eq} = E + C_{opt} + C_{ref} - D_{afs} - D_{lucht} - D_{bodem} - D_{meteo} - D_{barrier}$				
Parameter	**Equation**	**Definition**		**Solution**
E	$E = 10.\log(10^{\frac{E_{lv}}{10}} + 10^{\frac{E_{mv}}{10}} + 10^{\frac{E_{hv}}{10}})$ $E_{lv} = 69.4 + 27.6\log\left(\frac{V_{lv}}{V0}\right) + 10\log\left(\frac{Q_{lv}}{V_{lv}}\right) + C_{wegdek,lv}$ $E_{mv} = 73.2 + 19.0\log\left(\frac{V_{mv}}{V0}\right) + 10\log\left(\frac{Q_{mv}}{V_{mv}}\right) + C_{wegdek,mv}$ $E_{hv} = 76.0 + 17.9\log\left(\frac{V_{hv}}{V0}\right) + 10\log\left(\frac{Q_{hv}}{V_{hv}}\right) + C_{wegdek,hv}$	Light vehicle velocity=V_{lv} Medium vehicle velocity **=** V_{mv} Heavy vehicle velocity **=** V_{hv} Reference velocity **=** V0 Light vehicle volume **=** Q_{lv} Medium vehicle volume **=** Q_{mv} Heavy vehicle volume **=** Q_{hv} Pavement factor in table 2 **=** C_{wegdek}	V_{lv} = 105 V_{mv}= 99 V_{hv} = 106 V0 = 80 Q_{lv}= 19901 Q_{mv} = 4213 Q_{hv} = 1201 C_{wegdek} = 2	**85.48**
C_{opt}	-	The sound from the brakes because of the insignificance of the highway is zero	0	0
C_{ref}	$C_{ref} = 1.5 \times f_{obj}$	The coefficient of sound barriers= f_{obj}	f_{obj} = 0	0
D_{afs}	$D_{afs} = 10\log(r)$	Measured noise from the source of noise **=** r	r = 7.5	8.75
D_{lucht}	$D_{lucht} = 0.01 \times r^{0.9}$	Measured noise from the source of noise **=**r	r = 7.5	0.061
D_{bodem}	$D_{bodem} = B[2 + 4(1 - e^{-0.04r}) \times \left(e^{-0.65hw} + e^{-0.65(hweg-0.75}\right)]$	Constant factor of barrierB = height **=** h_w height of noise measurng **=** h_{weg}	B = 0	0
D_{meteo}	$D_{meteo} = 3.5 - 3.5e^{\frac{-0.04r}{(hweg+hw+0.75)}}$		h_w = 1 h_{weg} = 1.5 r = 7.5	0.31
$D_{barrier}$	**-**	No barrier in the case study	-	0

Table 3. The technical specifications for traditional asphalt.

Marshall sample density	Percentage filled with aggregate	Percent filled with bitumen	The percentage of void	Marshall resistance of asphalt	Percent bitumen compared to asphalt	Technical specifications for traditional asphalt
g/cm^3	%	%	%	kg	%	Unit
MS-2	MS-2	MS-2	MS-2	MS-2	ASTM D2172	Standard
2.19	**18**	**55.0**	**7.9**	**1412**	**5**	Used sample

specifications are in Table 3. For analysis of the area, initially we referred to the operation on Friday 6/11/2014 for taking the warm asphalt sample chosen for conducting grading tests and characterizing the asphalt. Examination showed that 5% bitumen has been used in the asphalt and grading test results are shown in Table 3

Figure 1. Interchange between Sattari Street and Azadegan highway.

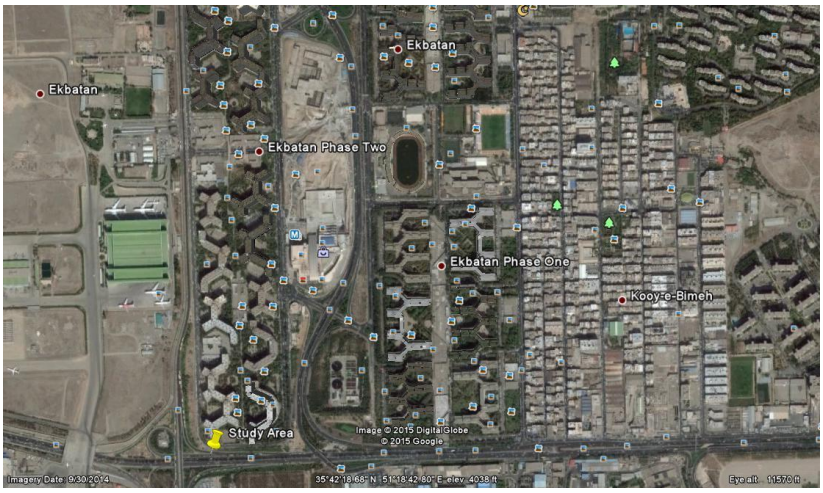

Figure 2. Point of noise measuring in the study.

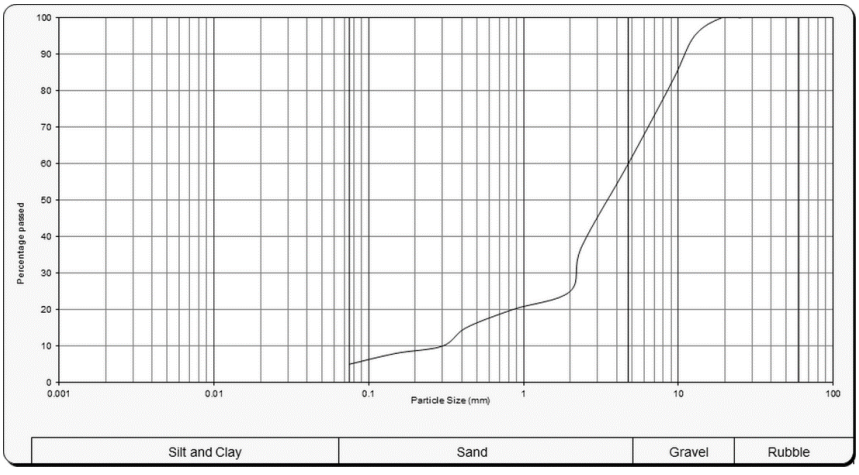

Figure 3. Grading diagram for asphalt mixed materials.

Table 4. Road surface correction.

	Road surface classification	Noise level correction		
Road surface coefficient	Porous	0-60 km/h	61-80 km/h	81-130 km/h
		-1 dB	-2 dB	-3 dB
	(Concrete or bitumen) young smooth asphalt		0 dB	
	(Concrete or bitumen) old smooth asphalt		2 dB	
	Cement and wavy asphalt mixture		2 dB	
	Pavement stones		3 dB	

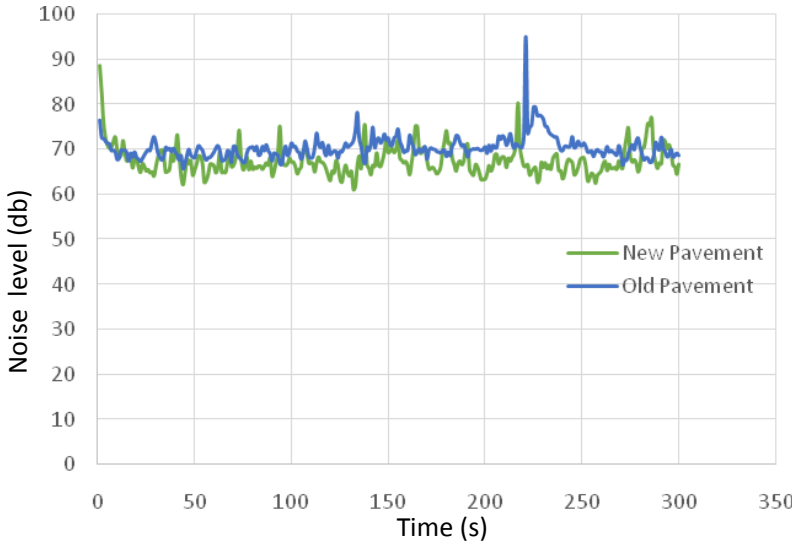

Figure 4. Observed noise level in studied area.

and Figure 3. After few days of sampling date, we again referred to the site for analyzing the noise generated by the asphalt. It let us compare the new asphalt and old one quantitatively. Therefore, we again referred to the asphalt site on 6/26/2014 and measured the sound; the data gained were analyzed.

DISCUSSION

Road surface corrections are seen in the correction applied over the sound emission model, SMM1. The results of the studies are summarized in Table 4. We examined in this study the difference caused by correcting the old asphalt and replacing it with new one. It was due to more porosity in the new asphalt layer. Over time and heavy traffic flows make the pavement surface compressed and as a result its porosity percentage decreased. It continues until the current asphalt is replaced with a new one. In other words, the environment's noise pollution increases whenever the asphalt layer is compressed under vehicles' tires. However, one should note that the increasing trend of noise pollution is stronger in the initial phases of asphalt lifespan than its final phases; because initial phases of utilization are accompanied with more pounding and compression of the layer compared to the phases the layer experiences in final days.

Figure 4 shows two sets of measurements carried out in the site. The blue-colored diagram indicates the news asphalt, which has been spread and utilized recently, while the red one reflects the band with the old pavement, which has not been repaired so far. As it is clear, the average sound vibrations are lesser on the new asphalt in comparison to the old one. For the old pavement the average sound level or L_{eq} is equal to 73 dB, whose maximum measure level stands at 97.1 dB. Compared to the other side of the street where a new pavement has been applied, the average noise level measured 69.9 dB with the maximum rate of 88.8 dB.

It can be seen that the new asphalt and the type of the asphalt used in the road are effective in minimizing noise pollution. On the other hand, the red curve shows the noise generated by the vehicles used the old asphalt. In this regional comparison, it became evident that the noise pollution decreased about by 3 dB, which is a

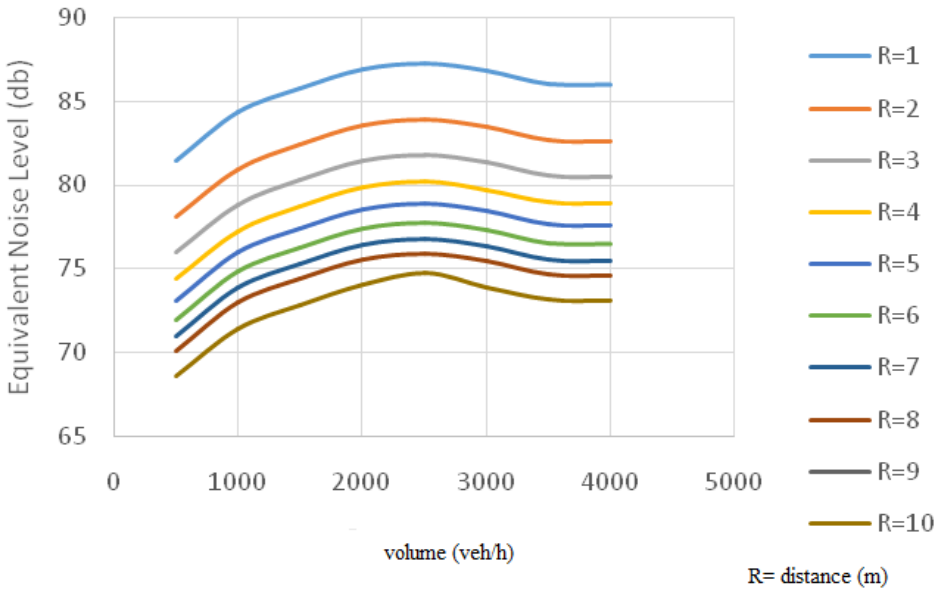

Figure 5. Equivalent noise level in different distances.

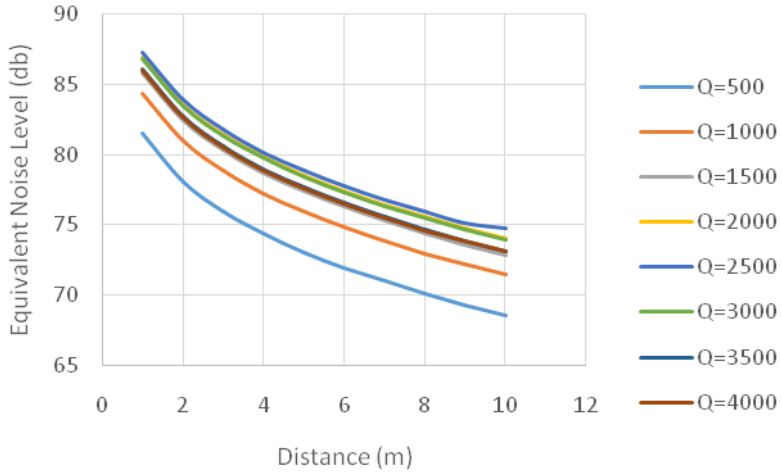

Figure 6. Equivalent noise level in different traffic volumes.

considerable amount, using the new asphalt. The decreased noise pollution in the environment can be assigned to more porosity in the new asphalt. Over time and due to using more vehicle of the street surface, the compression of the used pavement increased and hence its porosity decreased. Asphalt's pores trap the wave, generated by the engine, and also the noise, caused by rolling of tires, in the pavement, wasting its energy considerably. It is very effective in decreasing noise pollution.

Figures 5 and 6 show how noise is emitted by various distances and traffic loads. The first figure indicates the ratio of equivalent noise level to different traffic loads. Parallel lines in this figure represent different distance to the sound origin. In this figure, the highest diagram shows the 1 m distance to the sound origin, while the lowest line represents the 10-m distance to the noise origin, that is, axis of the street. As the diagrams suggest, noise initially is decreased considerably when the distance is increased, but when the distance is further increased, then the noise decline is ebbed away. However, lower noise is generated when the traffic load is increased and the average velocity is decreased. It suggests that not only number of vehicles, but also their velocity play a key role in generating noise; in that when the traffic load exceeds the standard capacity of the street, the generated noise is more despite fewer vehicles in the street.

Figure 5 shows the relationship between distance and noise level. As the figure shows, there is a reverse relation between distance and noise level. Different lines of the diagram have been designed to show different traffic flows of the model. The highest line indicates a traffic flow with at least 4000 vehicles, while the lowest line shows a traffic load with 500 various light, medium and heavy vehicles per hour. As the figure shows there is a reverse relation between distance and diagram's gradient. It suggests that when the distance is increased, noise pollution decline is ebbed away. Several factors affect this including further hindrances in streets, physical properties of waves, trees and other obstacles around the streets, etc.

In this research, in order to reduce the computation time, the noise standard German first method was used, given the parameters of the mathematical method used to calculate the mean of the noise reduction parameters. The accuracy of the method of calculation of noise is obtained with the field testing.

Eventually, it can be concluded that there are various parameters than can affect the noise generated through the streets. Of them, the most important ones are type of pavement, asphalt lifespan, and distance to the voice origin. These parameters were used in the mathematical model of the study and tests carried out in the site confirmed the accuracy of the model. However, future studies can examine the exact effect of asphalt lifespan on noise emission in terms of mathematical viewpoint and when it can be considered serious in the noise pollution studies. It is necessary to do sufficient studies on traffic noise.

Conflict of Interest

The authors have not declared any conflict of interest.

REFERENCES

Golmohammadi R, Abbaspour M, Nassiri P, Mahjub H (2007). Road traffic noise model. J. Res. Health Sci. pp. 13-17.

Ranjbar H, Gharagozlu A, Vafainejad A (2012). Tehran: s.n Air pollution map modeling with SMM1 method, 20th national geomathic congress.

Department, Transportation and Road. Porous Asphalt. Tehran: Transportation research (2007). 86/RRRI/228.

Jalilzadeh R, Nasiri P, Bakhshi MH (2004). Study on Asphalt effect in reducing noise pollution in city transportation. Tehran: Environment research Institute.

Hampshire (2009). University of new. UNHCS Design specifications for Porous asphalt pavement.

Wikipedia (2014). Wikipedia Website. [Online] 96. http://fa.wikipedia.org/wiki.

Laboratory, Soil mechanic Technical. Asphalt Extraction and Sieve analysis (2014). Tehran: Soil mechanic Technical Laboratory.

Serkan O, Hasan Y, Murat Y, Pervin Y (2009). Evaluation of noise pollution caused by vehicles in the city of Tokat, Turkey. Sci. Res. Essay 4(11):1205-1212.

ElifEbru S, Emin U (2011). Evaluation of traffic noise pollution in Corlu, Turkey. Sci. Res. Essays 6(14):3027-3033.

Turgut Ö, Zübeyde Ö (2012). A case study on acoustic performance and construction costs of noise barriers, and Metehan ÇALIS (2012). Sci. Res. Essays. 7(50):4213-4229.

Johnson DR, Saunders EG (1968).The evaluation of noise from freely flowing road traffic, J. Sound. Vib. 7(2):287-309.

Department of Transport, Calculation of Road Traffic Noise, HMSO, UK, 1988, 2008.

Sandberg U (2005).“State-of-the-art of low-noise pavements.” Presentations from SILVIA Final Seminar, Brussels.

Sandberg U, Ejsmont JA (2002). Tyre/road noise reference book. Informex, Kisa, Sweden.

Camomilla G, Malgarini M, Gervasio S (1990). “Sound absorption and winter performance of porous asphalt pavement" Transportation Research Record. 1265, Transportation Research Board, Washington, D.C., pp. 1-8.

Colwill DM, Bowskill GJ, Nichols JC, Daines ME (1993). “Porous asphalt trials in the United Kingdom.” Transportation Research Record. 1427, Transportation Research Board, Washington, D.C., pp. 13–21.

McNerney MT, Landsberger BJ, Turen T, Pandelides A (2000). “Comparative field measurements of tire/pavement noise of selected Texas pavements.” Research Rep. No. 7-2957-2, Center of Transportation Research, The Univ. of Texas at Austin, Austin, Texas.

Nelson PM (1994). Designing tyre and road surfaces to reduce traffic noise, TRL Annual Review, Transportation Research Laboratories, Crowthorne, U.K.

Olayinka OS (2012). Noise Map: Tool for Abating Noise Pollution in Urban Areas. Open Access Scientific Reports 1:185.

Garg N, Maji S (2014). A critical review of principal traffic noise models: Strategies and implications, Environ. Impact Assessment Rev. Elsevier. 46:68-81.

academicJournals

Vol. 10(6), pp. 218-231, 30 March, 2015
DOI: 10.5897/SRE2015.6196
Article Number:B479B7651820
ISSN 1992-2248

http://www.academicjournals.org/SRE

Scientific Research and Essays

Full Length Research Paper

The (G'/G)-expansion method and the $\exp(-\phi(\xi))$-expansion method with applications to a higher order dispersive nonlinear Schrödinger equation

Elsayed M. E. Zayed*, Yasser A. Amer and Reham M. A. Shohib

Mathematics Department, Faculty of Sciences, Zagazig University, Zagazig, Egypt.

Received 23 February, 2015; Accepted 17 March, 2015

In this article, we study the connection between the (G'/G)-expansion method and the $\exp(-\phi(\xi))$-expansion method with the aid of a suitable transformation. We employ these two methods to derive families of exact solutions for a higher order dispersive nonlinear Schrödinger equation describing the propagation of the optical pulse in a medium. Comparison between these two methods is presented. We show that the two methods as well as their results are equivalent.

Key words: Higher order dispersive nonlinear Schrödinger equation, The (G'/G)-expansion method, the $\exp(-\phi(\xi))$-expansion method, exact solutions.

INTRODUCTION

Exact solutions of nonlinear partial differential equations (PDEs) are of fundamental and important in applied science because they are widely employed to explain some of the nonlinear phenomena and dynamical processes existed in nature world. Nonlinear wave phenomena appear in various scientific and engineering fields, such as fluid mechanics, plasma physics, optical fibers, biology, solid state physics and so on. In the recent decades, several powerful methods for finding the exact solutions of the nonlinear PDEs have been proposed such as the tanh-method and its various extension (Parkes and Duffy, 1996; Fan, 2000; Yan, 2001), the Jacobi-elliptic function expansion method (Liu et al., 2001; Yan, 2003; Fu and Liu, 2003), the homogeneous balance method (Wang, 1995, 1996; Wang et al., 1996; Zayed and Arnous, 2012), the F-expansion method and its extension (Wang and Zhou, 2003; Zhou et al., 2004; Wang and Li, 2005a, b; Zhang et al., 2006; Wang. et al., 2007), the sub-ODE expansion method (Li and Wang, 2007; Wang et al., 2007; Yomba,

*Corresponding author. E-mail: e.m.e.zayed@hotmail.com

PACS: 02.30.Jr, 04.20. JB, 05.45.Yv.

2006; Li et al., 2006), the exp-function method (He and Wu, 2006; Zayed and Abdelaziz, 2011; Zhu, 2007), the (G'/G)-expansion method (Wang et al., 2008; Zhang et al., 2008; Zayed and Gepreel, 2009a, b; Zayed, 2009a, b;Zayed and Abdelaziz, 2010), the first integral method (Feng, 2002; Zheng, 2011; Taghizadeh et al., 2011; Sharma and Kushel, 2010; Bekir and Unsal, 2012; Lu et al., 2010), the extended hyperbolic auxiliary equation (Zhu, 2007), the subsidiary ODE (Zhang et al., 2006), the $\exp(-\phi(\xi))$-expansion method (Zhao and Li, 2014); Khan and Akbar, 2013; Harun-Or-Roshid and Rahman, 2014), the transformed rational function method (Ma and Lee, 2009), the multiple exp-function method (Ma and Zhu, 2012; Ma et al., 2010), the generalized Riccati equation method (Ma and Fuchssteliner, 1966), the Frobenius decomposition technique (Ma et al., 2007), the local fractional differential equations (Yang, 2011; Yang, 2012), the local fractional variation iteration method (Yang and Baleanu, 2012), local fractional Fourier series method (Hu et al., 2012), the cantor-type cylindrical coordinate method (Yang et al., 2013), the Yang-Fourier and Yang-Laplace transforms (He, 2012) and the fractional complex transform method (Su et al., 2013) . For further effective methods we refer to the recent articles (Chun-Guang et al., 2014; Hristov, 2012; Hristov and El Ganaoui, 2013; Zhang et al., 2014; Rui and Hui-Qin, 2014; Rui et al., 2013; Rui et al., 2015; Hui-Qin and Jian-Wen, 2015) which are very interested to the readers.

The objective of this paper is to study the connection between the (G'/G)-expansion method and the $\exp(-\phi(\xi))$ -expansion method with applications for constructing new families of exact solutions of the following higher order dispersive nonlinear Schrödinger equation with both fourth order dispersion effects and a quintic nonlinearity (Zhu, 2007; Zhang et al., 2006):

$$iu_z = \frac{\beta_2}{2}u_{tt} + i\frac{\beta_3}{6}u_{ttt} + \frac{\beta_4}{24}u_{tttt} - \gamma_2|u|^2 u - \gamma_4|u|^4 u \quad (1)$$

Where $u(z,t)$ is the slowly varying envelope of the electromagnetic field, t represents the time (in the group velocity frame) , z represents the distance along the direction of propagation (the longitudinal coordinate), $\beta_2, \beta_3, \beta_4$ represent group velocity dispersive (or second order dispersive), third order dispersive and fourth order dispersive respectively , γ_2 and γ_4 are cubic and quintic nonlinearity coefficients respectively. Equation (1) describes the propagation of optical pulses in a medium that exhibits a parabolic nonlinearity law. However, the exact analytic solutions to Equation (1) have been obtained in Zhu (2007) by using the extended hyperbolic auxiliary equation method and in Zhang et al. (2006) by using the subsidiary ODE method.

DESCRIPTION OF THE (G'/G)-EXPANSION METHOD

Suppose we have the following nonlinear PDE:

$$F(u,u_t,u_x,...) = 0 \quad (2)$$

where F is a polynomial in $u(x,t)$ and its partial derivatives in which the highest order derivatives and the nonlinear terms are involved. In the following, we give the main steps of this method [Wang et al., 2008; Zhang et al., 2008; Zayed and Gepreel, 2009a, b; Zayed, 2009a, b; Zayed and Abdelaziz, 2010]:

Step 1

We use the wave transformation:

$$u(x,t) = u(\xi),\ \xi = x - ct \quad (3)$$

where c is a constant, to reduce Equation (2) to the nonlinear ODE:

$$P(u,u',u'',...) = 0 \quad (4)$$

where P is a polynomial in $u(\xi)$ and its total derivatives with respect to ξ .

Step 2

We assume that Equation (4) has the formal solution:

$$u(\xi) = \sum_{i=0}^{N} a_i \left(\frac{G'}{G}\right)^i \quad (5)$$

where $G = G(\xi)$ is the solution of the linear ODE:

$$G'' + \lambda G' + \mu G = 0 \quad (6)$$

Where λ, μ, a_i are arbitrary constants.

Step 3

We determine the positive integer N in Equation (5) by balancing the highest order derivatives and the nonlinear terms in Equation (4). More precisely, we define the degree of $u(\xi)$ as $D[u(\xi)] = N$, which gives rise to the degree of other expressions as follows:

$$D\left[u^{P}(\xi)\left(\frac{d^{q}u(\xi)}{d\xi^{q}}\right)^{s}\right]=NP+s(q+N).$$

Hence, we can get the value of N in Equation (5).

In some nonlinear equations the balance number N is not a positive integer. In this case, we make the following transformations:

(a) When $N=\frac{q}{p}$, where $\frac{q}{p}$ is a fraction in the lowest term, we let:

$$u(\xi)=V^{\frac{q}{p}} \quad (7)$$

and substitute Equation (7) into Equation (4) to get a new equation in terms of the function $V(\xi)$ with a positive balance number in integer.

(b) When N is a negative number, we let

$$u(\xi)=V^{N} \quad (8)$$

and substitute Equation (8) into Equation (4) to get a new equation in terms of the function $V(\xi)$ with a positive balance number in integer.

Step 4

We substitute Equation (5) along with Equation (6) into Equation (4), collecting all terms of the coefficients of $\left(\frac{G'}{G}\right)^{i}$ $(i=0,1,2,...,N)$ and setting them to zero, we get a set of algebraic equations which can be solved by using the Maple or Mathematica.

Step 5

On solving Equation (6), we have the values of (G'/G) as follows:

$$\left(\frac{G'}{G}\right)=\begin{cases}\frac{\sqrt{\lambda^2-4\mu}}{2}\left[\frac{c_1\sinh\left(\frac{\sqrt{\lambda^2-4\mu}}{2}\xi\right)+c_2\cosh\left(\frac{\sqrt{\lambda^2-4\mu}}{2}\xi\right)}{c_1\cosh\left(\frac{\sqrt{\lambda^2-4\mu}}{2}\xi\right)+c_2\sinh\left(\frac{\sqrt{\lambda^2-4\mu}}{2}\xi\right)}\right]-\frac{\lambda}{2}, & \lambda^2-4\mu>0\\ \frac{\sqrt{4\mu-\lambda^2}}{2}\left[\frac{-c_1\sin\left(\frac{\sqrt{4\mu-\lambda^2}}{2}\xi\right)+c_2\cos\left(\frac{\sqrt{4\mu-\lambda^2}}{2}\xi\right)}{c_1\cos\left(\frac{\sqrt{4\mu-\lambda^2}}{2}\xi\right)+c_2\sin\left(\frac{\sqrt{4\mu-\lambda^2}}{2}\xi\right)}\right]-\frac{\lambda}{2}, & \lambda^2-4\mu<0\\ \frac{c_1}{c_1\xi+c_2}-\frac{\lambda}{2}, & \lambda^2-4\mu=0\end{cases} \quad (9)$$

where c_1 and c_2 are arbitrary constants. Peng (2009)has simplified Equations (9) and has shown that:

(1) If $\lambda^2-4\mu>0$ and $|c_1|>|c_2|$, we have:

$$G'/G=-\frac{\lambda}{2}+\frac{\sqrt{\lambda^2-4\mu}}{2}\tanh\left(\frac{\sqrt{\lambda^2-4\mu}}{2}\xi+\psi_1\,\mathrm{sgn}(c_1c_2)\right) \quad (10)$$

where $\psi_1=\tanh^{-1}\left(\frac{|c_2|}{|c_1|}\right)$ and $\mathrm{sgn}(c_1c_2)$ is the sign function:

(2) If $\lambda^2-4\mu>0$ and $|c_2|>|c_1|\neq 0$, we have:

$$G'/G=-\frac{\lambda}{2}+\frac{\sqrt{\lambda^2-4\mu}}{2}\coth\left(\frac{\sqrt{\lambda^2-4\mu}}{2}\xi+\psi_2\,\mathrm{sgn}(c_1c_2)\right) \quad (11)$$

Where $\psi_2=\tanh^{-1}\left(\frac{|c_1|}{|c_2|}\right)$.

(3) If $\lambda^2-4\mu>0$ and $|c_2|>|c_1|=0$, we have:

$$G'/G=-\frac{\lambda}{2}+\frac{\sqrt{\lambda^2-4\mu}}{2}\coth\left(\frac{\sqrt{\lambda^2-4\mu}}{2}\xi\right). \quad (12)$$

(4) If $\lambda^2-4\mu>0$ and $|c_1|=|c_2|$, we have:

$$G'/G=-\frac{\lambda}{2}\pm\frac{\sqrt{\lambda^2-4\mu}}{2}, \text{ if } c_1=\pm c_2. \quad (13)$$

(5) If $\lambda^2-4\mu<0$, we have:

$$G'/G=-\frac{\lambda}{2}-\frac{\sqrt{4\mu-\lambda^2}}{2}\tan\left(\frac{\sqrt{4\mu-\lambda^2}}{2}\xi-\psi_3\right) \quad (14)$$

where $\psi_3=\tan^{-1}\left(\frac{c_2}{c_1}\right)$.

Step 6

We substitute the values of a_i,λ,μ,c and (G'/G) given by Equations (10) to (14) into Equations (5) to find the exact solutions (including hyperbolic, trigonometric

and rational solutions) of Equation (2).

Description of the $\exp\left(-\phi\left(\xi\right)\right)$-expansion method and its connection with the $\left(G'/G\right)$-expansion method

First of all, let us now explain the connection between these two methods as follows: With reference to the articles [Zhao and Li (2014); Khan and Akbar, 2013; Harun-Or-Roshid and Rahman, 2014], we see that the description of the $\exp\left(-\phi\left(\xi\right)\right)$-expansion method follows directly from the $\left(G'/G\right)$-expansion method described previously if we replace $\left(G'/G\right)$ by $\exp\left(-\phi\left(\xi\right)\right)$. That is, if we use the transformation:

$$\left(G'/G\right)=\exp\left(-\phi\left(\xi\right)\right) \quad (15)$$

then the $\left(G'/G\right)$-expansion (Equation 5) along with Equation (6) can be reduced to the $\exp\left(-\phi\left(\xi\right)\right)$-expansion

$$u\left(\xi\right)=\sum_{i=0}^{N}a_i\left[\exp\left(-\phi\left(\xi\right)\right)\right]^i \quad (16)$$

where $\phi\left(\xi\right)$ is the solution of the nonlinear auxiliary ODE:

$$\phi'\left(\xi\right)=\exp\left(-\phi\left(\xi\right)\right)+\mu\exp\left(\phi\left(\xi\right)\right)+\lambda \quad (17)$$

Note that this connection is new and not discussed in the articles [Zhao and Li (2014); Khan and Akbar, 2013; Harun-Or-Roshid and Rahman, 2014] or elsewhere. Now, the main steps of the $\exp\left(-\phi\left(\xi\right)\right)$-expansion method follows directly from the Steps 3 to 6 of the $\left(G'/G\right)$-expansion method described previously, with replacing $\left(G'/G\right)$ by $\exp\left(-\phi\left(\xi\right)\right)$, where:

$$\phi\left(\xi\right)=-\ln\left(G'/G\right) \quad (18)$$

Substituting Equations (10) to (14) into Equation (18), we have the following solutions of Equation (17) which are new and not obtained in the articles (Zhao and Li, 2014; Khan and Akbar, 2013; Harun-Or-Roshid and Rahman, 2014) or elsewhere:

(a) If $\lambda^2-4\mu>0$ and $\left|c_1\right|>\left|c_2\right|$, we have:

$$\phi\left(\xi\right)=-\ln\left[-\frac{\lambda}{2}+\frac{\sqrt{\lambda^2-4\mu}}{2}\tanh\left(\frac{\sqrt{\lambda^2-4\mu}}{2}\xi+\psi_1\,\mathrm{sgn}(c_1c_2)\right)\right] \quad (19)$$

(b) If $\lambda^2-4\mu>0$ and $\left|c_2\right|>\left|c_1\right|\neq 0$, we have:

$$\phi\left(\xi\right)=-\ln\left[-\frac{\lambda}{2}+\frac{\sqrt{\lambda^2-4\mu}}{2}\coth\left(\frac{\sqrt{\lambda^2-4\mu}}{2}\xi+\psi_2\,\mathrm{sgn}(c_1c_2)\right)\right] \quad (20)$$

(c) If $\lambda^2-4\mu>0$ and $\left|c_2\right|>\left|c_1\right|=0$, we have:

$$\phi\left(\xi\right)=-\ln\left[-\frac{\lambda}{2}+\frac{\sqrt{\lambda^2-4\mu}}{2}\coth\left(\frac{\sqrt{\lambda^2-4\mu}}{2}\xi\right)\right] \quad (21)$$

(d) If $\lambda^2-4\mu>0$ and $\left|c_1\right|=\left|c_2\right|$, we have:

$$\phi\left(\xi\right)=-\ln\left[-\frac{\lambda}{2}\pm\frac{\sqrt{\lambda^2-4\mu}}{2}\right]\text{if}c_1=\pm c_2 \quad (22)$$

(e) If $\lambda^2-4\mu<0$, we have:

$$\phi\left(\xi\right)=-\ln\left[-\frac{\lambda}{2}-\frac{\sqrt{4\mu-\lambda^2}}{2}\tan\left(\frac{\sqrt{4\mu-\lambda^2}}{2}\xi-\psi_3\right)\right] \quad (23)$$

(f) If $\lambda^2-4\mu=0$, we have

$$\phi\left(\xi\right)=-\ln\left[\frac{2c_1-\lambda(c_1\xi+c_2)}{2(c_1\xi+c_2)}\right] \quad (24)$$

On the other hand, the authors [Zhao and Li (2014); Khan and Akbar, 2013; Harun-Or-Roshid and Rahman, 2014] applied the $\exp\left(-\phi\left(\xi\right)\right)$-expansion method (Equation 16) and (Equation 17) to some nonlinear PDEs, where $\phi\left(\xi\right)$ is the solution of the nonlinear ODE (17). On using the separation of variables in Equation (17) and integrating where C is the constant of integration, we have the following solutions of Equation (17) which are listed in Zhao and Li (2014); Khan and Akbar (2013) and Harun-Or-Roshid and Rahman (2014):

.

(a) If $\lambda^2-4\mu>0$, $\mu\neq 0,\lambda\neq 0$, we have:

$$\phi(\xi)=\ln\left[\frac{-\sqrt{\lambda^2-4\mu}\tanh\left(\frac{\sqrt{\lambda^2-4\mu}}{2}(\xi+C)\right)-\lambda}{2\mu}\right] \quad (25)$$

(b) If $\lambda^2-4\mu>0$, $\mu=0,\lambda\neq 0$, we have

$$\phi(\xi)=-\ln\left[\frac{\lambda}{\exp(\lambda(\xi+C))-1}\right] \quad (26)$$

(c) If $\lambda^2-4\mu=0$, $\lambda\neq 0$, $\mu\neq 0$, we have:

$$\phi(\xi)=\ln\left[-\frac{2\lambda(\xi+C)+4}{\lambda^2(\xi+C)}\right]. \quad (27)$$

(d) If $\lambda^2-4\mu=0$, $\lambda=0$, $\mu=0$, we have:

$$\phi(\xi)=\ln(\xi+C). \quad (28)$$

(f) If $\lambda^2-4\mu<0,\mu\neq 0$, we have:

$$\phi(\xi)=\ln\left[\frac{\sqrt{4\mu-\lambda^2}\tan\left(\frac{1}{2}\sqrt{4\mu-\lambda^2}(\xi+C)\right)-\lambda}{2\mu}\right] \quad (29)$$

Subsequently, we will solve Equation (1) by using the (G'/G)-expansion method (Equation 5) along with Equation (6) with the aid of Equation (10) to (14) and by using the $\exp(-\phi(\xi))$-expansion method (Equation 16) along with Equation (17) with the aid of Equations (20) to (24). We will show that these two methods and their results are equivalent.

APPLICATIONS

Here, we determine the exact solutions of Equation (1) by using the two methods described previously, namely the (G'/G)-expansion method and the $\exp(-\phi(\xi))$-expansion method. To this end, we first use the transformation (Zhang et al., 2006):

$$u(z,t)=\psi(\xi)\exp(i\theta) \quad (30)$$

Where

$$\xi=qz-\omega t\ ,\ \theta=kz-ct\ ,\ i=\sqrt{-1} \quad (31)$$

and $\psi(\xi)$ is a real-valued function, q,ω,k,c are constants to be determined later.

Substituting Equation (30) along with Equation (31) into Equation (1) and separating the real and imaginary parts, we have:

$$\beta_4\omega^4\psi^{(4)}+(12\beta_2\omega^2+12\beta_3\omega^2c-6\beta_4\omega^2c^2)\psi''+(24k-12\beta_2c^2-4\beta_3c^3+\beta_4c^4)\psi -24\gamma_2\psi^3-24\gamma_4\psi^5=0, \quad (32)$$

and

$$(\beta_3\omega^3-\beta_4\omega^3c)\psi'''+(6q-6\beta_2\omega c-3\beta_3\omega c^2+\beta_4\omega c^3)\psi'=0. \quad (33)$$

There are two cases to be considered. The case are as follows:

Case 1

If $(\beta_3\omega^3-\beta_4\omega^3c)\neq 0$

In this case, we differentiate Equation (33) and substitute the result into Equation (32) to get the equation

$$\left[\beta_4\omega^4(6q-6\beta_2\omega c-3\beta_3\omega c^2+\beta_4\omega c^3)-(\beta_3\omega^3-\beta_4\omega^3c)(12\beta_2\omega^2+12\beta_3\omega^2c-6\beta_4\omega^2c^2)\right]\psi'' -(\beta_3\omega^3-\beta_4\omega^3c)\left[(24k-12\beta_2c^2-4\beta_3c^3+\beta_4c^4)\psi-24\gamma_2\psi^3-24\gamma_4\psi^5\right]=0 \quad (34)$$

Balancing ψ'' with ψ^5 in Eq. (34) yields $N=\frac{1}{2}$. Since the balance number N is not integer, then in this case, we use the transformation

$$\psi(\xi)=V^{\frac{1}{2}}(\xi) \quad (35)$$

where $V(\xi)$ is a new function of ξ satisfying the following nonlinear ODE:

$$A(V'^2-2VV'')-4B(24k-12\beta_2c^2-4\beta_3c^3+\beta_4c^4)V^2+96B(\gamma_2V^3+\gamma_4V^4)=0, \quad (36)$$

where $A\neq 0,B\neq 0$ which are given by:

$$A=\omega^3(\beta_3-\beta_4c)(12\beta_2\omega^2+12\beta_3\omega^2c-6\beta_4\omega^2c^2)-\beta_4\omega^4(6q-6\beta_2\omega c-3\beta_3\omega c^2+\beta_4\omega c^3) \quad (37)$$

and

$$B=\omega^3(\beta_3-\beta_4c). \quad (38)$$

Balancing VV'' with V^4 in Equation (36) yields $N=1$. Let us now first apply the (G'/G)-expansion method to find the exact solutions of Equation (36). To this end, we have the formal solution of Equation (36) in the form:

$$V(\xi)=a_0+a_1\left(\frac{G'}{G}\right) \tag{39}$$

where a_0, a_1 are constants to be determined, such that $a_1\neq 0$.

Substituting (39) along with Equation (6) into Equation (36), collecting all coefficients of $\left(\frac{G'}{G}\right)^j$ $(j=0,1,2,3,4)$ and setting them to zero, we have the following system of algebraic equations:

$$\begin{aligned}
&\left(\frac{G'}{G}\right)^4: -3a_1^2(A-32a_1^2B\gamma_4)=0,\\
&\left(\frac{G'}{G}\right)^3: -4a_1\left[A(a_0+a_1\lambda)-24Ba_1^2(\gamma_2+4a_0\gamma_4)\right]=0,\\
&\left(\frac{G'}{G}\right)^2: -a_1\left[A(a_1\lambda^2+2a_1\mu+6a_0\lambda)+4a_1B(24k-12\beta_2c^2-4\beta_3c^3+\beta_4c^4)-288a_0a_1B(\gamma_2+2a_0\gamma_4)\right]=0,\\
&\left(\frac{G'}{G}\right): -2a_0a_1\left[A(\lambda^2+2\mu)+4B(24k-12\beta_2c^2-4\beta_3c^3+\beta_4c^4)-48a_0B(3\gamma_2+4a_0\gamma_4)\right]=0,\\
&\left(\frac{G'}{G}\right)^0: A(a_1^2\mu^2-2a_0a_1\mu\lambda)-4a_0^2B(24k-12\beta_2c^2-4\beta_3c^3+\beta_4c^4)+96a_0^3B(\gamma_2+a_0\gamma_4)=0.
\end{aligned} \tag{40}$$

On solving the above algebraic Equations (40) using the Maple or Mathematica, we have the results:

$$\begin{aligned}
&k=\frac{1}{24}\left(12\beta_2c^2+4\beta_3c^3-\beta_4c^4\right)-\frac{3}{16}\frac{\gamma_2^2}{\gamma_4},\ \mu=0,\ \lambda=3\gamma_2\sqrt{\frac{2B}{A\gamma_4}},\\
&a_0=0,\ a_1=\frac{1}{4}\sqrt{\frac{A}{2B\gamma_4}}.
\end{aligned} \tag{41}$$

where $A\gamma_4/B>0$.

From Equations (30), (35), (39) and (41) we deduce that:

$$u(z,t)=\left[\frac{1}{4}\sqrt{\frac{A}{2B\gamma_4}}\left(\frac{G'}{G}\right)\right]^{\frac{1}{2}}\exp(i\theta), \tag{42}$$

where $A\gamma_4/B>0$.

Substituting the formulas (10) to (14) of $\left(\frac{G'}{G}\right)$ obtained previously, into Equation (42) we see that the Schrödinger Equation (1) has the following families of exact solutions:

If $\lambda^2-4\mu>0$ and $|c_1|>|c_2|$, then we have the solution:

$$u(z,t)=\sqrt{\frac{-3\gamma_2}{4\gamma_4}}\left[\frac{1}{2}\mp\frac{1}{2}\tanh\left(\frac{3\gamma_2}{2}\sqrt{\frac{2B}{A\gamma_4}}\xi+\psi_1\operatorname{sgn}(c_1c_2)\right)\right]^{\frac{1}{2}}\exp(i\theta), \tag{43}$$

where $\psi_1=\tanh^{-1}\left(\frac{|c_2|}{|c_1|}\right)$, $A\gamma_2/B<0$ and $A\gamma_4/B>0$.

If $\lambda^2-4\mu>0$ and $|c_2|>|c_1|\neq 0$, then we have the solution:

$$u(z,t)=\sqrt{\frac{-3\gamma_2}{4\gamma_4}}\left[\frac{1}{2}\mp\frac{1}{2}\coth\left(\frac{3\gamma_2}{2}\sqrt{\frac{2B}{A\gamma_4}}\xi+\psi_2\operatorname{sgn}(c_1c_2)\right)\right]^{\frac{1}{2}}\exp(i\theta), \tag{44}$$

where $\psi_2=\tanh^{-1}\left(\frac{|c_1|}{|c_2|}\right)$, $A\gamma_2/B<0$ and $A\gamma_4/B>0$.

If $\lambda^2-4\mu>0$ and $|c_2|>|c_1|=0$, then we have the solution:

$$u(z,t)=\sqrt{\frac{-3\gamma_2}{4\gamma_4}}\left[\frac{1}{2}\mp\frac{1}{2}\coth\left(\frac{3\gamma_2}{2}\sqrt{\frac{2B}{A\gamma_4}}\xi\right)\right]^{\frac{1}{2}}\exp(i\theta), \tag{45}$$

provided $A\gamma_2/B<0$ and $A\gamma_4/B>0$.

If $\lambda^2-4\mu>0$ and $|c_1|=|c_2|$, then we have the solution:

$$u(z,t)=\sqrt{\frac{-3\gamma_2}{4\gamma_4}}\exp(i\theta) \tag{46}$$

provided $\gamma_2/\gamma_4<0$.

If $\lambda^2-4\mu<0$, then we have not any real solution:

If $\lambda^2-4\mu=0$, then we deduce from Equation (9) that the rational solution has the form:

$$u(z,t)=\left[\frac{1}{4}\sqrt{\frac{A}{2B\gamma_4}}\left(\frac{c_1}{c_1\xi+c_2}\right)\right]^{\frac{1}{2}}\exp(i\theta), \tag{47}$$

where $A\gamma_4/B>0$.

Let us now apply the $\exp(-\phi(\xi))$-expansion method to find the solutions of Equation (36). To this end, we see that the formal solution of Equation (46) has the form:

$$V(\xi) = a_0 + a_1 \exp(-\phi(\xi)) \tag{48}$$

where a_0 , a_1 are constants to be determined, such that $a_1 \neq 0$. Substituting Equation (48) along with Equation (17) into Equation (36), collecting the coefficients of $\left[\exp(-\phi(\xi))\right]^j$, $(j = 0,1,2,3,4)$ and setting them to zero, we have the following system of algebraic equations:

$$e^{-4\phi} : -3a_1^2(A - 32a_1^2 B\gamma_4) = 0,$$
$$e^{-3\phi} : -4a_1\left[A(a_0 + a_1\lambda) - 24Ba_1^2(\gamma_2 + 4a_0\gamma_4)\right] = 0,$$

$$e^{-2\phi} : -a_1\left[A(a_1\lambda^2 + 2a_1\mu + 6a_0\lambda) + 4a_1B(24k - 12\beta_2c^2 - 4\beta_3c^3 + \beta_4c^4) - 288a_0a_1B(\gamma_2 + 2a_0\gamma_4)\right] = 0, \tag{49}$$

$$e^{-\phi} : -2a_0a_1\left[A(\lambda^2 + 2\mu) + 4B(24k - 12\beta_2c^2 - 4\beta_3c^3 + \beta_4c^4) - 48a_0B(3\gamma_2 + 4a_0\gamma_4)\right] = 0,$$

$$e^0 : A(a_1^2\mu^2 - 2a_0a_1\mu\lambda) - 4a_0^2B(24k - 12\beta_2c^2 - 4\beta_3c^3 + \beta_4c^4) + 96a_0^3B(\gamma_2 + a_0\gamma_4) = 0.$$

Note that the algebraic equations (49) have the same form as (40) .Therefore, the solutions of the system (49) have the same forms as (41).

From Equations (30), (35), (48) and (41) we deduce that:

$$u(z,t) = \left[\frac{1}{4}\sqrt{\frac{A}{2B\gamma_4}}\exp(-\phi(\xi))\right]^{\frac{1}{2}}\exp(i\theta) \tag{50}$$

where $A\gamma_4 / B > 0$.

Substituting the formulas (19) to (24) of $\exp(-\phi(\xi))$ obtained previously, into (50), we have the same forms as (43) to (47). This proves that the (G'/G)-expansion method is equivalent to $\exp(-\phi(\xi))$-expansion method. Furthermore, substituting (26) into (50) we have the exact solution

$$u(z,t) = \sqrt{\frac{3\gamma_2}{4\gamma_4}}\left[\frac{1}{\exp\left(3\gamma_2\sqrt{\frac{2B}{A\gamma_4}}(\xi + C)\right) - 1}\right]^{\frac{1}{2}}\exp(i\theta) \tag{51}$$

where $A\gamma_4 / B > 0$, $A\gamma_2 / B > 0$.

Case 2

If $(\beta_3\omega^3 - \beta_4\omega^3 c) = 0$

In this case, we have $c = \frac{\beta_3}{\beta_4}, \omega \neq 0$ and from Equation (33) we get:

$$q = \frac{\beta_3\omega}{3\beta_4^2}\left(\beta_3^2 + 3\beta_2\beta_4\right) \tag{52}$$

Consequently, Equation (32) reduces to the equation:

$$\beta_4\omega^4\psi^{(4)}(\xi) + \left(12\beta_2\omega^2 + 6\omega^2\frac{\beta_3^2}{\beta_4}\right)\psi''(\xi) + \left(24k - 12\frac{\beta_2\beta_3^2}{\beta_4^2} - \frac{3\beta_3^4}{\beta_4^3}\right)\psi(\xi) \tag{53}$$
$$-24\gamma_2\psi^3(\xi) - 24\gamma_4\psi^5(\xi) = 0.$$

Balancing $\psi^{(4)}$ with ψ^5 in Equation (53) yields $N = 1$. Let us now apply the $\left(\frac{G'}{G}\right)$-expansion method to Equation (53). To this end, we have the formal solution:

$$\psi(\xi) = b_0 + b_1\left(\frac{G'}{G}\right) \tag{54}$$

where b_0 , b_1 are constants to be determined and $b_1 \neq 0$.

Substituting (54) along with Equation (6) into Equation (53), collecting all the coefficients of $\left[\frac{G'(\xi)}{G(\xi)}\right]^j$, $(j = 0,1,2,3,4)$ and setting them to zero, we have the following system of algebraic equations:

$$\left(\frac{G'}{G}\right)^5 : 24b_1(\beta_4\omega^4 - \gamma_4 b_1^4) = 0,$$
$$\left(\frac{G'}{G}\right)^4 : 60b_1\left[\lambda\beta_4\omega^4 - 2b_0b_1^3\gamma_4\right] = 0,$$

$$\left(\frac{G'}{G}\right)^3 : \beta_4\omega^4\left(40b_1\mu + 50b_1\lambda^2\right) + 2b_1\left(12\beta_2\omega^2 + 6\omega^2\frac{\beta_3^2}{\beta_4}\right) - 24b_1^3\gamma_2 - 240b_0^2b_1^3\gamma_4 = 0, \tag{55}$$

$$\left(\frac{G'}{G}\right)^2 : \beta_4\omega^4\left(60b_1\mu\lambda + 15b_1\lambda^3\right) + 3b_1\lambda\left(12\beta_2\omega^2 + 6\omega^2\frac{\beta_3^2}{\beta_4}\right) - 72b_0b_1^2\gamma_2 - 240b_0^3b_1^2\gamma_4 = 0,$$

$$\left(\frac{G'}{G}\right) : \beta_4\omega^4\left(16b_1\mu^2 + 22b_1\mu\lambda^2 + b_1\lambda^4\right) + b_1\left(\lambda^2 + 2\mu\right)\left(12\beta_2\omega^2 + \frac{6\omega^2\beta_3^2}{\beta_4}\right)$$
$$+b_1\left(24k - \frac{12\beta_2\beta_3^2}{\beta_4^2} - \frac{3\beta_3^4}{\beta_4^3}\right) - 72b_0^2b_1\gamma_2 - 120b_0^4b_1\gamma_4 = 0,$$

$$\left(\frac{G'}{G}\right)^0 : \beta_4\omega^4\left(8b_1\mu^2\lambda + b_1\lambda^3\mu\right) + b_1\mu\lambda\left(12\beta_2\omega^2 + 6\omega^2\frac{\beta_3^2}{\beta_4}\right)$$
$$+b_0\left(24k - \frac{12\beta_2\beta_3^2}{\beta_4^2} - \frac{3\beta_3^4}{\beta_4^3}\right) - 24b_0^3\gamma_2 - 24b_0^5\gamma_4 = 0.$$

On solving the above algebraic equations (55) by Maple or Mathematica, we have the results:

$$b_0 = \frac{\lambda\omega}{2}\left(\frac{\beta_4}{\gamma_4}\right)^{\frac{1}{4}}, b_1^2 = \omega^2\left(\frac{\beta_4}{\gamma_4}\right)^{\frac{1}{2}}, \mu = \frac{1}{\omega^2}\left(\frac{3}{5}\frac{\gamma_2}{\beta_4}\sqrt{\frac{\beta_4}{\gamma_4}} + \frac{1}{4}\omega^2\lambda^2 - \frac{3}{5}\frac{\beta_2}{\beta_4} - \frac{3}{10}\frac{\beta_3^2}{\beta_4^2}\right) \quad (56)$$
$$, k = -\frac{1}{200}\left(24\frac{\gamma_2\beta_2}{\beta_4}\sqrt{\frac{\beta_4}{\gamma_4}} + 12\frac{\beta_3^2\gamma_2}{\beta_4^2}\sqrt{\frac{\beta_4}{\gamma_4}} - 72\frac{\beta_2^2}{\beta_4} + 48\frac{\gamma_2^2}{\gamma_4} - 43\frac{\beta_3^4}{\beta_4^3} - 172\frac{\beta_2\beta_3^2}{\beta_4^2}\right)$$

where $\beta_4 / \gamma_4 > 0$.

From Equation (30), (54) and (56) we deduce that:

$$u(z,t) = \left[\pm\omega\left(\frac{\beta_4}{\gamma_4}\right)^{\frac{1}{4}}\left[\frac{\lambda}{2} + \left(\frac{G'}{G}\right)\right]\right]\exp(i\theta) \quad (57)$$

where $\frac{\beta_4}{\gamma_4} > 0$.

Substituting the formulas (10) to (14) of $\left(\frac{G'}{G}\right)$ obtained into (57), we have the following exact solutions of Equation (1):

If $\lambda^2 - 4\mu > 0$ and $|c_1| > |c_2|$, we have:

$$u(z,t) = \left[\frac{1}{2}\left(\frac{\beta_4}{\gamma_4}\right)^{\frac{1}{4}}\sqrt{\frac{12}{5}\frac{\beta_2}{\beta_4} + \frac{6}{5}\frac{\beta_3^2}{\beta_4^2} - \frac{12}{5}\frac{\gamma_2}{\beta_4}\sqrt{\frac{\beta_4}{\gamma_4}}}\tanh\left(\frac{1}{2}\sqrt{\frac{12}{5}\frac{\beta_2}{\beta_4} + \frac{6}{5}\frac{\beta_3^2}{\beta_4^2} - \frac{12}{5}\frac{\gamma_2}{\beta_4}\sqrt{\frac{\beta_4}{\gamma_4}}}\xi + \psi_1\,\mathrm{sgn}(c_1c_2)\right)\right]\exp(i\theta) \quad (58)$$

where $\psi_1 = \tanh^{-1}\left(\frac{|c_2|}{|c_1|}\right)$

If $\lambda^2 - 4\mu > 0$ and $|c_2| > |c_1| \neq 0$, we have:

$$u(z,t) = \left[\frac{1}{2}\left(\frac{\beta_4}{\gamma_4}\right)^{\frac{1}{4}}\sqrt{\frac{12}{5}\frac{\beta_2}{\beta_4} + \frac{6}{5}\frac{\beta_3^2}{\beta_4^2} - \frac{12}{5}\frac{\gamma_2}{\beta_4}\sqrt{\frac{\beta_4}{\gamma_4}}}\coth\left(\frac{1}{2}\sqrt{\frac{12}{5}\frac{\beta_2}{\beta_4} + \frac{6}{5}\frac{\beta_3^2}{\beta_4^2} - \frac{12}{5}\frac{\gamma_2}{\beta_4}\sqrt{\frac{\beta_4}{\gamma_4}}}\xi + \psi_2\,\mathrm{sgn}(c_1c_2)\right)\right]\exp(i\theta) \quad (59)$$

where $\psi_2 = \tanh^{-1}\left(\frac{|c_1|}{|c_2|}\right)$,

If $\lambda^2 - 4\mu > 0$ and $|c_2| > |c_1| = 0$, we have:

$$u(z,t) = \left[\frac{1}{2}\left(\frac{\beta_4}{\gamma_4}\right)^{\frac{1}{4}}\sqrt{\frac{12}{5}\frac{\beta_2}{\beta_4} + \frac{6}{5}\frac{\beta_3^2}{\beta_4^2} - \frac{12}{5}\frac{\gamma_2}{\beta_4}\sqrt{\frac{\beta_4}{\gamma_4}}}\coth\left(\frac{1}{2}\sqrt{\frac{12}{5}\frac{\beta_2}{\beta_4} + \frac{6}{5}\frac{\beta_3^2}{\beta_4^2} - \frac{12}{5}\frac{\gamma_2}{\beta_4}\sqrt{\frac{\beta_4}{\gamma_4}}}\xi\right)\right]\exp(i\theta) \quad (60)$$

If $\lambda^2 - 4\mu > 0$ and $|c_1| = |c_2|$, we have:

$$u(z,t) = \left[\pm\frac{1}{2}\left(\frac{\beta_4}{\gamma_4}\right)^{\frac{1}{4}}\sqrt{\frac{12}{5}\frac{\beta_2}{\beta_4} + \frac{6}{5}\frac{\beta_3^2}{\beta_4^2} - \frac{12}{5}\frac{\gamma_2}{\beta_4}\sqrt{\frac{\beta_4}{\gamma_4}}}\right]\exp(i\theta) \quad (61)$$

In Equation (58) to (61) we have the conditions $\frac{\beta_4}{\gamma_4} > 0$, $\frac{12}{5}\frac{\beta_2}{\beta_4} + \frac{6}{5}\frac{\beta_3^2}{\beta_4^2} - \frac{12}{5}\frac{\gamma_2}{\beta_4}\sqrt{\frac{\beta_4}{\gamma_4}} > 0$.

If $\lambda^2 - 4\mu < 0$, we have:

$$u(z,t) = \left[-\frac{1}{2}\left(\frac{\beta_4}{\gamma_4}\right)^{\frac{1}{4}}\sqrt{\frac{12}{5}\frac{\gamma_2}{\beta_4}\sqrt{\frac{\beta_4}{\gamma_4}} - \frac{12}{5}\frac{\beta_2}{\beta_4} - \frac{6}{5}\frac{\beta_3^2}{\beta_4^2}}\tan\left(\frac{1}{2}\sqrt{\frac{12}{5}\frac{\gamma_2}{\beta_4}\sqrt{\frac{\beta_4}{\gamma_4}} - \frac{12}{5}\frac{\beta_2}{\beta_4} - \frac{6}{5}\frac{\beta_3^2}{\beta_4^2}}\xi - \psi_3\right)\right]\exp(i\theta) \quad (62)$$

where $\psi_3 = \tan^{-1}\left(\frac{c_2}{c_1}\right)$, $\frac{\beta_4}{\gamma_4} > 0$, $\frac{12}{5}\frac{\gamma_2}{\beta_4}\sqrt{\frac{\beta_4}{\gamma_4}} - \frac{12}{5}\frac{\beta_2}{\beta_4} - \frac{6}{5}\frac{\beta_3^2}{\beta_4^2} > 0$.

If $\lambda^2 - 4\mu = 0$, we have from (9) the solution:

$$u(z,t) = \left[\omega\left(\frac{\beta_4}{\gamma_4}\right)^{\frac{1}{4}}\left[\frac{c_1}{c_1\xi + c_2}\right]\right]\exp(i\theta) \quad (63)$$

where $\frac{\beta_4}{\gamma_4} > 0$.

Let us now apply the $\exp(-\phi(\xi))$-expansion method to Equation (53). To this end, we have the formal solution:

$$\psi(\xi) = b_0 + b_1\exp(-\phi(\xi)) \quad (64)$$

where b_0, b_1 are constants to be determined, such that $b_1 \neq 0$. Substituting (64) along with Equation (17) into Equation (53), collecting the coefficients of $\left[\exp(-\phi(\xi))\right]^j$, $(j = 0,1,2,3,4)$ and setting them to zero, we have the following system of algebraic

equations:

$$e^{-5\phi}: 24b_1(\beta_4\omega^4-\gamma_4 b_1^4)=0,$$
$$e^{-4\phi}: 60b_1\left[\lambda\beta_4\omega^4-2b_0b_1^3\gamma_4\right]=0,$$
$$e^{-3\phi}: \beta_4\omega^4\left(40b_1\mu+50b_1\lambda^2\right)+2b_1\left(12\beta_2\omega^2+6\omega^2\frac{\beta_3^2}{\beta_4}\right)-24b_1^3\gamma_2-240b_0^2b_1^3\gamma_4=0, \quad (65)$$
$$e^{-2\phi}: \beta_4\omega^4\left(60b_1\mu\lambda+15b_1\lambda^3\right)+3b_1\lambda\left(12\beta_2\omega^2+6\omega^2\frac{\beta_3^2}{\beta_4}\right)-72b_0b_1^2\gamma_2-240b_0^3b_1^2\gamma_4=0,$$
$$e^{-\phi}: \beta_4\omega^4\left(16b_1\mu^2+22b_1\mu\lambda^2+b_1\lambda^4\right)+b_1\left(\lambda^2+2\mu\right)\left(12\beta_2\omega^2+\frac{6\omega^2\beta_3^2}{\beta_4}\right)$$
$$+b_1\left(24k-\frac{12\beta_2\beta_3^2}{\beta_4^2}-\frac{3\beta_3^4}{\beta_4^3}\right)-72b_0^2b_1\gamma_2-120b_0^4b_1\gamma_4=0,$$
$$e^{0}: \beta_4\omega^4\left(8b_1\mu^2\lambda+b_1\lambda^3\mu\right)+b_1\mu\lambda\left(12\beta_2\omega^2+6\omega^2\frac{\beta_3^2}{\beta_4}\right)$$
$$+b_0\left(24k-\frac{12\beta_2\beta_3^2}{\beta_4^2}-\frac{3\beta_3^4}{\beta_4^3}\right)-24b_0^3\gamma_2-24b_0^5\gamma_4=0.$$

Note that the algebraic Equations (65) have the same forms as Equation (55). Therefore, the solutions of the system Equation (65) have the same forms as Equation (56).

From Equations (30), (64) and (56) we deduce that:

$$u(z,t)=\left[\pm\omega\left(\frac{\beta_4}{\gamma_4}\right)^{\frac{1}{4}}\left[\frac{\lambda}{2}+\exp\left(-\phi(\xi)\right)\right]\right]\exp(i\theta), \quad (66)$$

where $\frac{\beta_4}{\gamma_4}>0$.

Substituting the formulas (19) to (24) of $\left(\exp\left(-\phi(\xi)\right)\right)$ into Equation (66), we have the same solutions as Equations (58) to (63). This proves that the (G'/G)-expansion method is equivalent to the $\left(\exp\left(-\phi(\xi)\right)\right)$-expansion method.

Furthermore, substituting (25) to (29) into (66) we have the new exact solutions:

If $\lambda^2-4\mu>0$, $\mu\neq 0$, we have:

$$u(z,t)= \quad (67)$$
$$\omega\left(\frac{\beta_4}{\gamma_4}\right)^{\frac{1}{4}}\left[\frac{\lambda}{2}-\frac{\left(\frac{\lambda^2}{2}-\frac{6}{5}\frac{\beta_2}{\omega^2\beta_4}-\frac{3}{5}\frac{\beta_3^2}{\omega^2\beta_4^2}+\frac{6}{5}\frac{\gamma_2}{\omega^2\beta_4}\sqrt{\frac{\beta_4}{\gamma_4}}\right)}{\sqrt{\frac{12}{5}\frac{\beta_2}{\beta_4\omega^2}+\frac{6}{5}\frac{\beta_3^2}{\beta_4^2\omega^2}-\frac{12}{5}\frac{\gamma_2}{\beta_4\omega^2}\sqrt{\frac{\beta_4}{\gamma_4}}}\tanh\left(\frac{1}{2}\sqrt{\frac{12}{5}\frac{\beta_2}{\beta_4\omega^2}+\frac{6}{5}\frac{\beta_3^2}{\beta_4^2\omega^2}-\frac{12}{5}\frac{\gamma_2}{\beta_4\omega^2}\sqrt{\frac{\beta_4}{\gamma_4}}}(\xi+C)+\lambda\right)}\right]\exp(i\theta)$$

If $\lambda^2-4\mu>0$, $\mu=0,\lambda\neq 0$

$$u(z,t)=\frac{1}{2}\left(\frac{\beta_4}{\gamma_4}\right)^{\frac{1}{4}}\left[\sqrt{\frac{12}{5}\frac{\beta_2}{\beta_4}+\frac{6}{5}\frac{\beta_3^2}{\beta_4^2}-\frac{12}{5}\frac{\gamma_2}{\beta_4}\sqrt{\frac{\beta_4}{\gamma_4}}}\right] \quad (68)$$
$$*\left[1+\frac{2}{\exp\left(\sqrt{\frac{12}{5}\frac{\beta_2}{\beta_4\omega^2}+\frac{6}{5}\frac{\beta_3^2}{\beta_4^2\omega^2}-\frac{12}{5}\frac{\gamma_2}{\beta_4\omega^2}\sqrt{\frac{\beta_4}{\gamma_4}}}(\xi+C)\right)-1}\right]\exp(i\theta)$$

In Equation (67) and (68) we have the conditions $\frac{\beta_4}{\gamma_4}>0$,

$\frac{12}{5}\frac{\beta_2}{\beta_4}+\frac{6}{5}\frac{\beta_3^2}{\beta_4^2}-\frac{12}{5}\frac{\gamma_2}{\beta_4}\sqrt{\frac{\beta_4}{\gamma_4}}>0$.

If $\lambda^2-4\mu=0$, $\lambda\neq 0$, $\mu\neq 0$, we have:

$$u(z,t)=\lambda\omega\left(\frac{\beta_4}{\gamma_4}\right)^{\frac{1}{4}}\left[\frac{1}{\left(\lambda(\xi+C)\right)+2}\right]\exp(i\theta) \quad (69)$$

where $\frac{\beta_4}{\gamma_4}>0$.

If $\lambda^2-4\mu=0$, $\lambda=0$, $\mu=0$, we have:

$$u(z,t)=\omega\left(\frac{\beta_4}{\gamma_4}\right)^{\frac{1}{4}}\frac{1}{(\xi+C)}\exp(i\theta) \quad (70)$$

where $\frac{\beta_4}{\gamma_4}>0$.

If $\lambda^2-4\mu<0$, we have the solution:

$$u(z,t)= \quad (71)$$
$$\omega\left(\frac{\beta_4}{\gamma_4}\right)^{\frac{1}{4}}\left[\frac{\lambda}{2}+\frac{\left(\frac{\lambda^2}{2}-\frac{6}{5}\frac{\beta_2}{\omega^2\beta_4}-\frac{3}{5}\frac{\beta_3^2}{\omega^2\beta_4^2}+\frac{6}{5}\frac{\gamma_2}{\omega^2\beta_4}\sqrt{\frac{\beta_4}{\gamma_4}}\right)}{\sqrt{\frac{12}{5}\frac{\gamma_2}{\beta_4\omega^2}\sqrt{\frac{\beta_4}{\gamma_4}}-\frac{12}{5}\frac{\beta_2}{\beta_4\omega^2}-\frac{6}{5}\frac{\beta_3^2}{\beta_4^2\omega^2}}\left[\tan\left(\frac{1}{2}\sqrt{\frac{12}{5}\frac{\gamma_2}{\beta_4\omega^2}\sqrt{\frac{\beta_4}{\gamma_4}}-\frac{12}{5}\frac{\beta_2}{\beta_4\omega^2}-\frac{6}{5}\frac{\beta_3^2}{\beta_4^2\omega^2}}(\xi+C)\right)-\lambda\right]}\right]\exp(i\theta)$$

where $\frac{\beta_4}{\gamma_4}>0$ $\frac{12}{5}\frac{\gamma_2}{\beta_4\omega^2}\sqrt{\frac{\beta_4}{\gamma_4}}-\frac{12}{5}\frac{\beta_2}{\beta_4\omega^2}-\frac{6}{5}\frac{\beta_3^2}{\beta_4^2\omega^2}>0$

Finally, we notice that our solutions (43) to (47), (58) to (63) and (67) to (71) of Equation (1) are new and not published elsewhere.

PHYSICAL EXPLANATIONS FOR SOME OF OUR RESULTS

Here, we have presented some graphs for the modulus of the exact solutions (43), (44), (51), (58), (59), (62), (68), (71) constructed by taking suitable values of involved

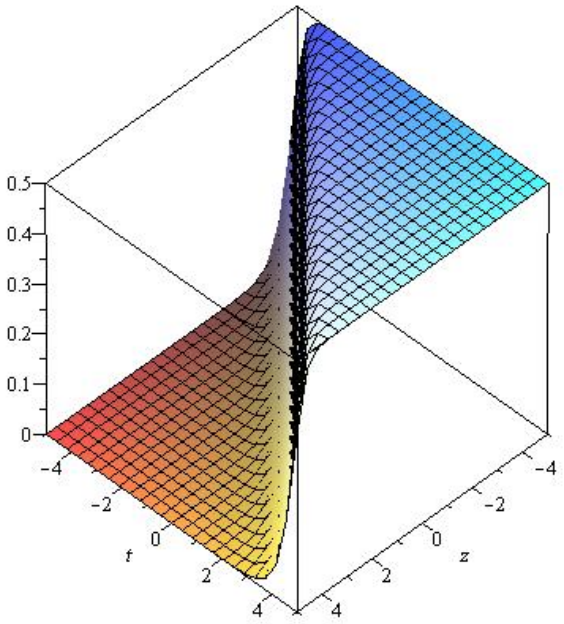

Figure 1. The plot of $\psi(z,t)$ of Equation (43) when $q=2,\omega=2,A=1,B=1,\ \gamma_2=-1,\ \gamma_4=3,c_2=0.$

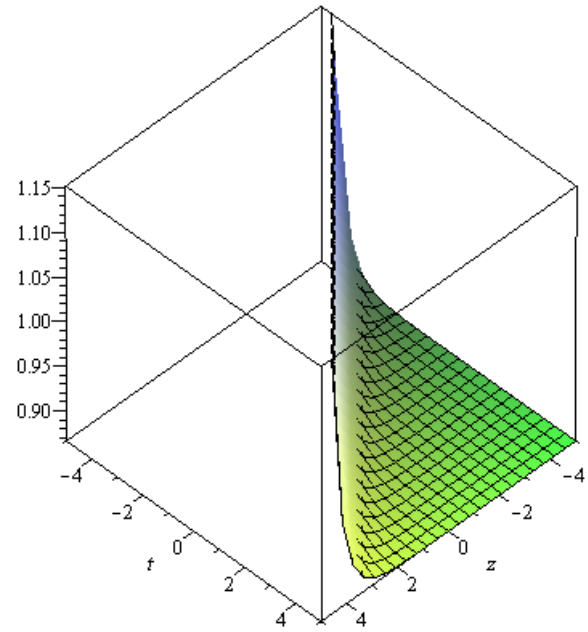

Figure 2. The plot of $\psi(z,t)$ of Equation (44) when $q=1,\omega=1,A=18,B=4,\ \gamma_2=-1,\ \gamma_4=1,c_1=0.$

trigonometric periodic solutions. For more convenience the graphical representations for the modulus of some of

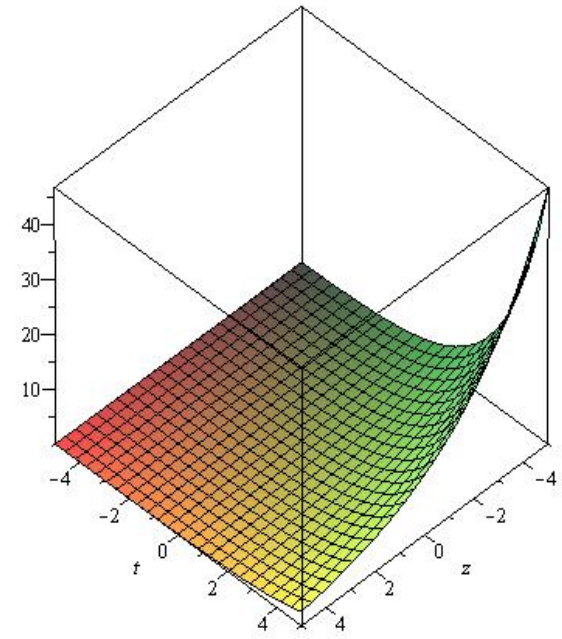

Figure 3. The plot of $\psi(z,t)$ of Equation (51) when $q=1,\omega=1,A=18,B=1,\ \gamma_2=1,\ \gamma_4=3,C=1.$

unknown parameters to visualize the mechanism of the original Equations (1). Some of these solutions are kink solutions, anti- kink-solutions, hyperbolic solutions and these solutions are shown in Figures 1 to 8.

Conclusions

New families of exact solutions including soliton solutions, the trigonometric function solutions and rational function solutions for the higher order dispersive nonlinear Schrödinger Equation (1) have been found using two methods, via the (G'/G)-expansion method and the $\exp(-\phi(\xi))$-expansion method. On comparing between these two methods and between their results, we conclude that the two methods are equivalent. Our results in this paper are new and not published elsewhere. By using the Maple or Mathematica, we have checked that all solutions obtained in this article satisfy the original Equation (1). Finally, our recent paper can be considered to be the first one which shows that the (G'/G)-expansion method and the $\exp(-\phi(\xi))$-expansion method are the same.

Conflict of Interest

The authors have not declared any conflict of interest.

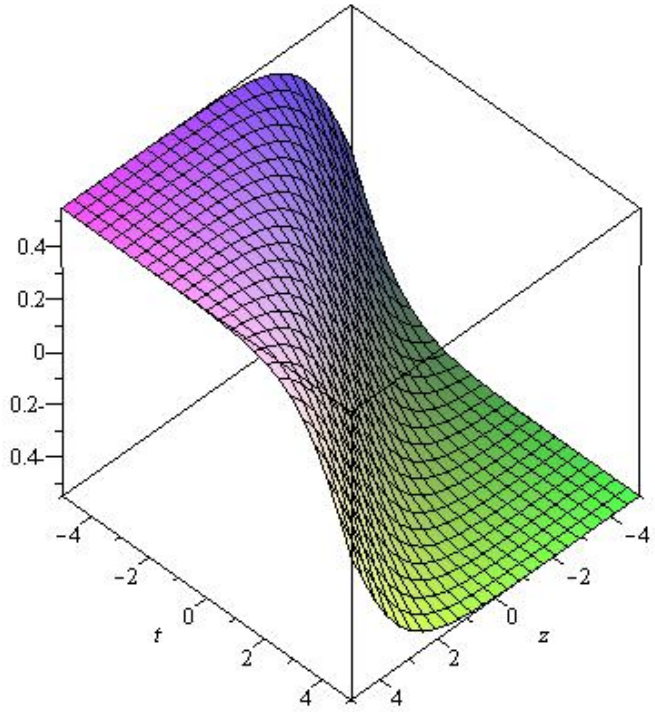

Figure 4. The plot of $\psi(z,t)$ of Equation (58) when $q=1,\omega=1,\beta_2=5,\beta_3=1,\beta_4=1,\ \gamma_2=5,\ \gamma_4=1,c_2=0.$

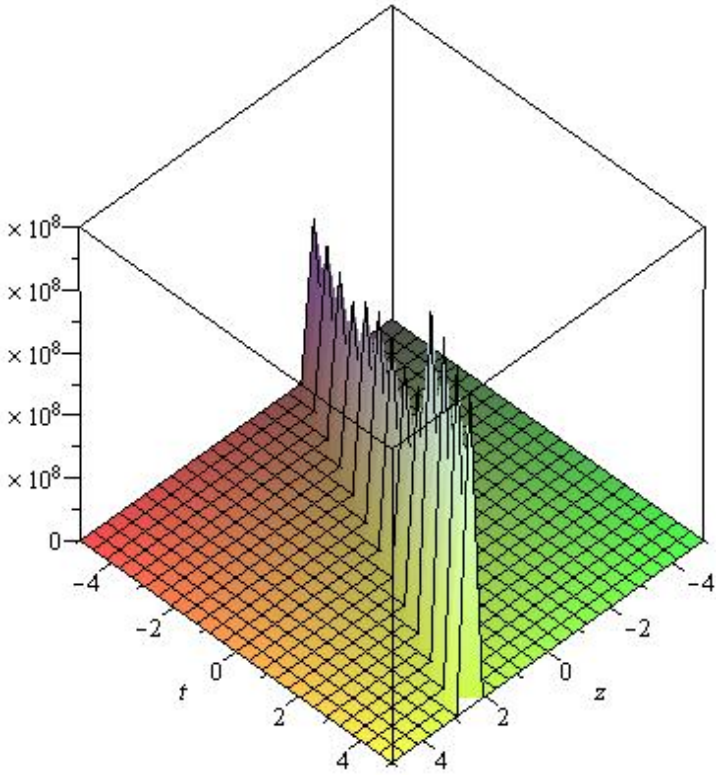

Figure 5. The plot of $\psi(z,t)$ of Equation (59) when $q=2,\omega=1,\beta_2=2,\beta_3=3,\beta_4=1,\ \gamma_2=1,\ \gamma_4=1,c_1=0.$

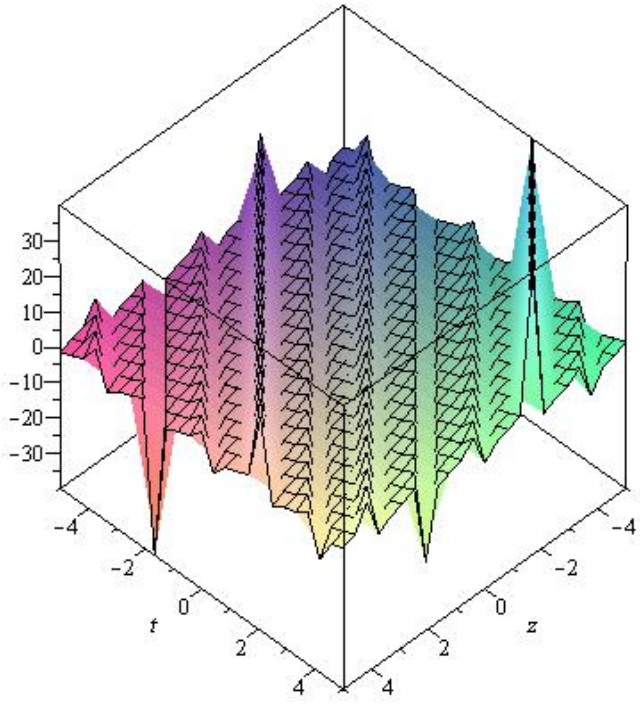

Figure 6. The plot of $\psi(z,t)$ of Equation (62) when $q=1, \omega=1, \beta_2=1, \beta_3=1, \beta_4=1, \gamma_2=6, \gamma_4=1, c_2=0.$

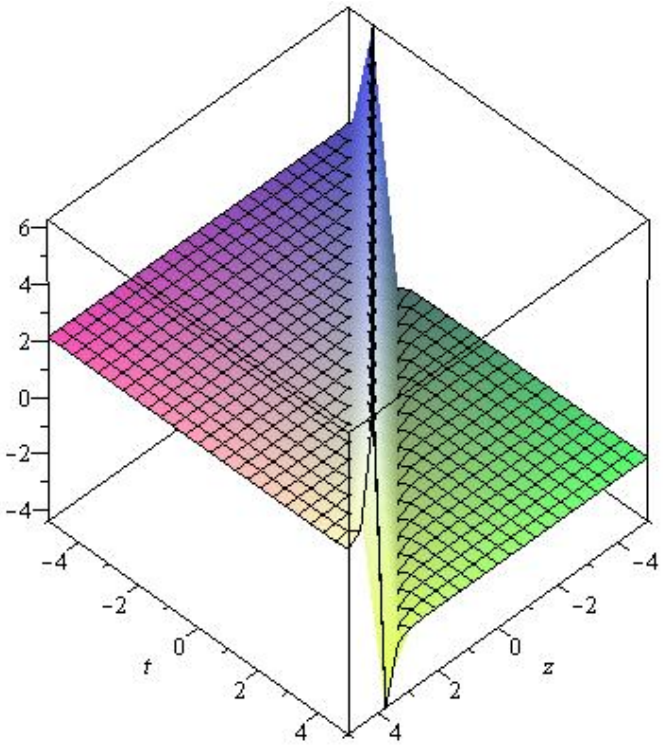

Figure 7. The plot of $\psi(z,t)$ of Equation (68) when $q=1, \omega=1, \beta_2=5, \beta_3=3, \beta_4=1, \gamma_2=2, \gamma_4=1, C=1.$

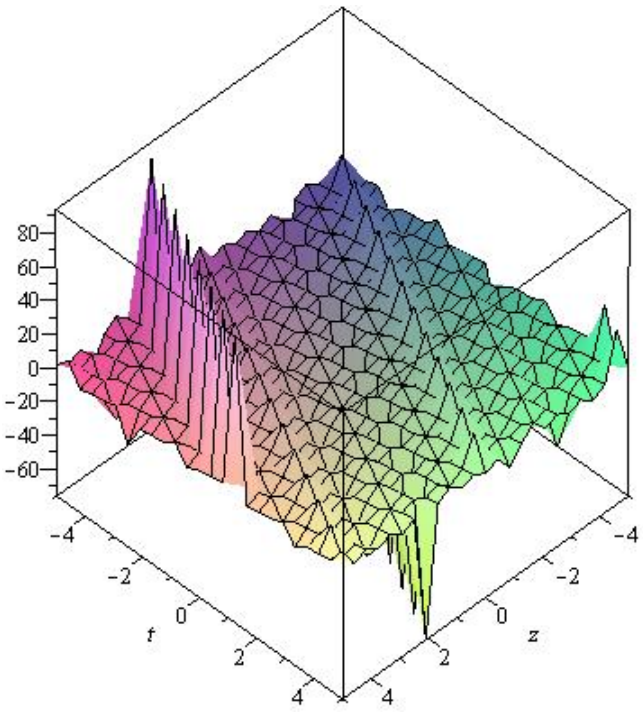

Figure 8. The plot of $\psi(z,t)$ of Equation (71) when $q=2, \omega=1, \beta_2=1, \beta_3=1, \beta_4=1, \gamma_2=6, \gamma_4=1, \lambda=1, C=1.$

REFERENCES

Parkes EJ, Duffy BR (1996). An automated tanh-function method for finding solitary wave solutions to non-linear evolution equation, Comput. Phys. Commun. 98:288-300.

Fan EG (2000). Extended tanh- function method and its applications to nonlinear equations, Phys. Lett. A 277:212-218.

Yan ZY (2001). New explicit travelling wave solutions for two new integrable coupled nonlinear evolution equations, Phys. Lett. A 292:100-106.

Liu SK, Fu ZT (2001). Jacobi elliptic function expansion method and periodic wave solutions of nonlinear wave equations, Phys. Lett. A 289:69-74.

Yan ZY (2003). Abundant families of Jacobi-elliptic function solutions of the (2+1)-dimensional integrable Davey-Stewartson-type equation via a new method, Chaos Solitons Fract.18:299-309.

Fu ZT, Liu SK (2003). A new approach to solve nonlinear wave equations, Commun. Theor. Phys. 39:27-30.

Wang ML (1995). Solitary wave solutions for variant Boussinesq equations, Phys. Lett. A 199:169-172.

Wang ML (1996). Exact solutions for a compound KdV-Burgers equation. Phys. Lett. A 213:279-287.

Wang ML, Zhou YB, Li ZB (1996). Application of a homogeneous balance method to exact solutions of nonlinear equations in mathematical physics, Phys. Lett. A 216:67-75.

Zayed EME, Arnous AH (2012). DNA dynamics studied using the homogeneous balance method. Chin. Phys. Lett. 29:080203-080205.

Wang ML, Zhou YB (2003). The periodic wave solutions for the Klein-Gordon-Schrodinger equations. Phys. Lett. A 318:84-92.

Zhou YB, Wang ML, Miao TD (2004). The periodic wave solution and solitary wave solutions for a class of nonlinear partial differential equations, Phys. Lett. A 323:77-88.

Wang ML, Li XZ (2005).Extended F-expansion method and periodic wave solutions for the generalized Zakharov equations, Phys. Lett. A 343:48-54.

Wang ML, Li XZ (2005). Applications of F-expansion to periodic wave solutions for a new Hamiltonian amplitude equation, Chaos Soliton Fract. 24:1257-1268.

Zhang JL, Wang ML, Li XZ (2006). The subsidiary ordinary differential equations and the exact solutions the higher order dispersive nonlinear Schrodinger equation. Phys. Lett. A 357:188-195.

Wang ML, Li XZ, Zhang JL (2007). Various exact solutions thenonlinear Schrödinger equation with two nonlinear terms, Chaos Soliton Fract. 31:594-601.

Li XZ, Wang ML (2007). A sub-ODE method for finding exact solutions of a generalized KdV and mKdV equation with high-order nonlinear terms, Phys.Lett. A 361:115-118.

Wang ML, Li XZ, Zhang JL (2007). Sub-ODE method and solitary wave solutions for higher order nonlinear Schrödinger equation, Phys. Lett. A, 363:96-101.

Yomba E (2007). The modified extended Fan sub-equation method and its application to the (2+1)-dimensional Broer-Kaup-Kupershmidt equation, Chaos Soliton Fract. 27:187-196.

Li XY, Li XZ, Wang ML (2006). Extended F-expansion method and periodic wave solutions for Klein-Gordon-Schrödinger equations, Commun. Theor. Phys. pp. 459-514.

He JH, Wu XH (2006). Exp-function method for nonlinear wave equations. Chaos, Solitons Fractals. 30:700-708.

Zayed EME, Abdelaziz MAM (2011). Exact solutions for the Schrödinger equation with variable coefficients using a generalized extended tanh function, the Sine-Cosine and the Exp-function methods. Appl. Math. Comput. 218:2259-2268.

Zhu SD (2007). Exp-function method for the discrete mKdV lattic, Int. J. Nonl. Sci. Numer. Simula. 8:465-469.

Wang ML, Zhang JL, Li XZ (2008). The (G`/G)-expansion method and traveling wave solutions of nonlinear evolutions in mathematical physics. Phys. Lett. A 372:417-423.

Zhang S, Tong JL, Wang W (2008). A generalized (G`/G)-expansion method for the mKdV equation with variable coefficients. Phys. Lett. A 372:2254-2257.

Zayed EME, Gepreel KA (2009). The (G`/G)-expansion method for finding traveling wave solutions of nonlinear partial differential equations in mathematical physics. J. Math.Phys. 50:013502-013513.

Zayed EME, Gepreel KA (2009). Some applications of the (G`/G)-expansion method to nonlinear partial differential equations. Appl. Math. Comput. 212:1-13.

Zayed EME (2009). New Traveling wave solution for higher dimensional nonlinear evolution equations using a generalized (G'/G) –expansion method. J. Phys. A: Math. Theor. 42:195202-195214.

Zayed EME (2009). The (G'/G) – expansion method and its applications to some nonlinear evolution equations in the mathematical physics. J. Appl. Math. Computing. 30:89-103.

Zayed EME, Abdelaziz MAM (2010). Traveling wave solution for the Burgers equation and the KdV equation with variable coefficients using a generalized (G'/G) expansion method, Z. Naturforsch, 65a:1065-1070.

Feng ZS (2002). The first integral method to study the Burgers-KdV equation. J. Phys. A: Math. Gen. 35:343-349.

Zheng B (2011).Traveling wave solution for some nonlinear evolution equations by the first integral method, WSEAS Transactions Math. 8:249-258.

Taghizadeh N, Mirzazadeh M, Farahrooz F (2011). Exact solutions of the nonlinear Schrödinger equation by the first integral method. J. Math. Anal. Appl.374:549-553.

Sharma P, Kushel OY (2010).The first integral method for Huxley equation. Int. J. Nonlinear Sci. 10:46-52.

Bekir A, Unsal O (2012). Analytical treatment of nonlinear evolution equations using first integral method. Pramana J. Phys. 79:3-17.

Lu B, Zhang H, Xie F (2010). Traveling wave solutions of nonlinear partial equations by using the first integral method. Appl. Math. Comput. 216:1329-1336.

Zhu S (2007). Exact solutions for the high-order dispersive cubic-quintic nonlinear Schrödinger equation by the extended hyperbolic auxiliary equation method ,Chaos, Solitons Fractals 34:1608-1612.

Zhang JL, Wang ML, Li XZ (2006). The subsidiary ordinary differential equations and the exact solutions of the higher order dispersive nonlinear Schrödinger equation, Phys. Lett. A, 357:188-195.

Zhao M, Li C (2014). The exp $(-\phi(\xi))$-expansion method to nonlinear

evolution equations, http://www.paper.edu.cn

Khan K, Ali M Akbar (2013). Application of exp $(-\phi(\xi))$ -expansion method to find the exact solutions of modified Benjamin-Bona-Mahony equation, World Appl. Sci. J. 24:1373-1377.

Harun-Or-R, Md.Azizur R (2014).The exp $(-\phi(\eta))$ -expansion method with application to the (1+1)-dimensional classical Boussinesq equations, Results in Physics, http://dx.doi.org/10.10161 j.rinp.2014.07.006.

Ma WX, Lee JH (2009). A transformed rational function method and exact solution to the (3+1)-dimensional Jimbo Miwa equation. Chaos Solitons Fractals. 42:1356-1363.

Ma WX, Zhu Z (2012). Solving the (3+1)-dimensional generalized KP and BKP by the multiple exp-function algorithm. Appl. Math. Comput; 218:11871-11879.

Ma WX, Huang T, Zhang Y (2010). A multiple exp-function method for nonlinear differential equations and its application. Phys. Script. 82:065003

Ma WX (1966) Bb. Fuchssteliner, Explict and exact solutions of KPP equation. Int. J. Nonlinear Mech. 31:329-338.

Ma WX, Wu HY, He JS (2007) Partial differential equations possessing Frobenius integrable decomposition technique. Phys. Lett. A 364:29-32.

Yang XJ (2011). Local Fractional Functional Analysis and Its Applications, Asian Academic Publisher Limited, Hong Kong.

Yang XJ (2012). Advanced Local Fractional Calculus and Its Applications, World Science Publisher, New York.

Yang XJ, Baleanu D (2012). Fractal heat conduction problem solved by local fractional variation iteration method, Thermal Science, 17 (2):625-628.

Hu MS, Agarwal RP, Yang XJ (2012).Local Fractional Fourier Series with Application to Wave Equation in Fractal Vibrating String. Abstract and Applied Analysis. Article ID 567401, 15 pp.

Yang XJ, Srivastava HM, He JH, Baleanu D (2013). Cantor-type cylindrical-coordinate method for differential equations with local fractional derivatives. Phys. Lett. A 377:1996-1700.

He JH (2012). Asymptotic methods for solitary solutions and compactons, Abst. Appl. Anal. article ID 916793,130 pages.

Su WH, Yang XJ, Jafari H, Baleanu D (2013). Fractional complex transform method for wave equations on Cantor sets within local fractional differential operator, Advances in Difference Equations.1:97.

Chun-Guang Z, Ai-Min Y, Hossein J, Ahmed H (2014). The Yang-Laplace transform for solving the IVPs with local fractional derivative, Abstract and Applied Analysis, Article ID 386459, 5 pp.

Hristov J (2012). An exercise with the He's variation iteration method to a fractional Bernoulli equation arising in a transient conduction with a non-linear boundary heat flux. Int. Rev. Chem. Eng. 4(5):489-497.

Hristov J, El Ganaoui M (2013). Thermal impedance estimations by semi-derivatives and semi-integrals: 1-D semi-infinite cases. Thermal Sci. 17(2):581-589.

Zhang YZ, Yang AM, Long Y (2014). Initial boundary value problem for fractal heat equation in the semi-infinite region by Yang-Laplace transform. Therm. Sci. 18(2):677–681.

Rui G, Hui-Qin H (2014). Breathers and localized solitons for the Hirota-Maxwell- Bloch system on constant backgrounds in erbium doped fibers. Annals Phys. 344:10-16.

Rui G, Hui-Qin H Ling-Ling Z (2013). Dynamic behaviors of the breather solutions for the AB system in fluid mechanics. Nonlinear Dynamics 74:701-709.

Rui G, Yue-Feng L, Hui-Qin H, Feng-Hua Q (2015). Coherently coupled solitons, breathers and rogue waves for polarized optical waves in an isotropic medium. Nonlinear Dynamics. DOI:10.1007/s11071-015-1938-z.

Hui-Qin H, Jian-Wen Z (2015). Integrability aspects and soliton solutions for the inhomogeneous reduced Maxwell-Bloch system in nonlinear optics with symbolic computation, Commun. Nonlinear Sci. Numer. Simulat. 22:1350-1359.

Peng Z (2009). Comment on Application of The (G`/G)-expansion method for nonlinear evolution equations [Phys. Lett. A 372 (2008)3400], Commu. Theor. Phys. 52:206-208.

academicJournals

Vol. 10(6), pp. 232-235, 30 March, 2015
DOI: 10.5897/SRE2015.6198
Article Number:EA8810651822
ISSN 1992-2248

http://www.academicjournals.org/SRE

Scientific Research and Essays

Full Length Research Paper

Antifungal activity of aqueous and ethanol extracts of seaweeds against sugarcane red rot pathogen (*Colletotrichum falcatum*)

S. Ambika* and K. Sujatha

Department of Seed Science and Technology, Agricultural College and Research Institute, Madurai- 625 104, Tamil Nadu, India.

Received 27 February, 2015; Accepted 17 March, 2015

The study was carried out to evaluate the effect of seaweed extracts of *Sargassum myricocystum* (brown alga) and *Gracilaria edulis* (red alga) against the mycelial growth of *Colletotrichum falcatum* with different extraction methods of aqueous and ethanol at concentrations of 5 and 10% along with control by poison food technique. The result revealed that extract of *S. myricocystum* (ethanol extract) showed significant antifungal activity against pathogen followed by *G. edulis*. *S. myricocystum* (ethanol extract – 10%) extract recorded the lowest mycelial growth of 52 mm where as control recorded 90 mm.

Key words: Seaweeds, pathogen, sugarcane, *Colletotrichum falcatum*.

INTRODUCTION

Sugarcane (*Saccharum* sp.) is one of the most important cash crop grown in India which contributes to the tune of 7.5% of agricultural production of the country (Viswanathan, 2010). India is known as original home of sugarcane and sugar. In India, it is widely cultivated in 4 million hectares with an average productivity of about 76 tonnes ha^{-1} as the main source of sugars and bio ethanol (FAO, 2008). The sugar requirement in India for 2030 is estimated to be 36 million tonnes for which the sugar recovery is to be 11% and average cane yield is to be 100 t/ha which can be fulfilled either by increasing the acreage or productivity (Premachandran, 2012). Sugarcane is widely affected by biotic and abiotic factors, of which the loss to fungal pathogens is critical. Red rot caused by *Colletotrichum falcatum* Went (Perfect state: *Glomerella tucumanensis* (Speg.) von Arx and Muller) is the dreadful fungal disease which severely affects and reduces cane weight by 29%, loss in sugar recovery by 31%, sucrose content by 75% and juice yield by 90% (Hussnain and Afghan, 2006).

This dual loss of juice content and quality results in great losses for both cane grower and the sugar factories. Annual loss of revenues by *C. falcatum* infection in India is estimated to be between 500 and 1000 million USD (Viswanathan and Samiyappan, 2002) and it was responsible for the elimination of many elite sugarcane varieties (Siddique et al., 1983). Various chemical fungicides are most commonly used for the controlling of plant diseases. Application of seaweeds for the control of soil borne plant diseases has

*Corresponding author. E-mail: ambikasingaram@gmail.com, Tel: 8489174468.

increased in recent years due to their environment friendly role. Macro algae are an attractive and natural source of bioactive molecules. Such natural products may have potential for the management of fungal diseases in sustainable agriculture such as organic farming. In recent years, there have been many reports of macro algae derived compounds that have a broad range of biological activities, such as antifungal, antibacterial, antiviral, antioxidant, anti-inflammatory, cytotoxic and antimitotic activities (Demirel et al., 2009). Marine bioactive substances extracted from seaweeds have been used for several decades to enhance plant growth and productivity (Rathore et al., 2009). Present investigation was undertaken to evaluate different seaweed extracts for their antifungal activity against *C. falcatum*.

MATERIALS AND METHODS

Isolation of pathogen

The pathogen was isolated from the diseased tissues of infected sets by tissue segment method (Rangaswami, 1958). The infected portions were cut into small pieces using sterilized scalpel and were surface sterilized with 0.1% mercuric chloride for one minute and washed in three changes of sterile water. The surface sterilized tissues were placed on PDA in sterile Petri plates and incubated at room temperature (28 ± 2°C). The hyphal tips of fungi grown from the pieces were transferred aseptically to PDA slants for maintenance of the culture. The fungus was further purified by single spore isolation and maintained on PDA. The pathogen was identified based on morphological characters.

Collection and preparation of extracts

The marine alga *Sargassum myricocystum* (brown alga) and *Gracilaria edulis* (red alga) collected from Mandapam coast, Tamil Nadu were washed with seawater initially to remove macroscopic epiphytes and sand particles and then with fresh water to remove adhering salt. The materials were shade dried for two weeks followed by oven drying at 40°C for 24 h and powdered.

Aqueous extract

About 20 g dried seaweed powder with 400 ml distilled water was autoclaved for 15 min at 100°C, 15 lbs then centrifuged at 10,000 rpm for 10 min. The supernatant was extracted and stored in a refrigerator till use.

Ethanol extract

Approximately 150 ml of alcohol was added to 20 g powder and kept for overnight with intermittent stirring and extracted through rotary evaporator at 40°C and 45 rpm. The liquid fertilizer was collected and stored in air tight container. Different concentrations were prepared by taking 5 and 10 ml of the stock preparation and mixing with distilled water to get 5 and 10% concentrations.

Antifungal activity

Poisoned food technique (Schmitz, 1930) was employed to screen the antifungal efficacy of seaweed extracts. Potato dextrose agar media amended with seaweed extracts (5 and 10%) was autoclaved and poured into sterile Petri plates. Fungal disc of 9 mm diameter were cut with the help of sterile cork borer from the periphery of 5 days old culture of *C. falcatum* and the disc were transferred aseptically on PDA plates poisoned with seaweed extracts. A plate only with PDA and fungal disc was considered as control and the diameter of growth of fungus in this plate was used as a control for the calculation of percent inhibition of test fungus.

Inhibition percentage

The inhibition percentage was calculated measuring the radial growth of the fungus grown on control and amended plates, using the following formula (Harlapur et al., 2007):

$I\% = 100 \times (C - T) / C$

Where, I% = inhibition percentage of pathogen growth, C = average radial growth in control plates and T = average radial growth in plates amended with seaweed extract.

Compatibility between antagonistic bacteria and seaweed extracts

King's B medium was amended with the *S. myricocystum* (brown alga) and *G. edulis* (red alga) with 5 and 10% concentration. Then, the antagonistic bacterial isolates were inoculated in the poisoned media. The plates were incubated under room temperature and the growth of bacteria was recorded visually and scored either as highly compatible or moderately compatible or not compatible.

Compatibility between antagonistic fungi and seaweed extracts

PDA medium was amended with the *S. myricocystum* (brown alga) and *G. edulis* (red alga) with 5 and 10% concentrations. Then, the antagonistic fungi isolates were inoculated in the poisoned media. The plates were incubated under room temperature and the growth of fungi was observed.

Data analysis

The data from various experiments were analysed statistically adopting the procedure described by Panse and Sukhatme (1985). Wherever necessary, the percentage values were transformed to arc sine values before carrying out the statistical analysis.

RESULTS AND DISCUSSION

Among the extracts tested, ethanol extract showed better performance for reducing the red rot pathogen growth in sugarcane. The percent reduction over control in ethanol extract was 33% where as in aqueous extract method 9%. Lowest mycelial growth (*C. falcatum*) was recorded in *S. myricocystum* at 10% (52 mm) (Figure 1), followed by *Gracillaria edulis* at 10% (57 mm) and *Caulerpa racemosa* at 10% (63 mm) in the ethanol extract compared to aqueous extract and other concentration (5%). Control recorded the highest mycelial growth of 90

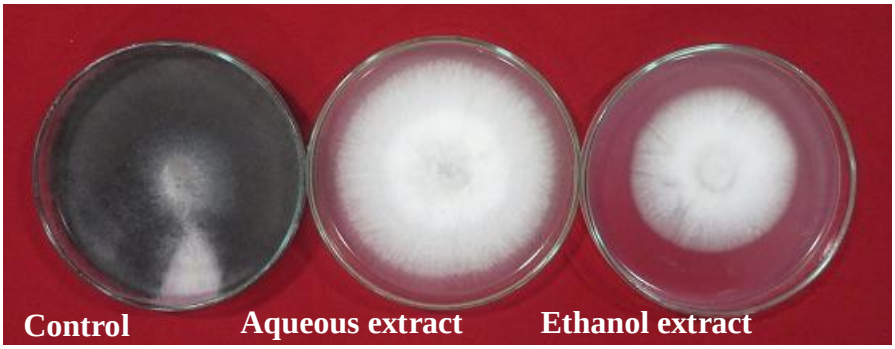

Figure 1. Effects of *Sargassum myricocystum* (10%) extracts on mycelial growth (mm) of *Colletotrichum falcatum in vitro.*

Table 1. Effect of aqueous and ethanol seaweed extracts on mycelial growth (mm) of *Colletotrichum falcatum in vitro.*

Treatment	Aqueous extract (mycelial growth (mm)	% reduction over control	Ethanol extract (mycelial growth (mm)	% reduction over control
Sargassum myricocystum (5%)	82	8.89	60	33.33
Sargassum myricocystum (10%)	79	12.22	52	42.22
Gracilaria edulis (5%)	85	5.56	71	21.11
Gracilaria edulis (10%)	80	11.11	57	36.67
Caulerpa *racemosa* (5%)	87	3.33	75	16.66
Caulerpa *racemosa* (10%)	83	7.77	63	30.00
Control	90	-	90	-
Mean	83.71	8.14	66.86	30.00
SEd	1.7443	0.7832	1.4138	0.6506
$CD_{(0.05)}$	3.62**	1.64**	2.94**	1.36**

Table 2. Compatibility between antagonistic fungi, bacteria and seaweed extracts.

Treatment	Aqueous extract		Ethanol extract	
	Trichoderma viride	***Pseudomonas fluorescens***	***Trichoderma viride***	***Pseudomonas fluorescens***
Sargassum myricocystum (5%)	+++	+++	+++	+++
Sargassum myricocystum (10%)	+++	+++	+++	+++
Gracilaria edulis (5%)	+++	+++	+++	+++
Gracilaria edulis (10%)	+++	+++	+++	+++
Caulerpa *racemosa* (5%)	++	++	++	++
Caulerpa *racemosa* (10%)	++	++	++	++
Control	+++	+++	+++	+++

+++: Highly compatible, ++: moderately compatible, +: slightly compatible -: No compatible.

mm (Table 1). The effect of different concentrations of seaweed extracts was tested for their compatibility with fungal antagonist *Trichoderma viride* and bacterial antagonist *Pseudomonas fluorescens* under *in vitro* condition. The results revealed that the growth of *T. viride* and *P. fluorescens* was found to be not sensitive to the extracts of seaweeds *S. myricocystum* and *G. edulis* (Table 2). Jayaraj et al. (2008) found that the application of seaweed extracts on carrot plants reduced leaf blights caused by *Alternaria* and *Botrytis* as effectively as the fungicide chlorothalonil. In carrot application of seaweed liquid fertilizer (SLF) enhanced activities of defense

related enzymes including peroxidase, polyphenyl oxidase, phenylalanine ammonia-lyase, chitinase and β-1,3- glucanase were significantly increased in plants treated with seaweed (Jayaraj et al., 2008; Solanki et al., 2012). Similar results were found in cucumber which showed enhanced activities of various defence-related enzymes including chitinase, B-1, 3-glucanase, peroxidase, polyphenol oxidase, phenylalanine ammonia lyase, and lipoxygenase due to SLF application (Jayaraman et al., 2011). The commercial extract from the brown seaweed *Ascophyllum nodosum* was found to reduce fungal diseases in cucumber (Jayaraman et al., 2011). The laminarin polysaccharide isolated from *Laminaria digitata* is able to elicit host defense responses in plants (Klarzynski et al., 2000). The brown seaweeds show high antifungal activity as compared to red and green alga. The brown seaweeds contain high amount of flavonoid and phenolic compounds which could be the reason for antifungal activity (Cowan et al., 1999). Lipophilic compounds (glycolipid, phenolic-terpenoids, unsaturated-fatty acids and hydroxylated unsaturated-fatty acids) are highly soluble in ethanol compared to water. These lipophilic compounds are having antifungal property (Hanaa et al., 2008). In another study, the authors (Tuney et al., 2006) found that ethanolic extract of *Padina pavonica* was active against *C. albicans,* however methanolic and acetonic extracts of the same algae were inactive against *C. albicans*.

Conclusion

Ethanol extracts of *S. myricocystum* at 10% concentration effectively controlled and inhibited the mycelial growth of *C. falcatum* in sugarcane under *in vitro* studies.

Conflict of Interest

The authors have not declared any conflict of interest.

REFERENCES

Cowan MM (1999). Plants products as antimicrobial agents. Clinical Microbiol. Rev. 12:564-582.

Demirel Z, Yilmaz-Koz F, Karabay-Yavasoglu U, Ozdemir G, Sukatar A (2009). Antimicrobial and antioxidant activity of brown algae from the Aegean Sea. J. Serb. Chem. Soc. 74(6):619-628.

FAO (2008). Faostat Database Collection http://apps.fao.org/page/collection.

Hanaa H, Abd El-Baky, Farouk K, Baz EL, Gamal SE, Baroty (2008). Evaluation of marine alga *Ulva lactuca* as a source of natural preservative ingredient. American- Eurasian J. Agric. Environ. Sci. 3(3):434-444.

Harlapur SI, Kulkarni MS, Wali MC, Srikantkulkarni H (2007). Evaluation of plant extracts, bio-agents and fungicides against *Exserohilum turcicum* causing *Turcicum* leaf blight of Maize. J. Agric. Sci. 20(3):541-544.

Hussnain Z, Afghan S (2006). Impact of major cane diseases on sugarcane yield and sugar recovery. Jhang, Pakistan, Shakarganj Sugar Research Institute, Annual report.

Jayaraj JA, Wan M, Rahman Punja ZK (2008). Seaweed extract reduces foliar fungal diseases on carrot. Crop Protect. 27:1360-1366.

Jayaraman J, Jeff N, Zamir P (2011). Commercial extract from the brown seaweed *Ascophyllum nodosum* reduces fungal diseases in greenhouse cucumber. J. Appl. Phycol. 23:353-361.

Klarzynski O, Plesse B, Joubert JM, Yvin JC, Kopp M, Kloareg B, Fritig B (2000). Linear beta -1,3 glucans are elicitors of defense responses in tobacco, Plant Physiol. 124:1027-1038.

Solanki MK, Singh N, Singh RK, Singh P, Alok K, Kumar SS, Prem L, Kashyap DKA (2012). Plant defense activation and management of tomato root rot by a chitin-fortified *Trichoderma*/Hypocrea formulation. Phytoparasitica 39(5):471-481.

Panse VG, and Sukhatme PV (1985). Statistical methods for Agricultural workers. ICAR, Publication, New Delhi: pp. 327-340.

Premchandran MN (2012).Breeding strategies for increasingproductivity and resistance to diseases in sugarcane. In: Sugarcanebreeding and pathologist meet, Coimbatore. pp. 11-26.

Rangaswami G (1958). An agar blocks technique for isolating soil micro organisms with special reference to phthiaceous fungi. Sci. Culture 24:85.

Rathore SS, Chaudhary DR, Boricha GN, Ghosh A, Bhatt BP, Zodape ST, Patolia JS (2009). Effect of seaweed extract on the growth, yield and quality of soybean (*Glycine max*) under rain fed conditions. S. Afr. J. Bot. 75:351-355.

Schmitz H (1930). Poisoned food technique. Industrial and Engineering Chemistry. Analyst. 2:361.

Siddique MM, Khanzada MI, Maazulla K (1983). Incidence and effects of sugarcane red rot caused by *Colletotrichum falcatum* in northern pakisthan. Pakistan J. Agric. Res. 4(3):208.

Tuney I, Cadirci BH, Unal D, Sukatar A (2006). Antimicrobial Activities of the Extracts of Marine Algae from the Coast of Urla (Izmir, Turkey). Turk. J. Biol. 30:171-175.

Viswanathan R (2010). Plant Disease: Red rot of sugarcane. Anmol Publishers, New Delhi, P. 305.

Viswanathan R, Samiyappan R (2002). Induced systemic resistance by fluorescent pseudomonads against red rot disease of sugarcane caused by *Colletotrichum falcatum*. Crop Protect. 21(1):1-10.

academicJournals

Vol. 10(6), pp. 236-242, 30 March, 2015
DOI: 10.5897/SRE2015.6065
Article Number:BF2F62551824
ISSN 1992-2248

http://www.academicjournals.org/SRE

Scientific Research and Essays

Full Length Research Paper

Improved production of β-galactosidase and β-fructofuranosidase by fungi using alternative carbon sources

Diandra de Andrades[1], Vanessa Cristina Arfelli[1], Alesandra Oriente[1], Caroline Henn[2], Veridiana Araujo Alves da Costa Pereira[2], Rita de Cássia Garcia Simão[3], Jose Luis da Conceição Silva[3] and Marina Kimiko Kadowaki[3]*

[1]Centro de Ciências Biológicas e da Saúde – UNIOESTE - Rua: Universitária 2069 CEP:85814-110, Cascavel, Paraná, Brazil.
[2]Divisão de Reservatório – MARR.CD, Itaipu Binacional, Avenida Tancredo Neves, 6731, CEP 85866-900 – Foz do Iguaçu, Paraná, Brazil.
[3]Centro de Ciências Médicas e Farmacêuticas – UNIOESTE - Rua: Universitária 2069 CEP:85814-110, Cascavel, Paraná, Brazil.

Received 4 August, 2014; Accepted 19 March, 2015

The influence of alternative carbon sources as inducers of β-galactosidase and β-fructofuranosidase by filamentous fungi (that are, *Aspergillus aculeatus, Chrysonilia sitophila, Gliocladium virens, Aspergillus fumigatus* and *Trichoderma longibrachiatum*), recently isolated from Brazil's Atlantic Forest biome has been investigated. The greatest levels of intracellular β-galactosidase activity were obtained using orange peel waste (56.31 U/mL) with *A. aculeatus*, rice straw (22.57 U/mL) with *G. virens*, sorghum straw (16.48 U/mL) with *C. sitophila*, and passion fruit peel with either *A. fumigatus* (17.26 U/mL) or *T. longibrachiatum* (17.53 U/mL). The most effective intracellular β-fructofuranosidase activity was obtained by *A. aculeatus* using trub (409.46 U/mL) or passion fruit peel (44.59 U/mL). Thus, alternative carbon sources, such as orange peel and trub, exhibit great potential as inducers for the production of these enzymes. Such fungal isolates from the Atlantic Forest of Paraná, Brazil are promising candidates for generating significant amounts of β-galactosidase and β-fructofuranosidase using abundant and inexpensive agro-industrial substrates.

Key words: Agro-industrial residue, Atlantic Forest, lactase, invertase, fungus.

INTRODUCTION

The use of agro-industrial wastes in bioconversion by microorganisms has been the subject of extensive research in the last year, especially with reference to the production of proteins, enzymes, organic acids and some secondary metabolites. As a developing country, Brazil continually undergoes extensive agricultural and industrial activity, and consequently annually generates an enormous amount of agro-industrial waste. In this

*Corresponding author. E-mail: marinakk@gmail.com, Tel: +55 45 3220-3292.

context, such biodegradable waste is recognized as a potential sustainable source for use in the production of various value-added products such as biofuel, animal feed, chemicals and enzymes (Saha and Ghosh, 2014). Thus, the exploitation of agro-industrial waste for microbial bioprocesses may be an answer in the search for alternative and inexpensive carbon sources. Some agro-industrial wastes such as cassava bagasse, sugarcane bagasse, sugar beet residues, sludge and coffee husks, the peel and pulp of citrus fruits and wheat meal, have been used as carbon sources, mainly in fermentation processes using microorganisms (Soccol and Vandenberghe, 2003). Hence, the selection of microorganisms capable of producing β-galactosidase and β-fructofuranosidase, using agro-industrial waste as a carbon source in fermentation processes, may aid in overcoming high enzyme production costs, particularly in relation to biotechnological applications.

β-D-fructofuranosidase (E.C. 3.2.1.26) or more commonly named of invertase, is an important enzyme in the food industry and is responsible for the irreversible hydrolysis of β1-2 sucrose to produce a mixture of equal amounts of glucose and fructose (Rustiguel et al., 2010). β-fructofuranosidase has been used extensively in the production of invert sugar syrups, mixtures of glucose and fructose, which are sweeter than sucrose due to the high degree of sweetness exhibited by fructose, because these sugars do not crystallize. This enzyme is widely used in processed foods, in lactic acid production, in the fermentation of cane sugar molasses, in calf feed production, in ethanol production and as food for honeybees (Ikram-ul-Haq et al., 2005; Rashad and Nooman, 2009). β-D-fructofuranosidase is also employed in the pharmaceutical industry in the form of digestive aid tablets and as powdered milk for infant food (Uma et al., 2012). β-fructofuranosidase is produced by various microorganisms, such as *Saccharomyces cerevisiae* (Andjelkovic et al., 2012), *Penicillium chrysogenum* (Nuero and Reyes, 2002), *Aspergillus ochraceus* (Guimarães et al., 2007) and *Aspergillus niger* (Madhan et al., 2010).

β-galactosidase (E.C. 3.2.1.23) also known as lactase, catalyzes the hydrolysis of lactose (Galβ1-4Glc) to produce glucose and galactose (Ansari and Satar, 2012). This enzyme is extensively used by the dairy industry in the hydrolysis of lactose in milk or products derived from whey. Furthermore, the enzyme is clinically important during the preparation of lactose-free milk and milk products for patients with lactose intolerance (Shaikh et al., 1999). In recent years, the transgalactosylation activity of β-galactosidase has also been exploited in the production of galactooligosaccharide (GOS) and other functional galactosylated products (Oliveira et al., 2011). In addition, a significant market for lactose-free milk and dairy products exists among ice cream and confectionery industries, to assist patients with lactose intolerance (Adam et al., 2005; Husain, 2010). β-galactosidase is commonly produced by animal cells, plants and microorganisms, including *A. niger, Aspergillus oryzae, Kluyveromyces fragilis* and *Kluyveromyces lactis* (Husain, 2010).

The use of sucrose and lactose are commonly cited for β-fructofuranosidase and β-galactosidase production by microorganisms, and, less often, unconventional sources such as from agricultural waste industries.

Therefore, the growth of microorganisms and subsequent enzyme production are strongly influenced by medium composition; the carbon source of medium is one of the most important components of culture media for fungal growth and enzyme production because it may regulate the biosynthesis of enzymes in microorganisms (Akcan, 2011). Thus, screening for appropriate carbon is one of the most critical step in the development of an efficient and economic bioprocess (Konsoula and Liakopoulou-Kyriakides, 2007; Akcan, 2011). In this context, the aim of the present study was to investigate the influence of agro-industrial waste as inducers of β-galactosidase and β-fructofuranosidase production by several fungal strains recently isolated from the Atlantic Forest biome in Paraná state, Brazil.

MATERIALS AND METHODS

Microorganisms

The filamentous fungi used in this study were isolated from samples of soil or decaying plants obtained from the Bela Vista Biological Refuge in Foz do Iguassu in the State of Paraná, Brazil. These fungal strains were taxonomically identified by mycology collection of the Federal University of Pernambuco, Brazil, as *Aspergillus aculeatus, Aspergillus fumigatus, Chrysonilia sitophila, Gliocladium virens* and *Trichoderma longibrachiatum*. The conidia of the strains were maintained on potato dextrose agar at 4°C for a month, and the stock culture was maintained in 10% glycerol solution at -80°C.

Culture conditions

Liquid medium for enzyme production consisted of Modified Czapek medium (g/L) with: yeast extract, 5; $(NH_4)_2SO_4$, 2.8; KH_2PO_4, 4; $MgSO_4 \cdot 7H_2O$, 0.9; and $CaCl_2 \cdot 2H_2O$, 0.9. Each culture was grown in 125 mL Erlenmeyer flasks containing 25 mL of sterile medium supplemented with 1% (w/v) dry matter agro-industrial waste (that are, banana peel, orange peel, passion fruit peel, walnut peel, pear peel, quinoa meal, soybean meal, rice straw, sorghum straw or trub). These alternative carbon sources were obtained from the market and industries of Cascavel, Paraná, Brazil. After a 1 mL inoculum (10^5 spores/mL) of mesophilic (that is, *A. aculeatus, C. sitophila* and *G. virens* were incubated at 28°C) or thermophilic fungus (*T. longibrachiatum and Aspergillus fumigatus* were grown at 42°C), fungi were grown in static conditions for five days. Each culture was vacuum filtered to obtain a cell-free filtrate of extracellular enzyme activity. Intracellular extracts were obtained from frozen mycelia (previously separated and washed with distilled water) after maceration in a porcelain mortar with twice their weight in glass beads (0.1 mm diameter), resuspended in distilled water and then centrifuged at 5000 × *g* for 5 min at 4°C. The filtrate was dialyzed overnight at 4°C against the buffer used for each enzymatic assay.

Enzymatic assay

β-fructofuranosidase activity was determined by analyzing reducing sugar that is released after incubation of the properly diluted enzyme with 0.2 M sucrose in 50 mM sodium acetate buffer (pH 4.0) at 60°C for 10 min. The amounts of reducing sugars were determined using dinitrosalicylic acid according to Miller (1959). One unit of enzyme activity was defined as the amount of enzyme capable of releasing 1 µmol of reducing sugar (glucose) per minute under the experimental conditions used.

The β-galactosidase activity assay was performed by mixing 100 µL of appropriately diluted enzyme with 500 µL of the synthetic substrate, β-D-galactopyranoside (ONPGal; 3 mM) dissolved in 50 mM sodium citrate buffer (pH 4.5), and incubating the mixture at 40°C for 10 min. The reaction was stopped by the addition of 2 mL of 0.2 M Na_2CO_3. Enzyme activity was determined from the amount of released o-nitrophenol, which was measured using a spectrophotometer at 410 nm. One unit of enzyme activity was defined as the amount of enzyme capable of releasing 1 µmol of o-nitrophenol per minute under the assay conditions used.

Statistical analysis

All experiments were performed in triplicate, and results are presented as mean ± standard deviation. Significant differences between the means of enzymatic activities were determined using an analysis of variance (ANOVA), followed by the Tukey test at a 5% level of significance ($P < 0.05$).

RESULTS AND DISCUSSION

Influence of agro-industrial waste on the production of fungal β-galactosidase

The use of agricultural residues as carbon sources in biotechnological processes can reduce the production costs of microbial fermentations. Thus, the search for both alternative carbon sources and fungal strains with the ability to produce appropriate enzymes is essential to obtain an economically viable fermentation process.

In this study, several alternative carbon sources were examined; among the agricultural residues tested, orange peel enhanced extracellular β-galactosidase production for most fungal strains tested (Table 1). The highest extracellular β-galactosidase activities were observed with orange peel by *G. virens* (8.47 U/mL), followed by pear peel (2.66 U/mL) by the same organism. Orange peel has also been reported to induce β-galactosidase by *A. niger, Aspergillus terreus, Aspergillus flavus, Penicillium brevicompactum* and *Fusarium oxysporum* (Vidya et al., 2014). However, an extracellular β-galactosidase (Bga1) from *Hypocrea jecorina* (*T. reesei*) was induced by D-galactose mediated by galactitol (Fekete et al., 2007). Raol and colleagues (2014) reported that in polysaccharides such as wheat bran, pectin and polygalacturonic acid, the β-galactosidase cleaves and releases galactose residues from the side-chains of galactan and it is suggested not to repress the biosynthesis of β-galactosidase. Thus, carbohydrates such as hemicellulose monomers or galactose found in these agro-residues may induce the production of β-galactosidase by fungi.

In this study, the induction of intracellular β-galactosidase by alternative carbon sources was higher than for the extracellular β-galactosidase produced by these fungal strains (Table 2). The highest value of intracellular β-galactosidase activity was obtained with the fungus *A. aculeatus* using orange peel waste (56.31 U/mL), rice straw (47.97 U/mL) and pear peel (44.45 U/mL); some other high values were obtained with rice straw and *G. virens* (22.57 U/mL), sorghum straw with *C. sitophila* (16.48 U/mL), and passion fruit peel with *A. fumigatus* (17.26 U/mL) or *T. longibrachiatum* (17.53 U/mL) (Table 2). To the best of our knowledge, this is the first report of β-galactosidase production by fungi of the genera *Gliocladium* and *Chrysonilia*. There are few reports of the use of agricultural waste as a carbon source for the production of β-galactosidase, but in one study, β-galactosidase from *Aspergillus tubengensis* GR-1 was produced using wheat bran (Raol et al., 2014).

However, there are many reports concerning β-galactosidase production induced with lactose or its derivatives, such as in the fungus *Trichoderma* sp. which reached 0.35 to 2.24 U/mL (Akinola et al., 2012); *Teratosphaeria acidotherma* AIU BGA-1 produced four intracellular β-D-galactosidases using lactose as a carbon source (Isobe et al., 2013). In this study, *T. longibrachiatum* produced significant amounts of β-galactosidase using alternative carbon sources, with enzymatic activities ranging from 1.46 to 17.53 U/mL. These results suggest that the fungi tested were capable of performing the bioconversion of these residues and of consequently providing monosaccharides such as arabinose, galactose and xylose; these, in turn, favored the induction and biosynthesis of β-galactosidase.

According to Fekete and colleagues (2002), the biosynthesis of β-galactosidase from *Aspergillus nidulans* was also induced by L-arabinose and hemicellulose monomers, and similar results were also observed in *A. niger* and *Penicillium canescens*. The reason for the induction of β-galactosidase by L-arabinose and D-xylose in *A. nidulans* was unknown, but according to the author, this induction was related to the concomitant release of D-galactose, L-arabinose and D-xylose from these sources of natural polysaccharide (Fekete et al., 2002).

β-fructofuranosidase production by fungi induced by agro-industrial wastes

The production of β-fructofuranosidase of these fungi was also examined in the presence of various agro-industrial wastes. Extracellular β-fructofuranosidase was induced by several carbon sources, such as soybean meal (9.48 U/mL), orange peel (4.09 U/mL) and passion fruit peel (4.07 U/mL) for *A. aculeatus,* whereas banana (4.64 U/mL) and pear peels (4.62 U/mL) favored the

Table 1. Production of extracellular β-galactosidase by filamentous fungi in liquid culture with agro-industrial residues as carbon sources.

Carbon source (1%)	*Aspergillus aculeatus*	*Aspergillus fumigatus*	*Chrysonilia sitophila*	*Gliocladium virens*	*Trichoderma longibrachiatum*
	β-galactosidase activity (U/mL)				
Banana peel	1.42 ± 0.08^{bc}	0.88 ± 0.10^{bc}	0.73 ± 0.04^{b}	1.63 ± 0.13^{cd}	1.12 ± 0.09^{b}
Pecan shell	0.27 ± 0.06^{e}	0.73 ± 0.07^{cd}	0.43 ± 0.18^{c}	0.81 ± 0.09^{f}	0.65 ± 0.08^{de}
Orange peel	1.66 ± 0.21^{ab}	2.12 ± 0.19^{a}	1.72 ± 0.18^{a}	8.47 ± 0.26^{a}	2.17 ± 0.06^{a}
Passion fruit peel	2.10 ± 0.26^{a}	1.17 ± 0.13^{b}	0.42 ± 0.14^{c}	1.98 ± 0.20^{c}	0.96 ± 0.12^{bc}
Pear peel	1.06 ± 0.14^{cd}	0.08 ± 0.02^{f}	0.33 ± 0.05^{cd}	2.66 ± 0.28^{b}	0.82 ± 0.06^{cd}
Quinoa meal	0.83 ± 0.10^{d}	0.47 ± 0.13^{de}	0.11 ± 0.02^{d}	1.59 ± 0.11^{cde}	0.21 ± 0.08^{g}
Rice straw	0.96 ± 0.09^{cd}	0.40 ± 0.05^{e}	0.14 ± 0.12^{cd}	1.95 ± 0.18^{c}	0.21 ± 0.04^{g}
Sorghum straw	0.93 ± 0.23^{cd}	0.62 ± 0.12^{cde}	0.40 ± 0.08^{cd}	1.45 ± 0.15^{de}	0.49 ± 0.11^{ef}
Soybean meal	1.39 ± 0.20^{bc}	0.67 ± 0.17^{cde}	0.26 ± 0.20^{cd}	0.92 ± 0.19^{f}	0.27 ± 0.12^{g}
Trub	0.88 ± 0.08^{d}	0.80 ± 0.21^{c}	0.10 ± 0.03^{d}	1.18 ± 0.10^{ef}	0.34 ± 0.08^{fg}

Values are mean ± SD of three replicates. Values followed by different letters in each column differ significantly according to the Tukey test ($P < 0.05$).

Table 2. Production of intracellular β-galactosidase by filamentous fungi in liquid culture with agro-industrial residues as carbon sources.

Carbon source (1%)	*Aspergillus aculeatus*	*Aspergillus fumigatus*	*Chrysonilia sitophila*	*Gliocladium virens*	*Trichoderma longibrachiatum*
	β-galactosidase activity (U/mL)				
Banana peel	7.58 ± 0.32^{g}	8.01 ± 0.10^{c}	7.37 ± 0.33^{de}	9.00 ± 0.13^{d}	2.58 ± 0.25^{d}
Pecan shell	0.56 ± 0.03^{h}	6.42 ± 0.27^{d}	1.29 ± 0.15^{g}	2.02 ± 0.10^{h}	6.35 ± 0.35^{c}
Orange peel	56.31 ± 0.56^{a}	12.44 ± 0.60^{b}	8.46 ± 0.30^{b}	18.51 ± 0.76^{c}	16.20 ± 0.59^{b}
Passion fruit peel	9.31 ± 0.13^{f}	17.26 ± 0.44^{a}	7.87 ± 0.22^{cd}	8.18 ± 0.15^{de}	17.53 ± 0.22^{a}
Pear peel	44.45 ± 0.34^{c}	1.88 ± 0.10^{ef}	7.65 ± 0.27^{cd}	6.49 ± 0.33^{f}	1.46 ± 0.23^{e}
Quinoa meal	18.88 ± 0.74^{e}	1.43 ± 0.12^{f}	7.60 ± 0.26^{cd}	9.29 ± 0.21^{d}	6.74 ± 0.19^{c}
Rice straw	47.97 ± 0.52^{b}	2.17 ± 0.12^{e}	8.01 ± 0.07^{bc}	22.57 ± 1.21^{a}	2.06 ± 0.14^{de}
Sorghum straw	20.43 ± 0.92^{d}	1.60 ± 0.19^{ef}	16.48 ± 0.23^{a}	7.54 ± 0.30^{ef}	2.22 ± 0.07^{d}
Soybean meal	19.80 ± 0.32^{de}	2.16 ± 0.12^{e}	6.55 ± 0.28^{f}	20.17 ± 0.49^{b}	6.98 ± 0.17^{c}
Trub	19.11 ± 0.54^{e}	1.71 ± 0.05^{ef}	6.83 ± 0.17^{ef}	4.84 ± 0.20^{g}	2.45 ± 0.21^{d}

Values are mean ± SD of three replicates. Values followed by different letters in each column differ significantly according to the Tukey test ($P < 0.05$).

production of β-frutofuranosidase by *A. fumigatus* (Table 3). Soybean meal also significantly induced extracellular β-fructofuranosidase by *C. sitophila* (3.98 U/mL). The use of alternative carbon sources by microorganisms as inducers of β-fructofuranosidase have been reported mainly for: sugar cane bagasse, cassava flour and corn cob (Alegre et al., 2009); food processing residues (Rashad and Nooman, 2009); and pineapple peels, sweet lime, pomegranate, orange and mosambi (Uma et al., 2012). The choice of carbon source for the production of β-fructofuranosidase is important for ensuring that this process is economical and feasible.

In contrast to *A. aculeatus* and *A. fumigatus*, *G. virens* and *T. longibrachiatum* exhibited low extracellular β-fructofuranosidase activity with the particular agro-industrial wastes used in this study (Table 3). The production of enzymes is influenced by both induction and catabolite repression. Thus, the low yield of β-fructofuranosidase, seen specifically with these fungi, may be due to the final products (glucose and fructose) released by polysaccharidases' action on waste, since the presence of these monomers does not favor the biosynthesis of β-fructofuranosidase due to a catabolite repression effect.

The production of intracellular β-fructofuranosidase was higher than for the extracellular enzyme in the presence of agro-industrial wastes used as carbon sources for all fungi in this study except *A. fumigatus* (Table 4).

Table 3. Production of extracellular β-fructofuranosidase by fungi in liquid culture with agro-industrial residues as carbon sources.

Carbon source (1%)	*Aspergillus aculeatus*	*Aspergillus fumigatus*	*Chrysonilia sitophila*	*Gliocladium virens*	*Trichoderma longibrachiatum*
	β-fructofuranosidase activity (U/mL)				
Banana peel	3.30 ± 0.26^{c}	4.64 ± 0.43^{a}	0.68 ± 0.17^{cd}	0.15 ± 0.04^{bcd}	0.28 ± 0.05^{b}
Nut shell	1.01 ± 0.18^{de}	3.80 ± 0.03^{b}	0.31 ± 0.04^{de}	0.15 ± 0.02^{bcd}	0.29 ± 0.0^{b}
Orange peel	4.09 ± 0.26^{b}	0.46 ± 0.10^{d}	0.23 ± 0.04^{de}	0.32 ± 0.14^{a}	0.42 ± 0.15^{b}
Passion fruit peel	4.07 ± 0.03^{b}	0.52 ± 0.13^{d}	1.79 ± 0.27^{b}	0.16 ± 0.02^{bcd}	2.86 ± 1.18^{a}
Pear peel	1.17 ± 0.03^{de}	4.62 ± 0.25^{a}	0.48 ± 0.09^{de}	0.13 ± 0.02^{bcd}	0.20 ± 0.03^{b}
Quinoa meal	0.87 ± 0.24^{e}	1.76 ± 0.09^{c}	1.03 ± 0.22^{c}	0.25 ± 0.03^{ab}	0.21 ± 0.03^{b}
Rice straw	0.21 ± 0.02^{f}	0.14 ± 0.02^{d}	0.22 ± 0.04^{de}	0.12 ± 0.03^{cd}	0.11 ± 0.02^{b}
Sorghum straw	1.41 ± 0.06^{d}	0.13 ± 0.02^{d}	0.10 ± 0.02^{e}	0.12 ± 0.02^{bcd}	0.23 ± 0.04^{b}
Soybean meal	9.48 ± 2.67^{a}	0.32 ± 0.05^{d}	3.98 ± 0.47^{a}	0.05 ± 0.0^{d}	0.03 ± 0.01^{b}
Trub	2.93 ± 0.10^{c}	3.78 ± 0.10^{b}	0.66 ± 0.17^{cd}	0.21 ± 0.04^{abc}	0.18 ± 0.04^{b}

Values are mean ± SD of three replicates. Values followed by different letters in each column differ significantly according to the Tukey test ($P < 0.05$).

Table 4. Production of intracellular β-fructofuranosidase by fungi in liquid culture with agro-industrial residues as carbon sources.

Carbon source (1%)	*Aspergillus aculeatus*	*Aspergillus fumigatus*	*Chrysonilia sitophila*	*Gliocladium virens*	*Trichoderma longibrachiatum*
	β-fructofuranosidase activity (U/mL)				
Banana peel	26.48 ± 1.32^{c}	2.94 ± 0.28^{b}	2.12 ± 0.81^{d}	0.13 ± 0.03^{d}	3.04 ± 0.23^{b}
Nut shell	4.75 ± 0.21^{e}	0.17 ± 0.05^{f}	0.21 ± 0.01^{d}	0.21 ± 0.03^{cd}	0.80 ± 0.10^{de}
Orange peel	23.49 ± 0.32^{cd}	3.20 ± 0.16^{b}	11.53 ± 0.34^{b}	0.93 ± 0.34^{bcd}	0.43 ± 0.01^{e}
Passion fruit peel	44.59 ± 2.90^{b}	2.39 ± 0.21^{c}	5.43 ± 0.16^{c}	0.95 ± 0.29^{bcd}	4.54 ± 0.39^{a}
Pear peel	11.47 ± 0.64^{de}	1.27 ± 0.07^{de}	0.27 ± 0.06^{d}	0.74 ± 0.28^{bcd}	1.13 ± 0.31^{cd}
Quinoa meal	40.60 ± 2.01^{b}	1.01 ± 0.08^{e}	27.91 ± 3.17^{a}	2.06 ± 0.44^{a}	1.44 ± 0.34^{c}
Rice straw	0.79 ± 0.10^{e}	0.25 ± 0.03^{f}	0.20 ± 0.01^{d}	0.16 ± 0.05^{cd}	0.62 ± 0.06^{de}
Sorghum straw	11.87 ± 2.02^{de}	0.18 ± 0.03^{f}	0.08 ± 0.02^{d}	0.34 ± 0.09^{bcd}	1.17 ± 0.06^{cd}
Soybean meal	19.08 ± 0.41^{cd}	1.65 ± 0.51^{d}	0.95 ± 0.03^{d}	1.06 ± 0.36^{b}	1.09 ± 0.20^{cd}
Trub	409.46 ± 17.79^{a}	4.00 ± 0.09^{a}	1.42 ± 0.45^{d}	0.97 ± 0.26^{bc}	4.14 ± 0.16^{a}

Values are mean ± SD of three replicates. Values followed by different letters in each column differ significantly according to the Tukey test ($P < 0.05$).

Enhanced production of intracellular β-fructofuranosidase by fungi was observed in *A. aculeatus* (409.46 U/mL) induced by trub (wastes obtained from brewing fermentation). Trub is commonly used as a supplement in animal feed because of its significant nutritional value, or discarded into the environment, and, thus, may be useful in microbial processes. Passion fruit peels were also effective in inducing intracellular β-fructofuranosidase by *A. aculeatus* (44.59 U/mL). Likewise, quinoa meal also significantly induced intracellular β-fructofuranosidase in *A. aculeatus* (40.60 U/mL) and *C. sitophila* (27.91 U/mL). On the other hand, carbohydrates such as sucrose or raffinose added to the medium induced large amounts of β-fructofuranosidase in *A. nidulans* (Vainstein and Peberd, 1991). Rubio and Navarro (2006) have also reported higher levels of β-fructofuranosidase obtained from *A. niger* using sucrose, turanose, raffinose and inulin; the authors suggested that carbohydrates that induce invertase synthesis have a β-link and a fructose located at the end of the molecule as a common feature in their structure. Nonetheless, the use of pure carbohydrates for the large-scale production of β-fructofuranosidase by fungi can become very expensive, and the choice of cheaper and renewable substrates, in the form of agro-industrial wastes may be advantageous. Agro-industrial residues are most commonly cited for the induction of xylanases, cellulases and pectinases by fungi. However, studies using lignocellulosic biomass sources for the induction of enzymes, such as β-galactosidase and β-fructofuranosidase, are still few in number; it is envisioned that the microbial process will become economically more feasible with time, while

retaining the potential to minimize the impact of industrial wastes on the environment.

Conclusion

In this study, screening for strong fungal producers of β-galactosidase and β-fructofuranosidase was performed using alternative carbon sources obtained from agro-industrial substrate. The highest β-galactosidase production was found as an intracellular enzyme produced by *A. aculeatus* and *G. virens* using orange peel, rice straw and pear peel. The most effective production of intracellular β-fructofuranosidase was obtained by *A. aculeatus* with trub (that is, brewing residue), passion fruit peel or quinoa meal as carbon sources, followed by the fungus *C. sitophila,* which also produced significant amounts of β-fructofuranosidase with quinoa meal. It was therefore concluded that these fungi can be exploited to generate significant amounts of β-galactosidase and β-fructofuranosidase using alternative agro-industrial substrates that are abundantly available, mainly in agricultural production regions. Thus, fungi isolated from the Atlantic Forest biome of Paraná, Brazil may be promising candidates for the production of β-galactosidase and β-fructofuranosidase for commercial use in the future. However, further studies on improved and optimized culture conditions will be needed to increase enzyme yield, particularly since the natural fungal sources of these enzymes have only relatively recently been isolated from nature and therefore their properties remain largely unknown.

Conflict of Interest

The authors do not have any financial or commercial conflicts of interest to declare.

ACKNOWLEDGEMENTS

This work was supported by grants from Fundação Araucária-Brazil. Marina K. Kadowaki is a Research Fellow for the State of Parana Research Support Foundation (Fundação Araucária-Brazil). Alesandra Oriente and Diandra de Andrades are recipients of the Brazilian Federal Agency for Support and Evaluation of Graduate Education (CAPES) Fellowship.

REFERENCES

Adam AC, Rubio-Texeira M, Polaina J (2005). Lactose: the milk sugar from a biotechnological perspective. Crit. Rev. Food Sci. Nutr. 44:553-557.

Alegre ACP, Polizeli MLTM, Terenzi HF, Jorge JA, Guimarães LHS (2009). Production of thermostable invertases by *Aspergillus caespitosus* under submerged or solid state fermentation using agroindustrial residues as carbon source. Braz. J. Microbiol. 40:612-622 .

Akcan N (2011). High level production of extracellular β-galactosidase from *Bacillus licheniformis* ATCC 12759 in submerged fermentation. Afr. J. Microbiol. Res. 5(26):4615-4621.

Akinola GE, Adebayo-Tayo B, Olonila OT (2012). Screening and production of β-galactosidase by *Trichoderma* species. Nat. Sci. 10(12):265-270. http://www.sciencepub.net/nature

Andjelkovic U, Theisgen S, Scheidt HA, Petkovic M, Huster D, Vujcic Z (2012). The thermal stability of the external invertase isoforms from *Saccharomyces cerevisiae* correlates with the surface charge density. Biochimie. 94:510-515.

Ansari SA, Satar R (2012). Recombinant β-galactosidases–past, present and future: A mini Review. J. Mol. Catal. B: Enzym. 81:1-6.

Fekete E, Karaffa L, Kubicek CP, Szentirmai A, Seiboth B (2007). Induction of extracellular β-galactosidase (Bga1) formation by D-galactose in *Hypocrea jecorina* is mediated by galactitol. Microbiol. 153:507-512.

Fekete E, Karaffa L, Sándor E, Seiboth B, Biró S, Szentirmai A, Kubicek CP (2002). Regulation of formation of the intracellular beta-galactosidase activity of *Aspergillus nidulans*. Arch. Microbiol. 179:7–14.

Guimarães LHS, Terenzi HF, Polizeli MLTM, Jorge JA (2007). Production and characterization of a thermostable extracellular β-D-fructofuranosidase produced by *Aspergillus ochraceus* with agroindustrial residues as carbon sources. Enzyme Microb. Tech. 42:52-57.

Husain Q (2010). B-galactosidases and their potential applications: A Review. Crc. Cr. Rev. Biotechn. 30:41-62.

Ikram-ul-Haq I, Baig MA, Ali S (2005.) Effect of cultivation conditions on invertase production by hyperproducing *Saccharomyces cerevisiae* isolates. World J. Microb. Biot. 21:487-492.

Isobe K, Yamashita M, Chiba S, Takahashi N, Koyama T (2013). Characterization of new β-galactosidase from acidophilic fungus, *Teratosphaeria acidotherma* AIU BGA-1. J. Biosci. Bioeng. 116(3):293–297.

Konsoula Z, Liakopoulou-Kyriakides M (2007). Co-production of α-amylase and β-galactosidase by *Bacillus subtilis* in complex organic substrates. Bioresour. Technol. 98(1):150-157.

Madhan SSR, Sathyavani R, Niket B (2010). Production and partial purification of invertase using *Cympopogan caecius* leaf powder as substrate. J. Microbiol. 50:318-324.

Miller GL (1959). Use of dinitrosalicylic acid for determination of reducing sugar. Anal. Chem. 31:424-426.

Nuero OM, Reyes F (2002). Enzymes for animal feeding from *Penicillium chrysogenum* mycelial wastes from *Penicillium manufacture*. Lett. Appl. Microbiol. 34:413-416.

Oliveira C, Guimarães PMR, Domingues L (2011). Recombinant microbial systems for improved β-galactosidase production and biotechnological applications. Biotech. Adv. 29:600-609.

Raol GG, Prajapatib VS, Raol BV (2014). Formulation of low-cost, lactose-free production medium by response surface methodology for the production of β-galactosidase using halotolerant *Aspergillus tubengensis* GR-1. Biocatal. Agric. Biotechnol. 3:181-187.

Rashad MM, Nooman MU (2009). Production, purification and characterization of extracellular invertase from *Saccharomyces cerevisiae* NRRL Y-12632 by solid-state fermentation of red carrot residue. Aust. J. Basic Appl. 3(3):1910-1919.

Rubio MC, Navarro AR (2006). Regulation of invertase synthesis in *Aspergillus niger*. Enzyme Microb. Tech. 39(4):601-606.

Rustiguel CB, Terenzi HF, Jorge JA, Guimarães LHS (2010). A novel silver-activated extracellular β-D-fructofuranosidase from *Aspergillus phoenicis*. J. Mol. Catal. B: Enzym. 67(1-2):10-15.

Saha SP, Ghosh S (2014). Optimization of xylanase production by *Penicillium citrinum* xym2 and application in saccharification of agro-residues. Biocatal. Agric. Biotechnol. 3(4):188-196.

Shaikh SA, Khire JM, Khan MI (1999). Characterization of a thermostable extracellular β-galactosidase from a thermophilic fungus *Rhizomucor sp.* Biochim. Biophys. Acta. 1472:314-322.

Soccol CR, Vandenberghe LPS (2003). Overview of applied solid- state fermentation in Brazil. Biochem. Eng. J. 13(2-3):205-218.

Uma C, Gomathi D, Ravikumar G, Kalaiselvi M, Gopalakrishnan VK

(2012). Production and properties of invertase from a C*ladosporium cladosporioides* in SMF using pomegranate peel waste as substrate. Asian Pac. J. Trop. Biomed. 2(2):S605-S611.
Vainstein MH, Peberd JF (1991). Regulation of invertase in *Aspergillus nidulans*: effect of different carbon sources. J. Gen. Appl. Microbiol. 137(3):15-321.
Vidya B, Palaniswamy M, Gopalakrishnan VK (2014). Screening and optimization of β-galactosidase from fungal strains by using agro residues. World J. Pharm. Sci. 3(6):1809-1821.

academicJournals

Vol. 10(6), pp. 243-250, 30 March, 2015
DOI: 10.5897/SRE2014.5872
Article Number:589695451826
ISSN 1992-2248

http://www.academicjournals.org/SRE

Scientific Research and Essays

Full Length Research Paper

Algorithm for wavelength assignment in optical networks

Gulzar Ahmad Dar*, Ifrah Amin and Hardeep Sing Saini

Department of ECE, Indo Global College of Engineering, Punjab Technical University, 141401, Chandigarh –India.

Received 9 March, 2014; Accepted 2 March, 2015

Wavelength division multiplexing (WDM) is a technology which multiplexes many optical carrier signals onto a single optical fiber by using different wavelengths. Wavelength assignment is one of the important components of routing and wavelength assignment (RWA) problem in WDM networks. In this article, to decrease the blocking probability, a new algorithm for wavelength assignment- Least Used Wavelength Conversion algorithm is introduced and is an enhancement to the previously used Least Used Wavelength assignment algorithm. The performance of this wavelength assignment algorithm is evaluated in terms of blocking probability and the results show that the proposed technique is very promising in future. The Least Used Wavelength Conversion algorithm is compared with algorithms such as first-fit, best-fit, random and most-used wavelength assignment algorithm.

Key words: Algorithm, wavelength division multiplexing (WDM), routing and wavelength assignment (RWA), first-fit, best-fit.

INTRODUCTION

Wavelength division multiplexing (WDM) is a very promising technology to meet the ever increasing demands of high capacity and bandwidth. The term wavelength-division multiplexing is commonly applied to an optical carrier. In a WDM network several optical signals are sent on the same fiber using different wavelength channels. WDM is used to address routing and wavelength assignment (RWA) problem. The first part of this problem is to route the network and the second is wavelength assignment. Wavelength assignment is one of the important issues in RWA. In general, if there are multiple feasible wavelengths between a source node and a destination node, then a wavelength assignment algorithm is required to select a wavelength for a given light path. Either distinct wavelength is assigned on each link of path or the same wavelength on each link can be used. When the wavelength conversion is not possible at intermediate routing nodes a light path must occupy the same wavelength on each link over its physical route. The clever algorithms are needed in order to ensure that RWA function is performed using a minimum number of wavelengths (Dar and Saini, 2013; Wason and Kaler, 2010).

The Least Used Wavelength Conversion Algorithm (LUWC) is an improvement over least used wavelength assignment algorithm. In LUWC, least– used wavelength assignment algorithm is executed until blocking. Also the

*Corresponding author. E-mail: drmushtaqpbg@gmail.com.

concept of wavelength conversion is used in this model. When the call is blocked, wavelength conversion is introduced and hence blocking probability is reduced. If the full wavelength conversion is used after least–used wavelength assignment algorithm, the blocking probability is reduced to a very large extent and its value reduces to a minimum possible value. Hence, the overall performance of the network increases. The Least Used Wavelength Conversion algorithm is compared with algorithms such as first-fit, best-fit, random and most-used wavelength assignment algorithm. Simulation results proved that the proposed approach is very effective for minimization of blocking probability of optical wavelength division multiplexed networks (Mukherjee, et al., 2004). All the results are taken using MATLAB.

WAVELENGTH ASSIGNMENT

There are two constraints that need to keep in mind while trying to solve RWA. One is distinct wavelength assignment constraint that is, all light paths sharing a common fiber must be assigned distinct wavelengths to avoid interference (Arun and Azizoglu, 2000). This applies not only with in alloptical networks but in access links as well. Another is wavelength continuity constraint which means the wavelength assigned to each light path remains the same on all the links while it traverses from source end-node to destination end-node (Murthy and Gurusamy, 2002; Qi and Chen, 2006). The most important wavelength assignment algorithms are as follows:

(i) First-fit algorithm: In this algorithm, firstly the wavelengths of the traffic matrix are sorted in non decreasing order. Then algorithm steps through this sorted list for selecting candidate chains joined. This process is carried on until all chains are considered to form a single chain representing linear topology. The idea of the first-fit scheme is to pack the usage of the wavelengths toward the lower end of the wavelengths so that high numbered wavelengths can contain longer continuous paths. By using first fit algorithm blocking can be reduced to a great extent as compared to random algorithm (Alyatama, 2005; Yuan and Zhou, 2000).
(ii) Random algorithm: In this algorithm, wavelength is selected randomly from available wavelengths. A number is generated randomly and the wavelength is assigned to this randomly generated number. As this technique chooses a random wavelength from the set of all wavelengths that are available along the path, the blocking probability cannot be minimized as much as compared to other wavelength assignment algorithms (Alyatama, 2005).
(iii) Most-used: The most-used scheme furthers the idea of the first-fit scheme in packing the usage of wavelengths. In this scheme, all the available wavelength that can be used to establish a connection are considered, the wavelength that has been used the most is selected for the connection. The wavelength usage using the most-used scheme is more compact than that using the first-fit scheme. Studies have shown that with precise global network state information, the most used scheme performs slightly better than the first-fit scheme (Yuan and Zhou, 2000).
(iv) Best-fit algorithm: Among all the wavelengths from the list, this algorithm chooses an efficient wavelength for the assignment and is known to be the best fit wavelength assignment. According to the previous study the best fit algorithm performs better than other existing algorithms. Depending upon the number of wavelengths and load given to the path per unit link, the blocking probability of the best fit increases and decreases respectively (Yuan and Zhou, 2000).

BLOCKING PROBABILITY

If there is no free wavelength available on any link, the call will be blocked. In simple terms blocking probability as per Poisson's formula can be calculated as the ratio of calls blocked to the total number of calls generated as given below

$$P_{Bavg} = \frac{Total\ no.of\ calls\ blocked}{\text{Total no.of calls generated}} \quad (1)$$

The network performance of any network can be measured through blocking probability, which is the statistical probability that a telephone connection cannot be connected due to insufficient transmission resources in the network. Also, the blocking probability on the link can be calculated by famous Erlang-B formula as given by Wan et al. (2003) Equation (2).

$$P_{b(L,W)} = \frac{\frac{L^W}{W!}}{\sum_{i=0}^{W}\frac{L^i}{i!}} \quad (2)$$

Where, $P_{b(L,W)}$ is blocking probability for L load and W wavelengths.

MODELING SETUP

Here, the enhanced algorithm is given and is evaluated in terms of blocking probability. Following assumptions are made to design the model:

(i) The network is connected in an arbitrary topology. Each link has a fixed number of wavelengths.
(ii) Point to point traffic.
(iii) There is no queuing of the connection request. The connection blocked will suddenly be discarded.

Table 1. For scenario 1.

S/No.	No. of nodes	No. of links	No. of wavelengths	Load per unit link (Erlang's)
1	20	20	20	20
2	20	20	20	20
3	20	20	20	40

Table 2. For scenario 2.

S/No.	No. of nodes	No. of links	No. of wavelengths	Load per unit link (Erlang's)
1	20	20	10	10
2	20	20	30	10
3	20	20	50	10

(iv) Link loads are mutually independent.
(v) Static routing.
(vi) Each station has an array of transmitters and receivers, where *W* is the wavelengths carried by the fiber.
Firstly, a source to destination pair is selected. Then using the shortest path routing algorithm, a route is selected. After that with the help of proposed algorithm, wavelength is assigned to the route. Until blocking, least–used wavelength assignment algorithm is executed. If the call is blocked, the concept of wavelength conversion is introduced which is done with the help of wavelength converters and hence blocking probability is reduced.

RESULTS AND DISCUSSION

Here, the simulation results of proposed algorithm are shown. The simulation is carried out on simulation software MATLAB 7.2 of The Mathworks, Inc. The blocking probability of network is compared according to the number of channels, load, wavelength and the number of links. Depending upon the varied values of these parameters, two scenarios have been set for obtaining results.

Scenario 1

In this scenario load per unit link is increased from 20 to 40 Erlang's and value of all the other three parameters remain fixed to 20. This scenario is set for comparison of proposed algorithm and existing algorithm (Table 1). Now we analyze that how well our wavelength assignment algorithm performs in comparison to existing wavelength assignment algorithm. In this we have fixed the number of nodes to 20; the total number of links used in the network is also fixed to 20; and the load is varying with the per unit link (Figures 1 to 4).

The graphs represent that the blocking probability of our proposed algorithm is increasing with respect to the increase in load. Further it is clear that our proposed algorithm is having less blocking probability as compared to conventional algorithms.

Scenario 2

Wavelength is changing by 10, 30 and 50 in this case. Number of nodes and number of links are constant as 20. Load per unit link is also fixed to 10. This case is also set for comparison between proposed algorithm and conventional algorithm (Table 2). Graph represents that there is a huge difference between the blocking probability of our proposed algorithm and other conventional algorithms. That means our proposed algorithm has less blocking probability (Figures 5 to 7).

It is clear from the graphs that the blocking probability of proposed algorithm is low in comparison to the conventional algorithms when we increase the wavelength. Scenario 1 graphs show that blocking probability of our proposed algorithm is much lower than the existing algorithms such as first fit, random, most used and best fit wavelength assignment algorithms. In the case of Scenario 2, blocking probability of proposed algorithm decreases as we increase the number of wavelengths. In this scenario, blocking probability of proposed algorithm is also reduces by the other conventional algorithms.

CONCLUSION

In this research paper, Least Used Wavelength Conversion algorithm has been proposed for wavelength assignment and its performance is evaluated in terms of blocking probability. In the first phase, the number of wavelengths is varied, keeping the other parameters

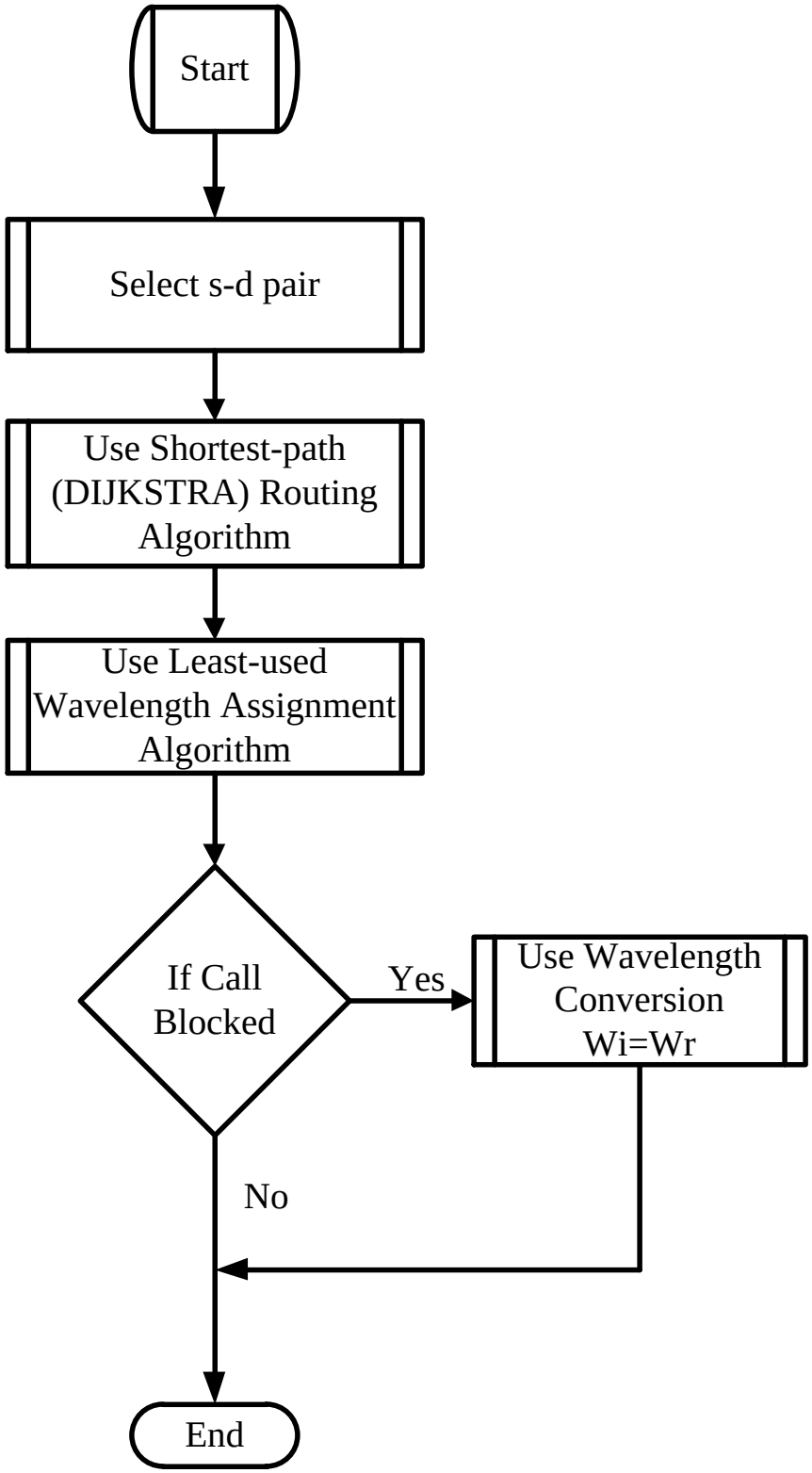

Figure 1. Flowchart of least used wavelength conversion algorithm.

constant. The results prove that the blocking probability of the proposed algorithm decreases with the increase in the number of wavelengths. In the second phase, the load per unit link is increased keeping the other

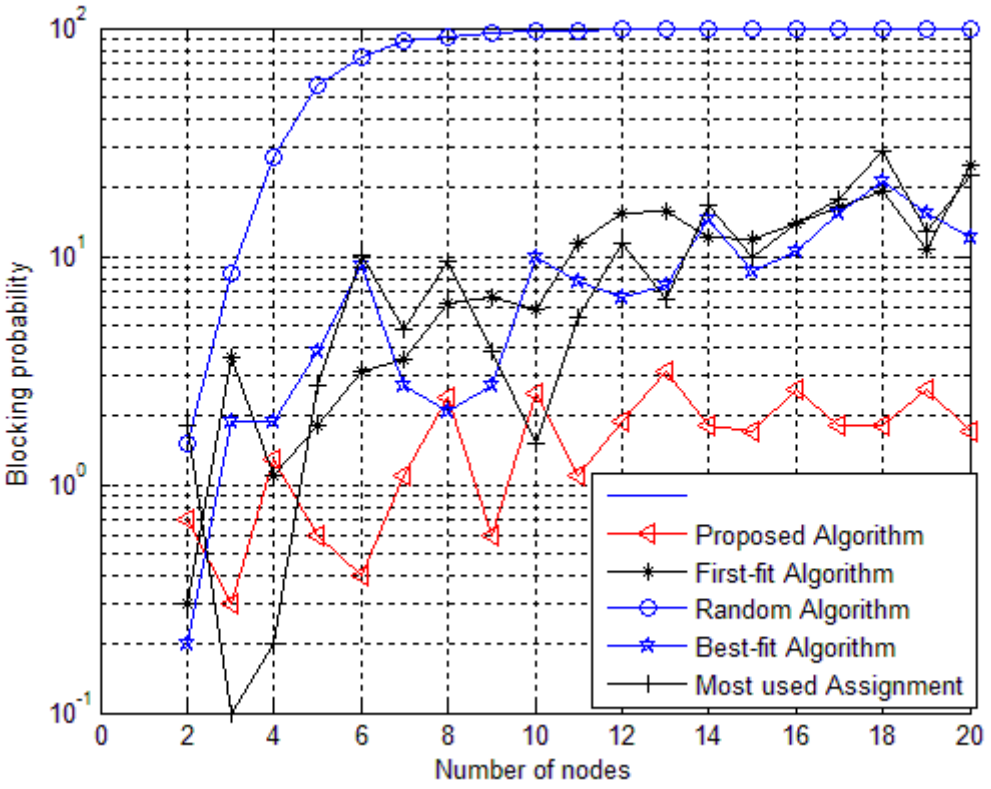

Figure 2. Comparison of the algorithm for load=10 Erlangs; W=20.

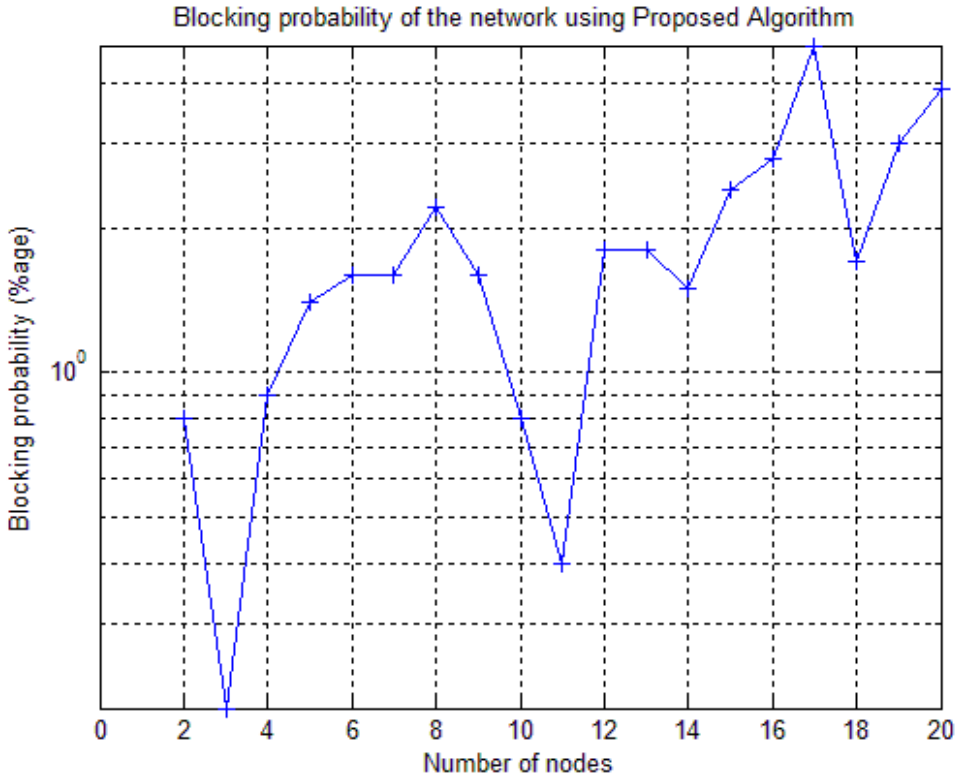

Figure 3. Comparison of the algorithm for load=20 Erlangs; W=20.

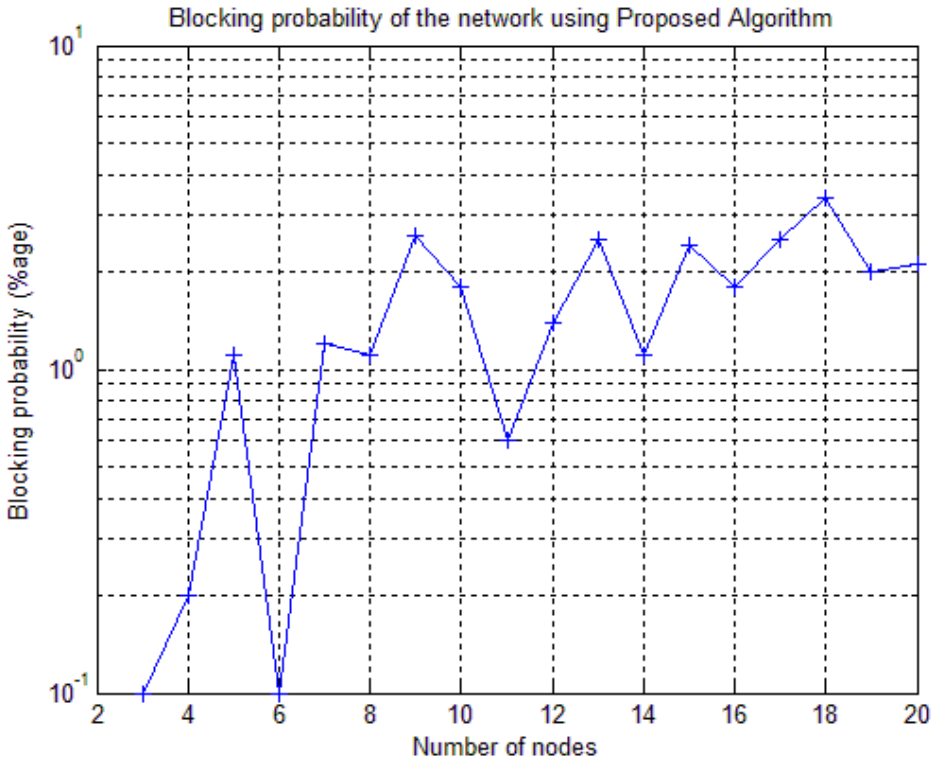

Figure 4. Comparison of the algorithm for load=30 Erlangs; W=20.

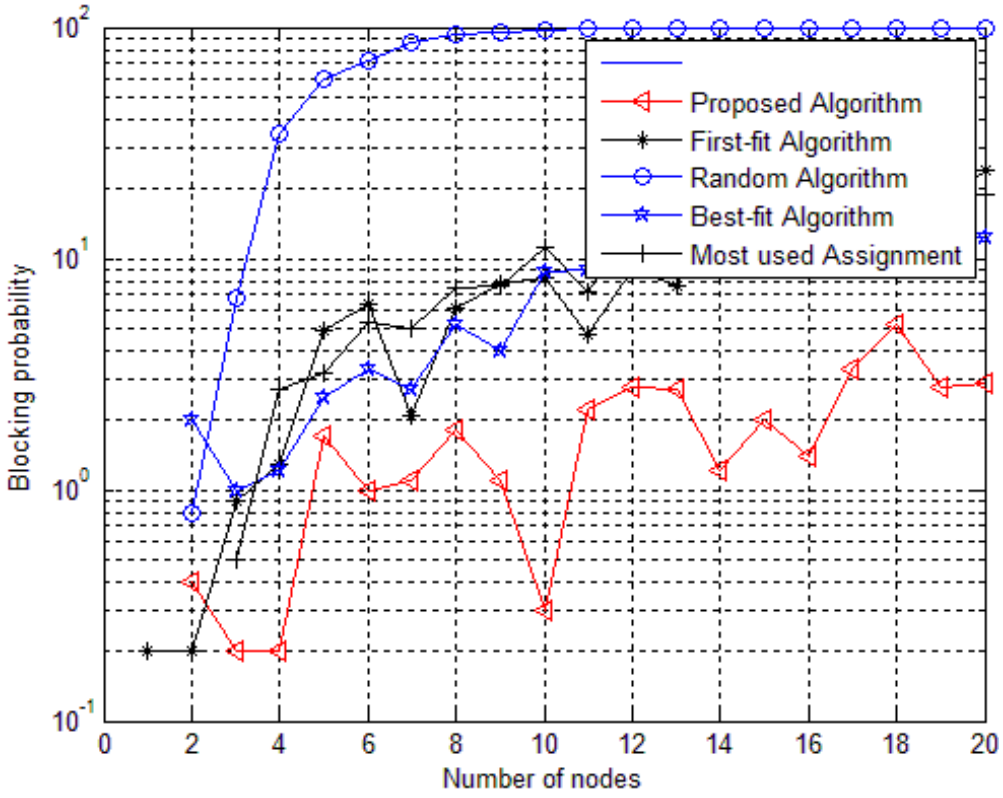

Figure 5. Comparison of the algorithm for load=10 Erlangs; W=10.

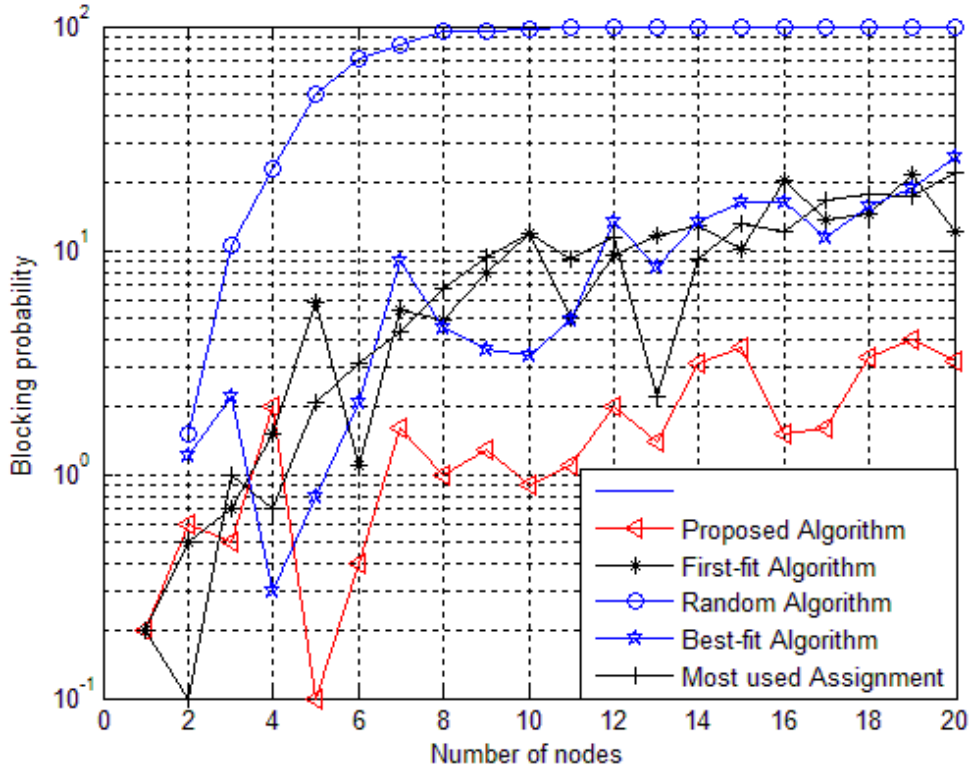

Figure 6. Comparison of the algorithm for load=10, Erlangs; W=30.

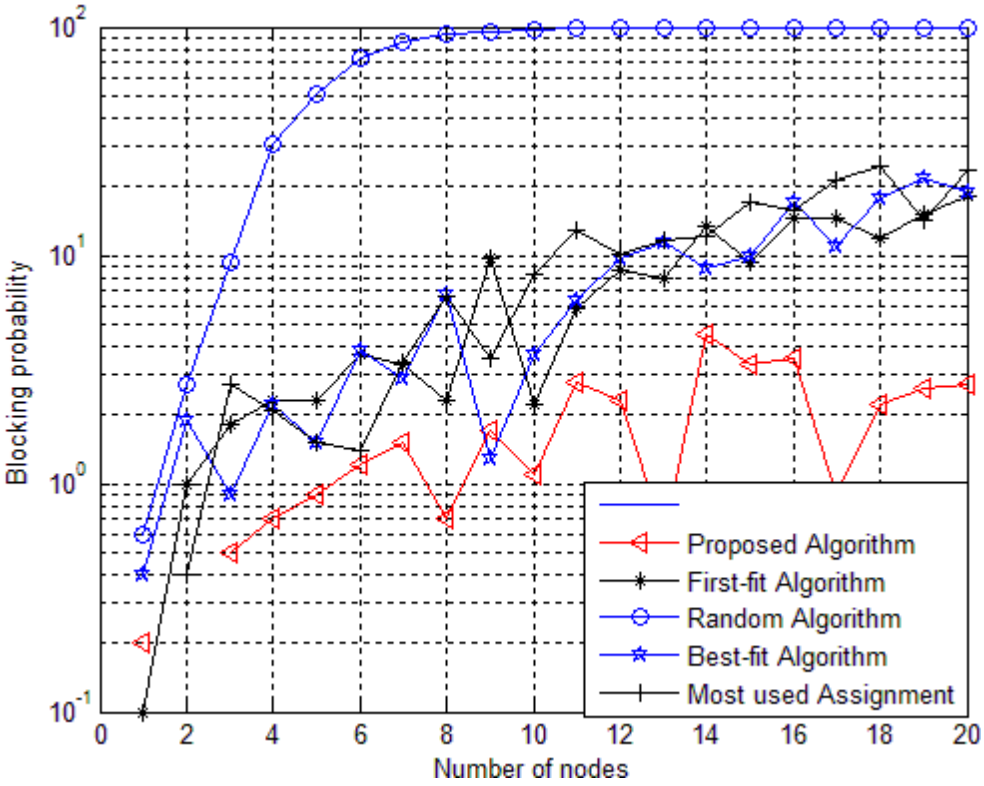

Figure 7. Comparison of the algorithm for load=10, Erlangs; W=50.

parameters constant. The results show that as the load is increased, the blocking probability of the network increases for the network. Clearly, the algorithm will prove to be a promising technique in near future when the requirement of keeping blocking probability low is a must. Hence the use of Least Used Wavelength Conversion algorithm is proposed.

Conflict of Interest

The authors have not declared any conflict of interest.

REFERENCES

Alyatama A (2005). Wavelength decomposition approach for computing blocking probabilities in WDM optical networks without wavelength conversions, Comput. Networks 49:727-742.

Arun K, Azizoglu SM (2000). Wavelength assignment algorithms for wavelength routed interconnection of LANs. J. Lightwave Technol. 18(12):1807-1817.

Dar GA, Saini HS (2013). Wavelength assignment algorithm for optical networks. Int. J. Comput. Technol. 9(2)1049-1054.

Mukherjee A, Singh SP, Chaubey VK (2004). Wavelength conversion algorithm in an intelligent WDM network, Optics Commun. 230:59-65.

Murthy CSR, Gurusamy M (2002). WDM optical networks -Concepts, Design and Algorithms, Prentice Hall of India Pvt. Limited.

Qi JWX, Chen B (2006). Wavelength Assignment for Multicast in All-Optical WDM Networks With Splitting Constraints, IEEE/ACM Transactions on Networking 14(1):169-182.

Wan J, Zhou Y, Sun X, Zhang W (2003). Guaranteeing quality of service in optical burst switching networks based on dynamic wavelength routing. Optics Commun. (220):85-95.

Wason A, Kaler RS (2010). Blocking in wavelength-routed all-optical WDM networks, Optik .International J. Light Electron Optics- Elsevier Sci. 121(10):903-907.

Yuan X, Zhou J (2000). A study of dynamic routing and wavelength assignment with Imprecise Network State Information, IEEE ICCCN.

academicJournals

Vol. 10(6), pp. 251-253, 30 March, 2015
DOI: 10.5897/SRE2014.5878
Article Number:071D88551828
ISSN 1992-2248

http://www.academicjournals.org/SRE

Scientific Research and Essays

Short Communication

The law of symmetry and its application

Yang Hongyu*, Huang Chunyi, Wang Zhiyang, Lin Ying and Zhang Shue

North China Electric Power University, China.

Received 11 March, 2014; Accepted 20 June, 2014

In this paper, the content of the law of symmetry and its application in science and production is introduced. It emphasizes the law`s effect on scientific law.

Key words: Symmetry principle, scientific law, translation variant, symmetry, geometrical, rotational.

INTRODUCTION

Since modern times, more and more scientific laws have been discovered. These laws usually fit one or a few aspects. Is there any relationship between these laws? Is there a law that is obeyed by all fields of science? The law of symmetry is the law of this kind.

THE CONTENT OF THIS LAW

The law of symmetry contains several sub laws:

Translation invariant: if the conditions are the same, no matter when and where it happens, the results are the same.
Geometrical symmetry: if the starting condition is symmetrical, the result is symmetrical.
Rotational symmetry: if 2 objects are of the same attributes, and the starting conditions are the same, the results of the 2 objects are the same.

THE 2 DESCENDABLE LAWS

(1) For any group of given conditions, there must be only one result.

(2) If all functions in a process are linear, the result function must be linear.

NOTICE

The law of symmetry is fit with any field of science, but it cannot be used wrongly.
For example,'1+1' paradox: if it`s known that a+b=2, can we conclude a=b=1?
The wrong answer is yes, because a and b are of the same attribute, if we suppose a>b, we conclude a<b, so a=b.
The lead to this wrong answer is that we do not realize a and b are not certain, the premise of the law of symmetry is that the answer is certain.
For another example, Rabbit paradox: if the 2 identical twin rabbits are fed in the same condition, can we conclude that their blood pressure is the same?
The wrong answer is yes, because the 2 rabbits are of the same attribute, and the starting condition is the same, so their blood pressure is the same.
The lead to this wrong answer is that we do not realize the factors that affect blood pressure are very complex, but we simply think that they are in the same condition.

*Corresponding Author. Email: sgrass@qq.com.

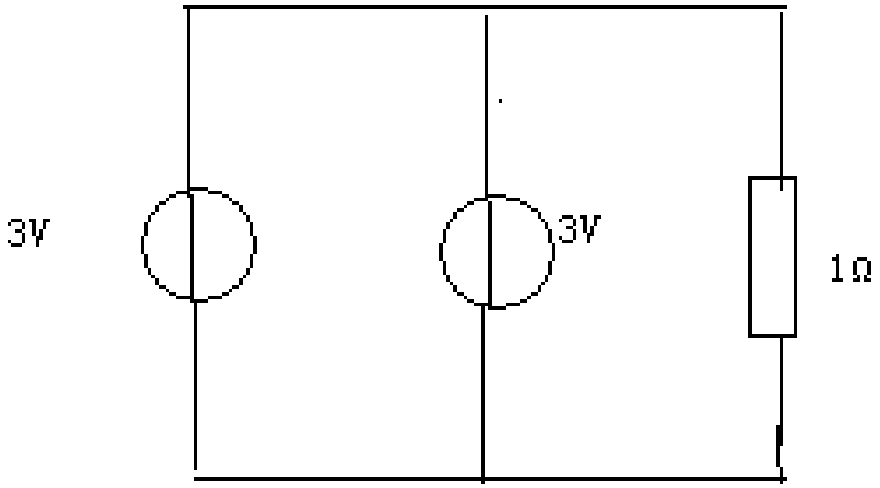

Figure 1. An electric circuit.

The real factors may not be the same.

THE APPLICATION OF THIS LAW

Mathematics

For example, to do this question, (Chunfeng, 2013):

$$A = \iint_D \frac{\sqrt{a}}{\sqrt{a}+\sqrt{b}}\,da * db$$ D: $a^2+b^2 \le 1$,

In this question, a and b are rotationally symmetrical, so the answer A= B= $\iint_D \frac{\sqrt{b}}{\sqrt{a}+\sqrt{b}}\,da * db$
so we can add these two answers, A+B= $\iint_D \frac{\sqrt{a}+\sqrt{b}}{\sqrt{a}+\sqrt{b}}\,da * db = \iint_D 1\,da * db$,
that is so easy. 2A= $\iint_D 1\,da * db$, we can easily know the value of A.

Results

If the area of D is 1, that is 2A=1, so we can know A=0.5.The answer is easy to get.

Discussion

From the above example, if we do not use this law, it is very hard to solve the problem. But if we use this law, the problem is very easy to solve. So we can see, using this law can make some problem easier to solve.

We can prove some models are not exact

For example, as shown in Figure 1 (Xiyou, 2013), the electric current of the 2 powers` wires can be any value. It contracts the 1st descendable law, so it is wrong. In fact, any electric power source has resistance.

Results

For the electric current of the 2 powers` wires to be any value, this model isn`t exact.

Discussion

We sometimes use the model shown in Figure 1, but this model is not exact. If we do not know this law, we may draw the wrong conclusion. This law can correct people`s wrong idea.

THE PROBLEM THAT CANNOT BE SOLVED NOW

The only thing that cannot be proved now is this one. Material wave is a kind of probability wave. Until now, we can only discuss its probability. It seems to contradict the 1st sublaw, but Einstein said that the god does not play the game which throws the dice. The real fact may not be known now.

Conclusion

The above cases show that this law is correct and exact. Using this law, we can avoid making mistakes and find what is wrong and not exact. We can also discover the mistakes or limitations of people`s current point of view.

Conflict of Interest

The author(s) have not declared any conflict of interest.

REFERENCES

Chunfeng L (2013). Advanced Mathematics, Tingshua Press, pp. 150-160.
Xiyou C (2013). Circuit Thoery. Higher Education Press. pp. 110-115.

academicJournals

Vol. 10(6), pp. 254-259, 30 March, 2015
DOI: 10.5897/SRE2014.5882
Article Number:6B1B1E051829
ISSN 1992-2248

http://www.academicjournals.org/SRE

Scientific Research and Essays

Full Length Research Paper

Evaluation of potential application of micromagnetic techniques for detection of corrosion in reinforced concrete

Carlos Henrique de Carvalho[1]*, Carlos Otávio Damas Martins[1], Sandro Griza[1], Thomas Gabriel Rosauro Clarke[2] and Ledjane Silva Barreto[1]

[1]Federal University of Sergipe, Brazil.
[2]Federal University of Rio Grande do Sul, Brazil.

Received 16 March, 2014; Accepted 5 March, 2015

Despite the constant development of new materials, reinforced concrete is still widely used in civil engineering. Corrosion of the steel armour in reinforced concrete structures has historically been one of the main causes of damage and early failure. The development of a reliable method of non-invasive corrosion inspection and evaluation has been a challenge for many years. This paper focused on magnetic inspection of the tendons in steel armours. Results show a good correlation between micromagnetic parameters and corrosion evolution, indicating that the method is a viable option for integrity monitoring of such structures.

Key words: Reinforced concrete, corrosion monitoring, micromagnetic tests.

INTRODUCTION

Steel reinforced concrete is one of the most common materials in civil construction due to its versatility and wide acceptability by designers. Once constructed, good quality concrete can last for many years without intervention (Andrade and Dal 1999). As a disadvantage, corrosion of the steel reinforcement has been one of the predominant factors leading to premature deterioration of concrete worldwide, especially of structures located in coastal areas. This process leads to considerable maintenance costs and demands frequent structure inspection or intervention (Arndt and Jalinoos, 2009).

Literature shows that the most important causes of corrosion initiation in reinforcing steel are the ingress and contact of chloride ions and carbon dioxide on the steel surface, which causes a change in the alkaline environment provided by the concrete, thus leading to incremental degradation processes. Corrosion detection and monitoring has therefore been a significant concern for engineers and researchers in the non destructive testing area (Arndt and Jalinoos, 2009; Breysse et al., 2009; McCann and Forde, 2001; Song and Saraswathy, 2007).

Song and Saraswathy (2007) showed a good review of the application of some of the most popular corrosion monitoring techniques to reinforced concrete structure evaluation.

*Corresponding author. E-mail: consvalho@hotmail.com

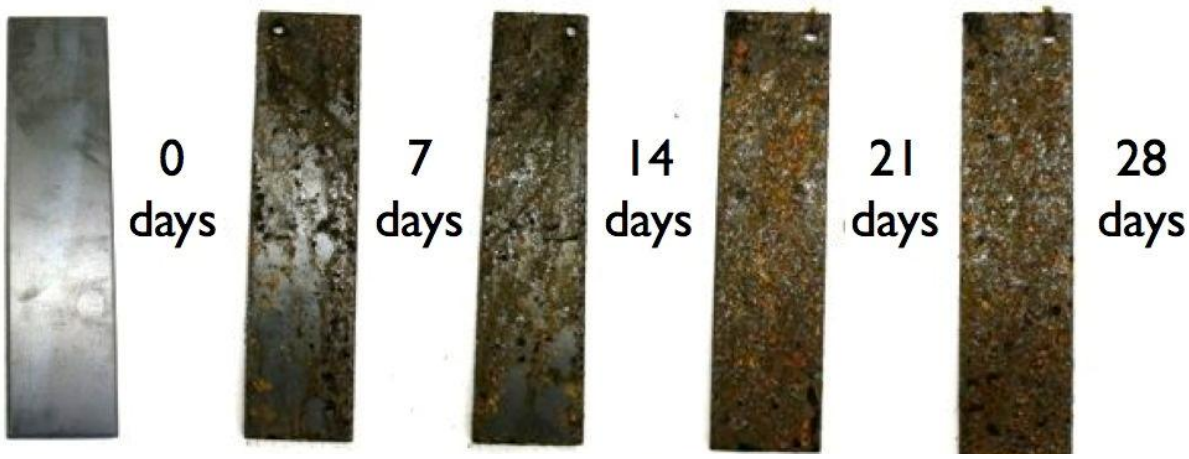

Figure 1. AISI 1020 steel samples, before and after the exposure to salt spray for the indicated period.

Arndt and Jalinoos (2009) evaluated conventional methods based on the detection of electrochemical changes in the structure. However, although cheap, these methods provide low sensitivity, and the authors acknowledge the need for further development of other non destructive techniques, such as radiography, ultrasound, thermography or electromagnetic testing.

Martins (2008), Martins and Reguly (2009, 2010) and Martins et al. (2013) showed results of micromagnetic methods applied to stress and toughness measurements in steels. In these techniques, microstructure-induced variations of the magnetisation characteristics of the material can be correlated to of some of its properties, traditionally those which strongly influence magnetic domain boundary motion (that is, grain boundaries, residual stresses, phase distribution) or cause changes to the induced eddy current fields.

This works aims at increasing the usual range of application of micromagnetic methods by analysing the influence of corrosion evolution on magnetic properties of AISI 1020 steels samples. Corrosion in this case is the irreversible consumption of material due to its interaction with the environment (Arndt and Jalinoos, 2009). During this process, the oxidative reactions occurring on the materials surface will alter its magnetisation characteristics, allowing this effect to be used to quantify the amount of corrosion taking place in the structure.

EXPERIMENTAL PROCEDURE

Flat samples of AISI 1020 steel (5 x 50 x 200 mm^3) were used in this work. This flat geometry was selected due better configuration with the equipments magnetic probe. Also, the low carbon AISI 1020 material was chosen due to its normal application as reinforcement in concrete combining a good strength and low cost (despite its low corrosion resistance).

In order to simulate the corrosion degradation, the samples were exposed to a 5% NaCl atmosphere for different periods of time (0, 7, 14, 21, and 28 days) in a salt spray chamber (manufactured by Bass Equipment Ltd.). The resulting aspect of the samples is shown in Figure 1.

Micromagnetic measurements were performed with a 3MA-II equipment manufactured and supplied by the IZFP Fraunhofer Institut from Germany. For magnetisation and analysis, a rectangular contact surface probe (with 50 x 75 mm^2) was proposed and used in this work. The basic parameters used in the measurements were: magnetic field intensity: 35 A/cm; magnetisation frequency: 200 Hz; analysing frequency for Barkhausen noise: 0.5 MHz, and analysing frequencies for multi-frequency Eddy current: 0.05, 0.1, 0.5, and 1 MHz. These parameters were selected by the authors' previous experience in the field of micromagnetic analysis (Martins, 2008; Martins and Reguly, 2009, 2010; Martins et al., 2013).

As shown in Martins (2008), Martins and Reguly (2009, 2010), Martins et al. (2013), Dobmann et al. (1998), Dobmann (2007) and Yelbay (2010) the 3MA technique is based on the interaction of an external magnetic field and the ferromagnetic sample followed by the signal analysis given by four micromagnetic techniques.

Measurements were performed 40 times on each of 3 points per sample. Two concrete blocks, with 7.5 and 15 mm-thickness each were used to vary the lift-off between the sensor and the steel sample.

This approach allowed 31 micromagnetic parameters to be obtained, which are derived from a combination of three micromagnetic techniques: harmonic analysis of the tangential field (HAHt), Barkhausen noise (MBN), and multi frequency Eddy current analysis (MFEC). Statistical analysis and correlations of the data were performed on the MMS Software, provided with the 3MA-II equipment. Table 1 in the Annex 1, shows the micromagnetic parameters given by the 3MA equipment (Dobmann et al., 1998). Figure 2 shows an image of the equipment and a schematic of the test configuration.

RESULTS

Results were divided in two groups depending on whether concrete lift-off layers were used or not. A statistical analysis based on multiple variable regression analysis was performed on the data obtained, and in this first analysis, in which no concrete layers were present, only parameters for one of the mentioned methods were

Table 1. Micromagnetic parameters derived from the 3MA approach (Song and Saraswathy, 2007; Martins, 2008).

	Symbol	Unit	Description
HAHt	Ax	A/cm	Amplitude of the harmonics of order x
	Px	[rad]	Phase angle of the harmonic of order x
	Hco	[A/cm]	Coercive field derived from technical HAHt
	Hro	[A/cm]	Harmonic higher Ht(0)
	K	%	Harmonic distortion
	SAH	[A/cm]	Sum of the amplitudes of the harmonics SAH =ΣAx
	Vmag	[V]	Amplitude of the output voltage to micromagnetic analysis
	HAHt	**-**	**Harmonic analysis of the tangential current field**
MBN	Mmax	[V]	Maximum amplitude of the curve M(H) for a cycle of magnetization
	Mmean	[V]	Average signal curve M(H) to a magnetization cycle
	Mr	[V]	Curve measured signal M(H) for H = 0 A/cm
	Hcm	[A/cm]	Coercive field derived from MBM
	□ hyym	[A/cm]	Expansion of the curve M(H) for M = 0,yy% de Mmax
	MBN	**-**	**Magnetic Barkhausen noise analysis**
MFEC	Re*	[V]	Real part of the eddy current signal to the frequency of No*
	Im*	[V]	Imaginary part of the signal for frequency eddy current of No*
	Mag*	[V]	Magnitude of the eddy current to the frequency of No*
	Ph*	[rad]	Phase angle of the eddy current signal to the frequency of No*
	MFEC	**-**	**Multi-frequency eddy current analysis**

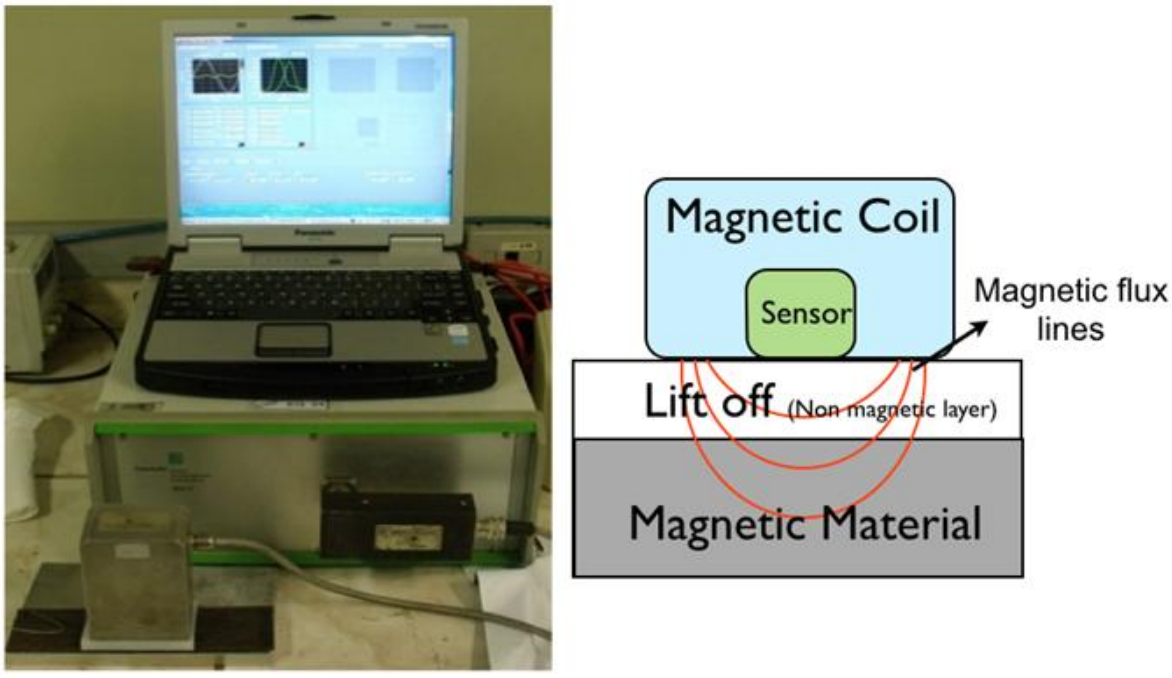

Figure 2. 3MA-II equipment and schematic of the experimental setup adopted for the measurements.

included in the analysis. Figure 3 shows the results obtained through this methodology; it shows significant data dispersion for the MBN technique (R^2 =0.836 (correlation)), which is an indicative of the low sensitivity of the MBN technique to corrosion evolution in ferromagnetic steel materials. The HAHt (R^2 = 0.987) and

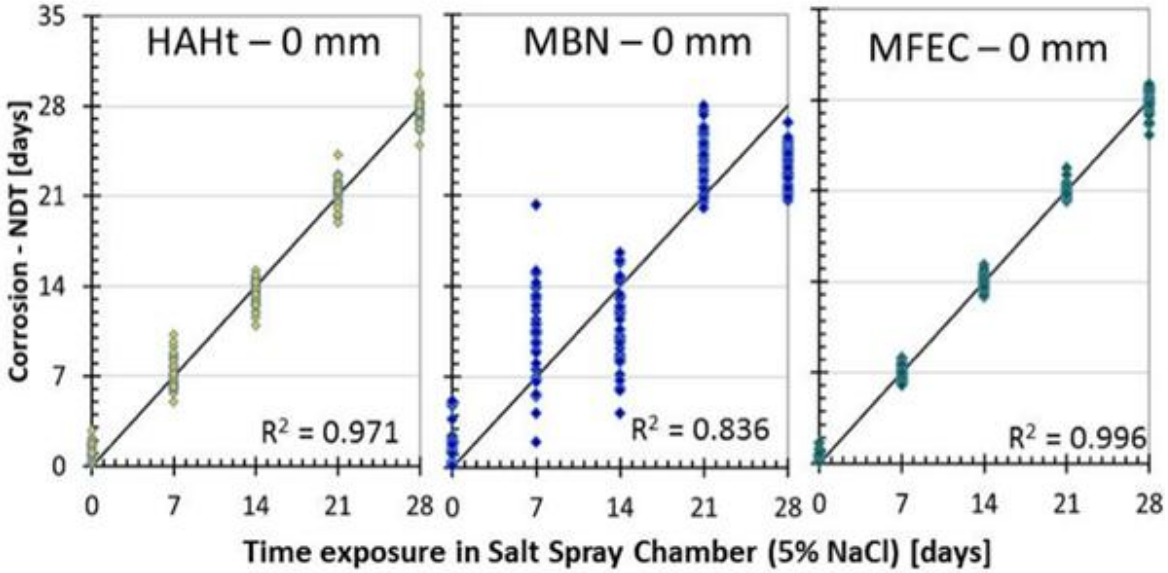

Figure 3. Micromagnetic parameters obtained from measurements on samples exposed to varying period lengths (without lift-off).

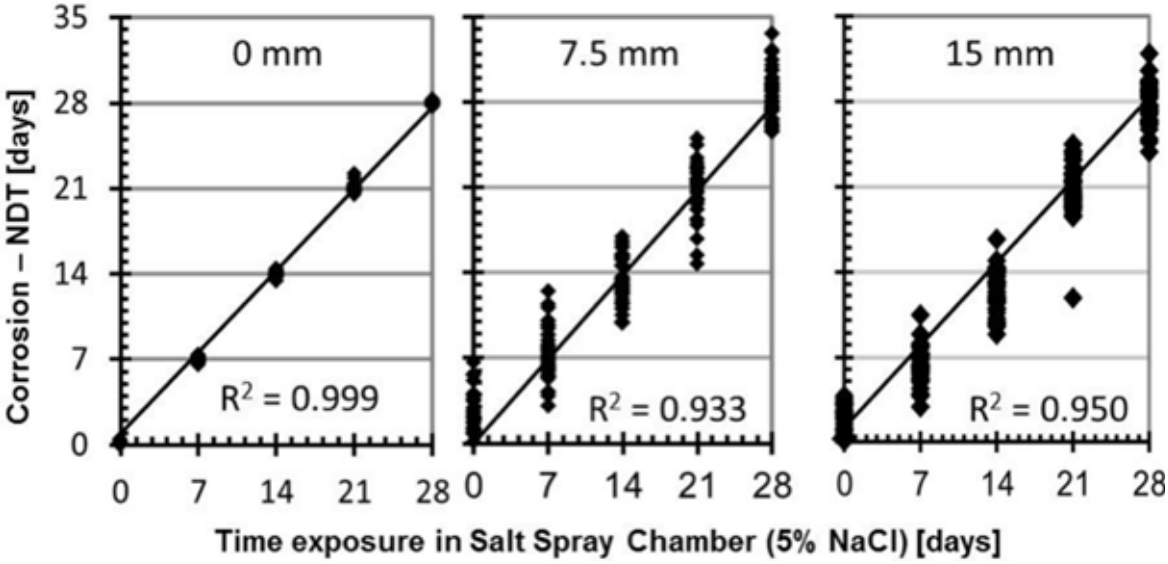

Figure 4. Micromagnetic parameters obtained from measurements on samples exposed to varying period lengths: without lift-off (0 mm), and with a 7.5mm-thick or 15mm-thick concrete layer used to impose different lift-offs.

MFEC (R^2 = 0.997) techniques provided better correlations with the corrosion evolution process, with less scatter. The equations obtained for each of the techniques after the analysis are shown in the Annex 2.

Improvements in the correlations are usually obtained if data of parameters of all methods are combined in a single regression analysis. For the measurements taken in the presence of concrete layers to simulate the lift-off seen in practical reinforced steel inspection, the lower signal-to-noise led to significantly worse result when parameters for a single method were combined.

Hence, a statistical analysis including parameters from the three techniques was performed on the data obtained when no lift-off concrete layer was present (0 mm), and on the data obtained when the two concrete lift-off layers (with two different thicknesses - 7.5 and 15 mm) were used. Figure 4 shows that, despite the expected loss in signal intensity and the distortion in the magnetic field caused by the presence of the lift-off concrete layers, the combination of the parameters of the three micromagnetic

techniques led to excellent correlations between the processed data and the period of exposure to salt spray.

DISCUSSION

As shown extensively in Martins (2008), Martins and Reguly (2009, 2010), Martins et al. (2013), Dobmann et al. (1998), Dobmann (2007) and Yelbay (2010), there is a basic interaction between the magnetisation characteristics and the microstructural properties of ferromagnetic materials, which allows their characterisation or inspection. During a corrosion process, the oxidation of the surface of the material will similarly influence its response to applied magnetic fields. In this sense, this work aimed at finding a good combination of magnetisation parameters, which allowed a good correlation between the measured data and the corrosion degree in these materials. If applied to reinforced concrete inspection in the civil engineering sector, the measurement procedure should also be robust when a concrete lift-off layer of different thicknesses is present. It is important to note that by the interaction of the magnetic field with the ferromagnetic material, these micromagnetic techniques can be applied for the steel bar localisation in reinforced concrete, prior to its corrosion analysis and evaluation.

Figure 3 shows the good sensitivity of the individual micromagnetic methods to the corrosion state on the samples, when no lift-off was imposed. The results were further improved when parameters of the different techniques where included in the regression analysis, as shown in Figure 4.

However, a loss of sensitivity was seen when the concrete blocks were inserted to create lift-offs of different heights. This is due to the lower intensity of the imposed magnetic field and the resulting lower signal-to-noise ratio obtained. In other words, the lift-off decreases the reliability of the micromagnetic method due to the increased path of the magnetic field from the sensor to the sample and back. Similar effects were seen in (Martins and Reguly, 2010).

The results shown in Figure 4 indicate that by combining parameters of different methods a good correlation can be obtained even when the thickest concrete block was used. If a sensor with a more adequate geometry is developed and used instead of the commercial sensor used in this work, these results are likely to improve. Nevertheless, the results indicate that a reliable procedure for micromagnetic non destructive analysis and monitoring of corrosion evolution in steel reinforcement in concrete has been demonstrated. This will be the focus of further developments of the authors.

Conclusions

Results showed good correlation between values obtained from multiple variable regression analysis of parameters given by three micromagnetic methods (harmonic analysis of the tangential magnetic field, Barkhausen noise, and multiple frequency Eddy current analysis) and the corrosion evolution obtained from exposure of steel samples to different periods of exposure to salt spray. Good correlations were found between the measured and processed data and the corrosion state of the sample even in the presence of 15 mm-thick concrete lift-off layers.

This indicates that micromagnetic measurements are a promising way of inspecting or monitoring corrosion evolution in reinforced concrete, contributing to the development of methodologies of structural integrity evaluation and conservation for constructors and engineers.

Conflict of Interest

The authors have not declared any conflict of interests.

ACKNOWLEDGEMENTS

The authors are grateful to FAPITEC/SE and CNPq for their financial support.

REFERENCES

Andrade J, Dal Molin DA (1999). case study about degradation of reinforced concrete structures in a marine macro-environment in Brazil", International Symposium on NDT Contribution to the Infrastructure Safety Systems, RS, Brazil.

Arndt R, Jalinoos F (2009). NDE for corrosion detection in reinforced concrete structures — a benchmark approach", NDTCE'09, France,

Breysse D (2009). How to improve the quality of concrete assessment by combining several NDT measurements", NDTCE'09, France,

McCann DM, Forde MC (2001). Review of NDT methods in the assessment of concrete and masonry structures", NDT&E international, P. 34.

Song HW, Saraswathy V (2007). Corrosion Monitoring of Reinforced Concrete Structures – A Review. Int. J. Electrochem. Sci. 2:1-28.

Martins COD (2008). Desenvolvimento de metodologias de inspeção e monitoramento de risers flexíveis através de técnicas micromagnéticas de análise de tensões", PhD Thesis, PPGE3M – UFRGS, P. 133.

Martins COD, Reguly A (2009). Micromagnetic stress evaluation of Flexible Riser tensile armours", Insight Vol. 51 N° 1, January.

Martins COD, Reguly A (2010). Lift-off influence analysis during the micromagnetic stress evaluation of flexible riser tensile armours", Insight N° 6, June P. 52.

Martins COD, Altenhofen A, Clarke TGR, Reguly A (2013). Applying Micromagnetic Methods for the Nondestructive Metallurgical Characterisation of an AISI 4140 Steel Materials", N° 3, March Insight P. 55.

Dobmann G (2007). Industrial Applications of 3MA – Micromagnetic Multi-parameter Microstructure and Stress Analysis", 5th ISCS2007, Romania.

Dobmann G, Altpeter I, Becker R, Kern R, Laub U, Theiner W (1998). Barkhausen noise measurements and related measurements in ferromagnetic steels", Sensing for Materials Characterisation. The ASNDT inc, P. 1.

Yelbay HI (2010). Non-destructive determination of residual stress state in steel weldments by Magnetic Barkhausen Noise technique, ND&T International 43:29-33.

ANNEX

Equations:

Equation 1: $R^2 = 0.987$; RMSE: 9.945 (Figure 3).

Corrosion $_{NDT\text{-}HAHt}$ [days] = $1316.66 - 587.5*V_{mag} + 441.67*A_3 + 150.42*A_5 - 216.67*P_3 - 54.16*P_5 - 92.91*K - 38.17*H_{ro}$.

Equation 2: $R^2 = 0.836$; RMSE: 8.183 (Figure 3).

Corrosion $_{NDT\text{-}MBN}$ [days] = $89.16* - 168.75*M_{max} + 172.08*M_{mean} - 4.5*H_{cm} - 2.64*\Delta H75M$.

Equation 3: $R^2 = 0.9960$; RMSE: 5.045 (Figure 3).

Corrosion $_{NDT\text{-}MFEC}$ [days] = $22.04 + 1150*Im_1 - 641.67*Mag_1 + 5.21*Ph_1 + 3658.3*Re_2 + 900*Im_2 + 770.83*Mag_2 - 9.625*Ph_2$.

Equation 4: $R^2 = 0.999$; RMSE: 3.202 (Figure 4).

Corrosion $_{NDT\text{-}ALL}$ [days] = $74.33 - 16.25*P_3 - 4.204*UHS - 4.51*H_{ro} - 1.25*M_{max} + 8.602*M_{mean} + 325.87*Im_3 - 541.56*Mag_3$.

Equation 5: $R^2 = 0.9331$; RMSE: 61.432 (Figure 4).

Corrosion $_{NDT\text{-}ALL}$ [days] = $2201.3 - 2310.92*V_{mag} + 2224.71*A_3 + 170.84*A_5 + 4{,}92*P_5 + 157{,}81*UHS - 948.84*K - 44.96*M_r - 8.44*Ph_3$.

Equation 6: $R^2 = 0.9505$; RMSE: 51.797 (Figure 4).

Corrosion $_{NDT\text{-}ALL}$ [days] = $2861.82 - 3089.52*V_{mag} + 1924.2*A_3 + 201.25*UHS - 853.05*K + 53.56*M_{max} - 51304.5*Im_2 - 12.3*Ph_3 - 19980.8*Im4$.

academicJournals

Related Journals Published by Academic Journals

- International NGO Journal
- International Journal of Peace and Development Studies